Mechanistic understanding of pH variations in capacitive deionization

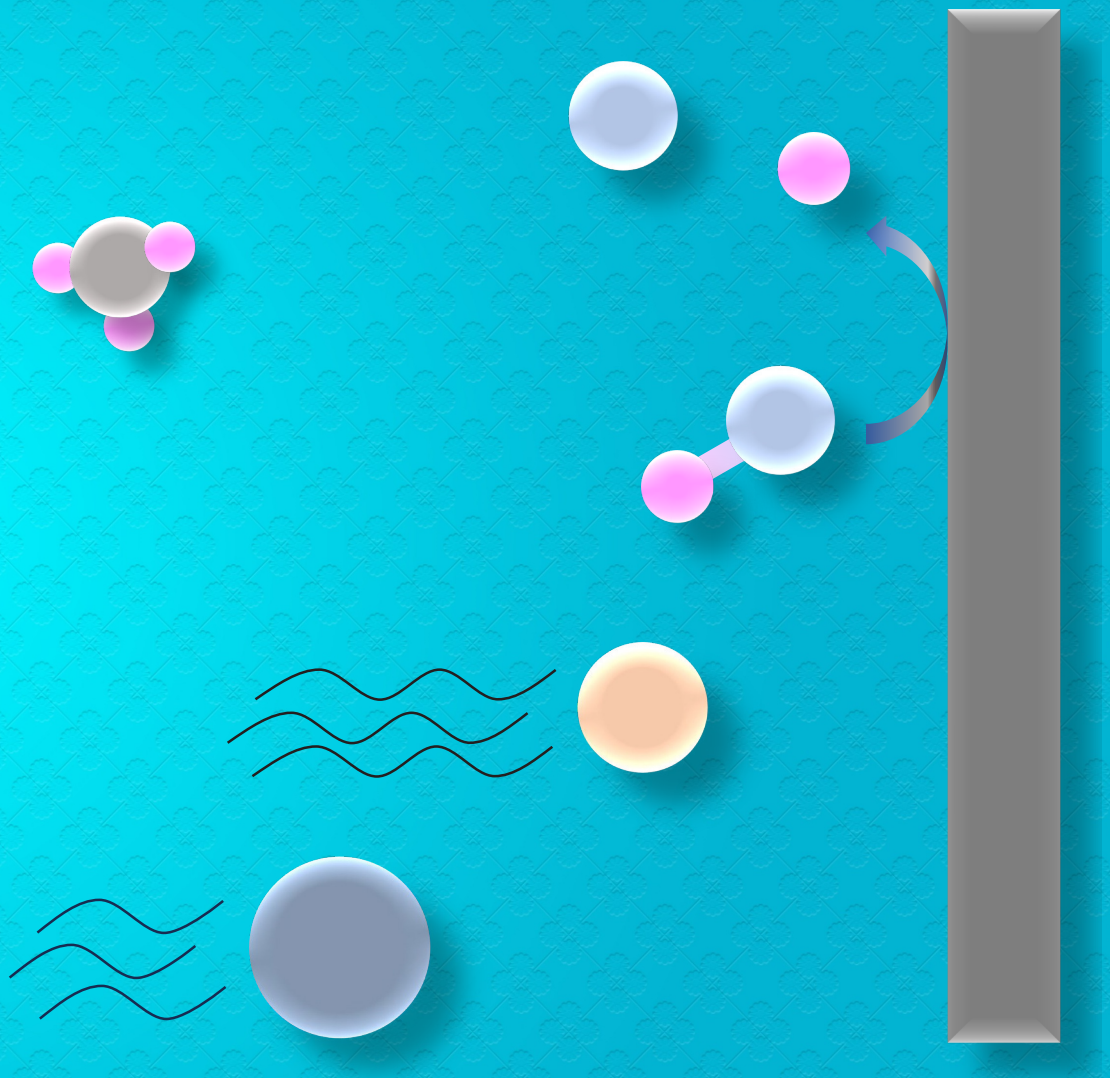

Antony Cyril Arulrajan

Propositions

1. pH changes in membrane capacitive deionization are primarily caused by non-faradaic processes rather than faradaic reactions.
   (this thesis)

2. pH variations in electrochemical desalination promote ion-selective separation.
   (this thesis)

3. The conclusions drawn from experiments conducted under ideal conditions have limited impact when solving problems in real-world situations.

4. Artificial intelligence will enable researchers to model complex systems without being a master of programming or mathematics.

5. Environmental activists lack awareness about technological possibilities.

6. Political participation without political awareness is dangerous.

Propositions belonging to the thesis, entitled

Mechanistic understanding of pH variations in capacitive deionization

Antony Cyril Arulrajan
Wageningen, 9 September
2024.

Mechanistic understanding of pH variations in capacitive deionization

Antony Cyril Arulrajan

Thesis committee

Promotor
Prof. Dr A. van der Wal
Special Professor, Electrochemical Water Treatment
Wageningen University & Research

Co-promotors
Dr S. Porada
Scientific project manager,
Wetsus, European Centre of Excellence for Sustainable Water Technology, Leeuwarden, The Netherlands.
Assistant professor,
Wrocław University of Science and Technology, Poland.

Dr J.E. Dykstra
Associate Professor, Environmental Technology
Wageningen University & Research

Other members
Prof. Dr L.C.P.M. de Smet, Wageningen University & Research
Prof. Dr D. van Halem, Delft University of Technology
Dr M.W.J. Luiten – Olieman, University of Twente, Enschede
Dr Akbar Asadi Tashvigh, Wageningen University & Research

This research was conducted under the auspices of the Graduate School for Socio-Economic and Natural Sciences of the Environment (SENSE)

Mechanistic understanding of pH variations in capacitive deionization

Antony Cyril Arulrajan

Thesis
submitted in fulfilment of the requirements for the degree of doctor
at Wageningen University
by the authority of the Rector Magnificus,
Prof. Dr C. Kroeze
in the presence of the
Thesis Committee appointed by the Academic Board
to be defended in public
on Friday 9 September 2024
at 1.00 p.m. in the Omnia Auditorium.

Antony Cyril Arulrajan
Mechanistic understanding of pH variations in capacitive deionization,
166 pages.

PhD thesis, Wageningen University, Wageningen, the Netherlands (2024)
With references, with summary in English

DOI https://doi.org/10.18174/669705

To my family

“Magic happens when you don’t give up even though you want to. The universe always falls in love with a stubborn heart.”

-J.M. Storm

TABLE OF CONTENTS

Chapter 1. Introduction

1.1. Water scarcity

The 21st century has witnessed a great water scarcity problem.[1–4] The diminishing availability of fresh water resources, coupled with the increasing demand for water across domestic, industrial, and agricultural sectors, has resulted in 4 billion people worldwide facing water shortages for at least one month a year.[5] The migration of people and increased industrial activities have led urban areas to experiencing sustained water stress throughout the year.[3,6] In addition, many countries are faced with severe droughts and irregular monsoon patterns in recent years, primarily attributed as the effects of climate change.[7–11] Water stress, caused by different factors, is exerting significant pressure on public health, economic development, and ecological stability.

Water treatment technologies have emerged as important and necessary tools in numerous regions around the world to address water scarcity.[10] Water desalination and wastewater treatment serve the dual purpose of providing a clean and potable water supply for domestic, agricultural, and industrial use, and facilitate the purification and reclamation of wastewater for subsequent reuse.[12]

1.2. Water demand in different sectors

The demand for fresh water comes from domestic, industrial, and agricultural sectors. Domestic desalination plants are often employed to address drinking water scarcity issues in water stressed areas. In addition to the production of drinking water from sea water or brackish water, desalination technologies are also used for municipal wastewater treatment which includes the purification and recycling of wastewater to reduce water consumption and the environmental impact of wastewater discharge.[13,14] The implementation of water treatment technologies in the domestic sector leads to sustainable management of domestic water resources.

In industries, water plays a crucial role in various processes, and the efficient management of this important resource is of primary importance.[15,16] Industrial water treatment is aimed at minimizing freshwater usage while reducing effluent discharge and it's environmental impact. In industries, multiple water treatment technologies are used in combination to treat industrial wastewater to enable reuse of water and recovered resources from water such as minerals to reach circularity. In some industries, policies such as zero liquid discharge (ZLD) are adopted to treat wastewater and enable complete reuse of water.[17]

In the agricultural sector, quality of water needs is depending on the specific farming practices, activities, and crop types. For livestock, clean and safe water is required. For irrigation purposes, water enriched with certain minerals is often required depending on the crop type. The implementation of water treatment techniques helps to meet the water requirements for agriculture in geological locations where freshwater availability is scarce.

The availability and type of water source, the quality requirements of the treated water, and regulations on treating (waste) water are considered for the choice of the treatment technologies.

1.3. The landscape of water treatment technologies

Water treatment technologies function based on various fundamental principles, utilizing factors like temperature, pressure, and electric field to separate salts and impurities from water, ultimately desalinating the water. The selection of a particular technology is based on several considerations, including the initial concentration and quality of the feed water, desired quality standards for the treated water, energy efficiency, overall cost-effectiveness, and the extent of chemical usage during the desalination process. Each desalination method possesses its unique strengths and weaknesses as shown in table 1, making it essential to match the technology with the specific requirements of the water treatment scenario.

Table 1. The strengths and weakness of different types of desalination technologies

Technology	Strength	Weakness
Temperature-driven desalination technologies	Suitable for brine treatment, zero liquid discharge treatment, and to produce high purity water	Energy intensive, cost intensive, lack of ion-selective separation, high operational cost, usage of cleaning chemicals
Pressure-driven desalination technologies	Suitable for sea water desalination, wastewater treatment, and to produce high purity water	Lack of ion-selective separation, high operational costs, usage of cleaning chemicals, low water recovery (30-60%)
Electric field-driven desalination technologies	Suitable for brackish water desalination, potential for ion-selective separation, potential for chemical free desalination, high water recovery (>90%)	Energy intensive for high concentration water (>5g/l), high capital costs, membrane maintenance.

The efficiency of each technology is depending upon factors such as feed water concentration, salt removal, water recovery, productivity etc. Therefore, it is hard to compare two different technologies straight away. However, energy consumption of a technology is considered an important criterion to choose suitable desalination technology as shown in figure 1.1. For seawater desalination, with its high salinity (approximately 35 g/L), thermal and pressure-driven technologies are well-suited. Thermal desalination offers effective treatment but demands a specific energy

consumption (SEC) between 13 and 22 kWh/m^3, depending on the specific technology employed and operational conditions.[18] Seawater reverse osmosis (SWRO) is the widely used desalination technology with a significantly lower SEC, typically ranging from 2 to 5 kWh/m^3 while forward osmosis (FO) has a SEC between 4 to 11 kWh/m^3 depending upon operational conditions[18–20]. In contrast, for brackish water with a lower salt concentration (typically less than 5 g/L), conventional thermal desalination becomes less efficient. Due to their higher energy requirements, thermal desalination technologies are not a preferred choice for brackish water desalination. Brackish water reverse osmosis (BWRO) has lower energy consumption typically requiring a SEC in the range of 0.3 to 0.7 kWh/m^3 for 50-90% of salt reduction with 20 to 60 l/h/m^2 of water productivity. Whereas, electric field driven technologies are comparatively more suitable for brackish water desalination with SEC

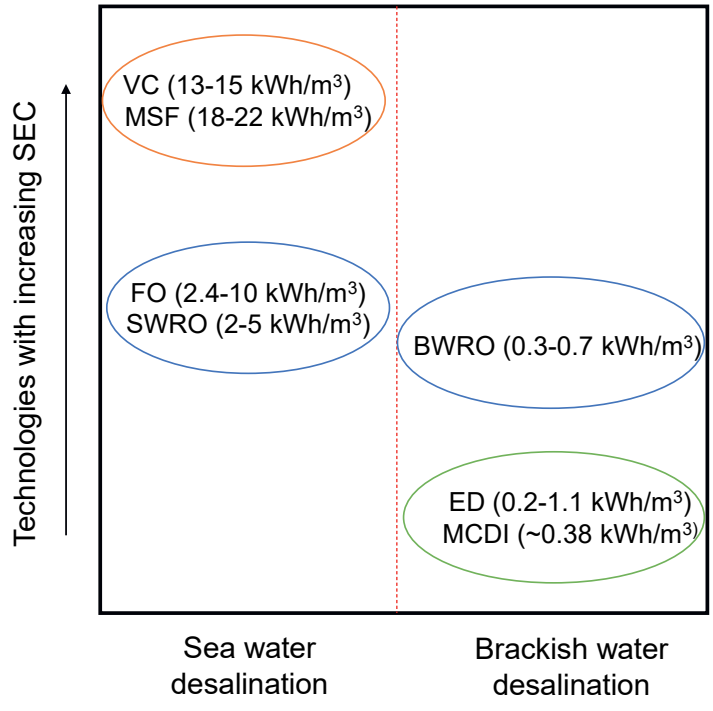

Figure 1.1. The landscape of desalination technologies suitable for sea water desalination and brackish water desalination with their SEC range. Brown circle represents temperature driven technologies, blue circles represent pressure driven technologies and green circle represents electric field driven technologies.

comparable to SWRO or even lower with SEC of between 0.2 to 1.1 kWh/m^3 depending upon technology and the operational conditions.[21,22]

1.3.1. Temperature-driven desalination technologies

Thermal desalination technologies utilize temperature as the principal force driving clean water production, with Multi-Effect Distillation (MED), Multi-Stage Flash (MSF) distillation, and Vapor Compression (VC) techniques emerging as prominent methods. In MED, saline water is heated to generate water vapor in one chamber, which is then condensed in subsequent chambers to yield fresh water, utilizing recovered heat to fuel further evaporation.[23,24] MSF operates by heating water in a high temperature-high pressure chamber, rapidly evaporating a portion in the first stage through pressure reduction (flash evaporation), with subsequent stages repeating this process at decreasing pressures.[23,25] In VC desalination, water is heated to produce vapor, mechanically compressed, and then introduced into chambers for evaporation and condensation, with the cyclic process repeating across multiple chambers. [23,26]

1.3.2. Pressure-driven desalination technologies

Pressure-driven technologies rely on a pressure gradient across semi-permeable membranes to separate salt and water. Reverse Osmosis (RO), Forward Osmosis (FO), and Nanofiltration (NF) are prominent pressure-driven technologies with each offering distinct advantages for water treatment. In RO, feed water is subjected to pressures exceeding osmotic pressure, compelling water molecules to pass through the RO membrane while blocking salt ions, resulting in desalinated water on one side and a concentrated salt solution on the other side.[26,27] The emerging method FO utilizes a semi-permeable membrane in contact with a highly concentrated draw solution on one side and lower-concentration feedwater on the other, creating an osmotic pressure that drives water passage from the feed to the draw solution which is subsequently diluted. Then a draw recovery step is used for fresh water recovery from diluted draw solution.[28] In NF, a porous

membrane is employed with a molecular weight cutoff (MWCO), selectively allowing smaller molecules such as water and monovalent salts to permeate under pressure while blocking larger molecules such as divalent ions/salt, yielding a desalinated water stream and a concentrated stream enriched in larger ions/salts, often utilized for removing hardness ions rather than fresh water production.[29,30]

1.3.3. Electric field-driven desalination technologies

In electric field-driven technologies, current or voltage is applied between two electrodes, resulting in positively and negatively charged electrodes. The charged electrodes remove salt ions from water either by capacitive processes i.e., electrostatic ion storage, or by faradaic reactions, to produce desalinated water. Electrodialysis (ED), bipolar membrane electrodialysis (BPED) and capacitive deionization (CDI) are well known and emerging electrochemical desalination technologies.

1.3.3.1. Electrodialysis

In conventional electrodialysis (ED), two electrodes are separated by alternatively arranged AEMs and CEMs. An electrolyte solution (for example, Na_2SO_4) is circulated through the electrode compartments. Feed water flows through the spacer channels placed between the IEMs. During ED operation, the electrodes are charged to drive faradaic reactions such as water splitting, resulting in the production/consumption of charged ions such as H^+ and OH^-, which require a counterion to maintain electroneutrality, and therefore salt ions migrate from one compartment to the other. Due the alternative arrangement of IEMs, and because anions are dominantly transported across the AEM and cations across the CEM, a separate desalinated stream and a concentrated stream are produced, as shown in figure 1.2a.[31–34]

1.3.3.2. Bipolar membrane electrodialysis

In bipolar membrane electrodialysis (BPED), bipolar membranes (BPM, a type of ion exchange membrane that contains both anion and cation exchange layers), are inserted in a conventional electrodialysis setup with AEMs and

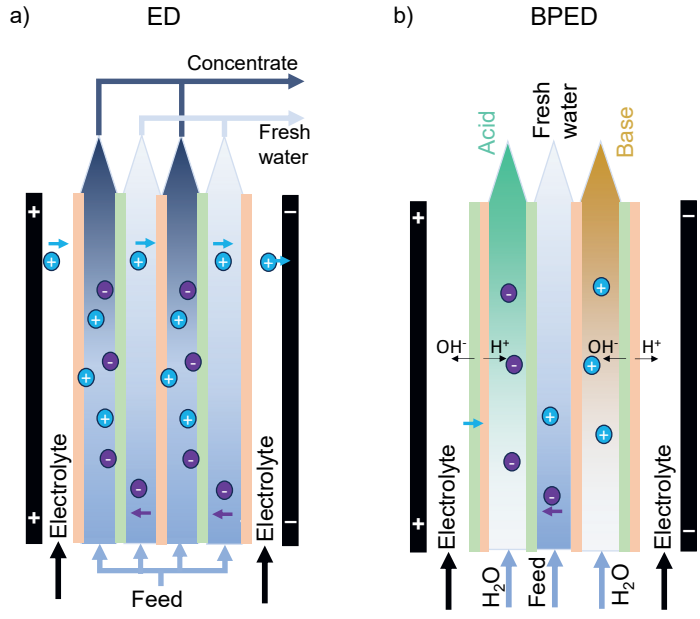

Figure 1.2. Working principle of ED (a) and BMED (b)

CEMs. As shown figure 1.2b, BPMs are positioned alongside the electrodes, with IEMs placed between BPMs and separated by spacer channels. An electrolyte solution is circulated through the electrode compartments, while spacer channels between membranes are for feed water flow. During charging of BPED, similar to ED, faradaic reactions at the electrodes generate ions. Additionally, the BPMs also split water into H^+ and OH^- inducing electromigration of salt ions to ensure charge neutrality. Electromigration of ions in this cell configuration leads to desalination in the flow channel between IEMs while producing an acid stream and a basic stream in the channels adjacent to the BPMs.[16,35]

1.3.3.3. Capacitive deionization

In capacitive deionization, two porous carbon electrodes separated by a porous spacer channel are used as shown in figure 1.3a. The activated carbon electrodes have micropores (< 2 nm in diameter) and macropores (> 2 nm in diameter). When the electrodes are charged, electrical double layers are formed throughout the electrode. The electronic charge is balanced by electrostatic adsorption (i.e., electrosorption) of salt ions of opposite charge (i.e., counterions), which are transported from the spacer channel, via the macropores in the electrodes, to the micropores. Due to the smaller size of the micropores, the electrical double layers in the micropores overlap.[36–38]

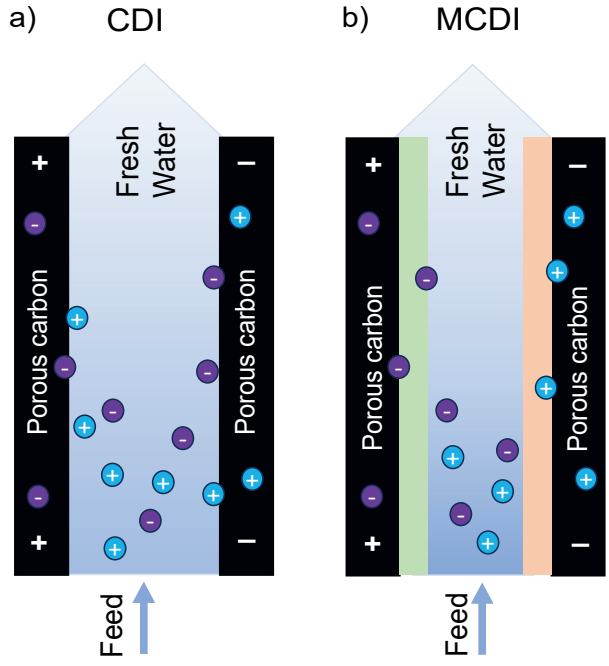

Figure 1.3. Cell configuration and working principle of CDI (a) and MCDI (b)

CDI is a cyclic process of charging and discharging, to produce, alternatingly, a desalinated water stream and a concentrated stream. When a CDI cell is charged, the cathode (i.e., negatively charged electrode) adsorbs cations while the anode (i.e., positively charged electrode) adsorbs anions, producing a

desalinated water stream. Once the electrodes reach their adsorption capacity, the cell is discharged by reversing the current/voltage or by short-circuiting the electrodes, resulting in the desorption of ions, and consequently in the production of a concentrated stream in the spacer channel. In CDI, the charge applied to the electrodes is not only utilized to adsorb counterions, but also to expel co-ions (i.e., ions of the same charge as the electrode) from the carbon electrodes to the flow which results in a reduced charge efficiency.[36–38]

1.3.3.4. Membrane capacitive deionization

Membrane capacitive deionization (MCDI) is a sub-class of CDI, where, in addition to carbon electrodes and a spacer, ion exchange membranes are also included. A cation exchange membrane (CEM) is placed in front of the cathode and an anion exchange membrane (AEM) in front of the anode, see figure 1.3b. The inclusion of ion exchange membranes increases the desalination efficiency by blocking co-ions from leaving the electrode compartment (i.e., the CEM blocks anions leaving the cathode compartment while the AEM blocks cations leaving the anode compartment). As the co-ions are confined within the electrode compartments, more counterions are transported from the spacer channel to maintain the charge balance in the electrode compartments resulting in increased salt removal and an overall efficiency increase. [36–39]

1.4. Advantages of electrochemical desalination technologies - The case of MCDI

Energy consumption

Energy consumption in desalination is a crucial metric as it contributes significantly to operation costs, and therefore it is used to determine the feasibility of using a specific desalination technology.[40,41] Comparative assessments of desalination technologies, particularly of membrane capacitive deionization (MCDI) and reverse osmosis (RO), rely on the existing data available on the literature that are obtained under diverse

experimental and operational conditions. As a result, there are significant variations in energy efficiency of these technologies for specific feedwater, such as brackish water.[42,43] However, in recent studies better comparisons are made by aligning the desalination conditions such as the feed water salt concentration, concentration reduction (i.e., Δc, 80%), and water recovery (WR 93%) for both MCDI and RO systems. The outcomes indicate that MCDI exhibits energy efficiency in brackish water desalination, boasting an energy consumption of approximately 0.38 kWh/m^3, whereas RO necessitates around 0.53 kWh/m^3 under analogous conditions.[22]

Levelized cost of water

The Levelized Cost of Water (LCOW) stands as a valuable and pragmatically significant metric for assessing the economic viability of contemporary deionization technologies.[44] It encompasses various cost components, including capital outlays, energy consumption costs, chemical expenses, and maintenance costs associated with membrane and electrode replacements. This comprehensive approach ensures a more accurate calculation of the cost per litre of desalinated water. In the context of brackish water desalination, MCDI demonstrates a LCOW ranging from 0.74 to 1.74 \$/m^3 for brackish water desalination.[45] In contrast, the reported LCOW for Brackish Water Reverse Osmosis (BWRO) falls between 0.18 and 0.33 \$/m^3.[46] Though these findings are in favour of RO, the LCOW of MCDI mainly arise from the replacement of IEMs and electrodes. With increasing research and developments on IEMs, cell and electrode materials, the lifespan of IEMs and electrodes is expected to be increased which can make MCDI competitive for brackish water desalination compared to a much more mature technology, RO.

Water recovery

In the process of water desalination, a fraction of the water becomes desalinated, while the remaining fraction becomes concentrated with salts. The water recovery (WR) is defined as the ratio of desalinated water over the total volume of water treated. A higher WR signifies a more efficient

utilization of water, minimizing wastage of water in the form of a concentrated stream. MCDI achieves water recoveries exceeding 80%, while some existing brackish water reverse osmosis (BWRO) plants achieve a WR between 10% to 70% with a single module.[47] Many existing RO plants for seawater desalination achieve consistently lower WR of 30-60%.[48] Often, anti-scaling chemicals, multiple RO stages, and water softening techniques are used to reach WR >80% with BWRO which can significantly increase LCOW for brackish water desalination.[49] Thermal desalination technologies can potentially achieve WR > 90% but their elevated energy requirements makes them less attractive. MCDI stands out by achieving high WR with lower/similar energy demands compared to conventional desalination technologies such as RO, positioning it as an alternative and sustainable desalination technology.[22]

Ion-selective separation & resource recovery

Thermal desalination technologies operate by separating clean water from water with dissolved salts, yielding a brine solution containing all the salts from the feedwater. While capable of producing ultrapure water, thermal desalination lacks the ability to selectively remove salts. Whereas, pressure-driven technologies employing membranes offer a degree of selectivity based on membrane pore size and surface modifications. Nanofiltration (NF) membranes, for instance, can selectively remove $CaSO_4$ while leaving NaCl in the treated water.[29,50,51] Reverse osmosis (RO), however, blocks all ions, allowing only water molecules to permeate, limiting room for selective salt separation. Given that the membrane is the sole active component in pressure-driven desalination technologies mentioned here, opportunities for inducing selectivity are confined to membrane properties.[52,53]

Different from both thermal and pressure-driven methodologies, MCDI separates ions from water to produce freshwater. This inherent distinction in MCDI introduces the potential for selective ion removal through four important components: the two electrodes, the cation-exchange membrane (CEM), and anion-exchange membrane (AEM). Carbon electrodes can be

chemically modified to selectively adsorb certain ions in the electrodes.[54,55] Likewise, non-carbon materials can also be employed to achieve ion-selective desalination[56,57] Beyond electrodes, both AEM and CEM can be fabricated or modified to selectively transport specific ions to the electrodes.[58–60] This approach in MCDI stands in contrast to conventional desalination methods, offering a promising avenue for selective ion separation for desalination and resource recovery.

Room for process developments

Thermal and pressure-driven desalination methodologies have been commercially deployed for more than six decades, marked by sustained operational efficacy achieved through continuous research and development. The refinement and optimization of these technologies have notably advanced, with particular emphasis on the enhancement of reverse osmosis (RO) performance, as seen by progress in process optimization, pretreatment steps, and membrane cleaning techniques.[61,62] In contrast, MCDI stands as a relatively recent addition into the technologies for desalination, initiating research and development activities ~15 years ago. The dynamic trajectory of MCDI research reflects its promising potential.

1.5. Challenges for improved MCDI operation

Mineral scaling

Mineral scaling poses a current challenge to the efficacy of desalination processes, impacting not only MCDI but also other electrochemical technologies, conventional pressure and temperature-driven technologies.[63–66] In the MCDI process, multiple factors, including the solubility limits of salts, the presence of hardness ions, and solution pH, contribute to the precipitation of salts such as $CaCO_3$ and $CaSO_4$.[65–67] This phenomenon leads to the deposition of mineral scaling on critical components such as spacers and membranes within the MCDI system. The consequences of mineral scaling include a decline in system efficiency, increased operational costs, diminished lifespan of MCDI systems, and the necessitated use of anti-scaling

chemicals [66,67] These anti-scalants, while effective in mitigating mineral scaling, introduce environmental concerns due to their inherent harmful properties. The interplay of these factors underscores the need for targeted research and innovative strategies to mitigate mineral scaling in MCDI, ensuring sustained operational efficiency and environmental sustainability.

Insufficient ion-selectivity

While MCDI holds promise for selective ion removal, the extent of its ion selectivity is constrained between certain important groups of ions such as Na^+/K^+, Cl^-/NO_3^-.[68] The factors determining ion selectivity in MCDI include the chemistry of surface groups on carbon electrodes, the chemical nature of non-carbon electrode materials, the selective transport of ions facilitated by membranes, and the valence of ions, which is, for some ions, pH dependent[56,69–71]

Activated carbon in MCDI exhibits inadequate selectivity towards common ions of interest, including Na^+, Ca^{2+}, Cl^-, and NO_3^-. To enhance ion selectivity, chemical modifications of carbon electrodes, involving the introduction of specific chemical groups such as amines, are implemented.[69] The ion adsorption mechanisms of certain chemical groups such as amines are based on the pH of the solution and the pKa values of the specific amine group. Apart from the selectivity induced by the nature of electrodes, the valence and the type of ions can also influence ion-selective removal. Amphoteric ions such as carbonate, phosphate, and borate exhibit pH-dependent speciation, rendering their selective and efficient removal based on the pH of the solution.[71]

Water productivity

Productivity (P), denoted in $L/h/m^2$, signifies the volume of treated water generated per unit time and unit area of the membrane/electrode.[72] MCDI operates cyclically, producing desalinated water intermittently. In contrast, other desalination technologies such as RO and ED yield a continuous output, simultaneously generating desalinated and concentrated streams. This

distinction in operational dynamics implies that, for example, an ED cell can achieve up to a twofold in water production compared to an MCDI cell within the same operational timeframe, given that the desalination conditions such as feed water concentration and concentration reduction are identical. To produce the same amount of desalinated water as ED, the MCDI stack size has to be increased by increasing the number of MCDI cells. However, it is crucial to acknowledge that increasing MCDI stack size comes at the expense of increased capital costs, presenting a challenge in balancing productivity gains against economic considerations.

1.6. pH changes in MCDI and its influence on mineral scaling and ion-selectivity

pH changes in MCDI

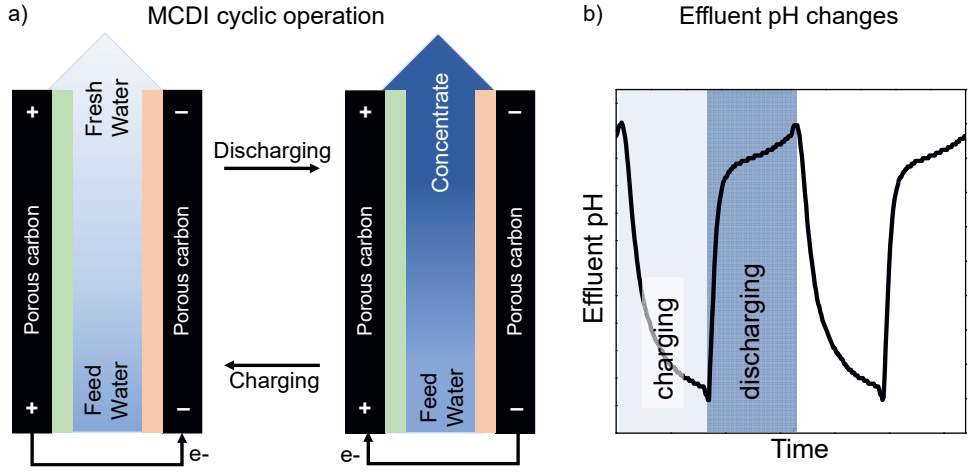

Figure 1.4. Cyclic operation of MCDI (a) and effluent pH changes during operation (b)

During the cyclic operation of MCDI, the effluent pH changes from feed water pH during charging and discharging, see figure 1.4. The effluent pH increases or decreases during charging or discharging and is also based on the water composition. In the literature, studies related to pH changes often identified faradaic reactions that are taking place at the electrodes as the

cause.[73,74] In MCDI, these faradaic reactions are undesired, resulting in a reduction of the efficiency.

Influence of pH changes on mineral scaling

Numerous factors contribute to mineral scaling in electrochemical desalination technologies; however, the concentration of hardness ions and solution pH stand out as primary factors in MCDI.[75,76] In the context of MCDI, the discharge phase is particularly prone to mineral scaling, as the concentration of hardness ions in the concentrate increases especially at higher water recovery levels (>50%), where an associated increase in pH within the concentrate can trigger the precipitation of hardness ions, thereby causing mineral scaling. It is known that MCDI systems are prone to mineral scaling when treating real brackish water which contains many other salts in addition to NaCl. To mitigate and control mineral scaling in MCDI, better understanding about pH changes in the spacer and strategies to control the changes are important research directions.

Influence of pH changes on ion-selectivity

During MCDI operation, pH changes are observed at the boundaries of the electrodes and membranes. While pH changes in the spacer have a direct impact on mineral scaling, those occurring within the electrode compartments have an influence on ion adsorption.

Chemical surface modification of carbon electrodes is a strategy to develop ion selectivity of the electrodes. The protonation or deprotonation of those groups is based upon both their pKa values and the localized pH environment. This protonation-deprotonation equilibrium defines the charge of these chemical groups. For instance, carboxylic acid groups, possessing a pKa value of ~3, exist in their deprotonated form (COO^-) above their pKa making them capable of adsorbing cations.[54] Similarly, amine-containing chemical groups often exhibit pKa values above 8, existing in a protonated form (example, NH_4^+) at pH levels below their respective pKa, facilitating the adsorption of anions.[54] Thus, the local pH at the electrodes plays a crucial role

in influencing the chemical properties of surface groups, thereby impacting their adsorption capacity and selectivity towards ions.

Furthermore, the local pH at the electrodes also impacts the speciation of amphoteric ions. For instance, the speciation of dissolved CO_2 (i.e., H_2CO_3, HCO_3^-, CO_3^{2-}) in water is affected by the local pH.[77] These distinct valences play an important role during electrostatic adsorption processes. By leveraging the pH-specific speciation of dissolved CO_2, electrochemical desalination technologies can capture CO_2.[78] Analogously, the design of MCDI cells is optimized to maintain an optimal pH at the cathode, facilitating the removal of boric acid in the form of borate ions.[71]

1.7. Scope and thesis outline

The demand for clean water and the need for recovery and reuse of valuable resources in (waste)water, essential for enabling a sustainable and circular society, underscores the need for technological advancements in water treatment. Electrochemical desalination technologies, particularly MCDI, exhibit significant potential in water treatment processes, manifesting a dual capability of generating fresh water and selectively extracting minerals from water. In order to utilise the full potential of MCDI, there is a need for dedicated research and development efforts targeting prevailing challenges, including mineral scaling, lower water productivity, and ion-selective salt removal. Given that pH changes in MCDI are a common factor influencing these challenges, this thesis focuses on developing pH changes during MCDI operation. The insights gained in pH changes are subsequently harnessed to effectively address the previously mentioned challenges of MCDI.

Chapter 2 discusses the investigation of pH changes in MCDI during long-term operation with aged electrodes using two different feed water solutions: a NaCl solution and tap water. The pH changes at the effluent during the cyclic charging and discharging of electrodes are investigated. To reveal the effect of long-term MCDI operation under practical operational voltages, pH studies are carried out with aged electrodes and lower operational voltages

(<1.2 V). Between faradaic processes and non-faradaic processes, the type of process that causes pH changes during long-term MCDI operation is identified. The pH changes between synthetic single salt water (NaCl feed water) and real water (tap water) are studied which shows the difference in behaviour between these different feed waters, and the factor causing the difference in pH changes is attributed to the presence of HCO_3^- and CO_3^{2-} ions in tap water.

Chapter 3 discusses how a change in dissolved inorganic carbon (H_2CO_3, HCO_3^-, CO_3^{2-}) during MCDI operation results in pH changes at the effluent, specifically showing the adsorption and desorption of HCO_3^- ions and the distribution of other DIC species during charging and discharging. This chapter further discusses mineral scaling in MCDI systems which is a consequence of pH changes. It is revealed that the desalination of tap water or synthetic water with hardness ions under higher water recovery conditions increases mineral scaling. To mitigate mineral scaling, a strategy is developed which can reduce anti-scaling agent consumption and enhance system stability.

Chapter 4 discusses a comprehensive examination of pH dynamics within different compartments of an MCDI cell, namely, at the effluent, in the cathode, and in the anode during NaCl desalination. An ultra-micro pH sensor with precise positioning capabilities near the electrodes is used to record pH changes under both non-faradaic and faradaic conditions. By comparing the results with existing theoretical and experimental studies, the chapter offers valuable insights into the observed pH variations across various compartments of the MCDI cell. The findings provide essential understanding for optimizing mineral scaling, facilitating the removal of pH-sensitive compounds such as boric acid, and to utilize the benefits of pH sensitive chemical groups to modify electrodes in MCDI applications.

Chapter 5 discusses an innovative design of an (M)CDI cell, different from the conventional MCDI cell design. Building on the concept proposed by Smith and Dmello in 2016, wherein two cation-selective electrodes prepared

using chemical modification of carbon electrodes and a single AEM were employed, this chapter extends the idea by introducing anion-selective electrodes prepared by modifying carbon with pH sensitive amine groups and with a single CEM. The experimental data are verified with theoretical predictions, and the energy consumption of the new cell design is compared with a conventional MCDI system. The novel cell design also leads to a continuous CDI desalination system with a twofold increase in productivity compared to conventional MCDI.

Chapter 6 discusses the understandings gained from this thesis on pH changes in MCDI systems, strategy for mitigating mineral scaling, possible new cell designs and their implications on improving the MCDI technology. It explores the advantages of understanding gained on the mechanisms of pH changes to limit mineral scaling and the volume of cleaning chemicals needed, aiming towards sustainable operation and enhanced efficiency during long-term desalination processes. It also discusses near-electrode pH changes and their potential utilization in targeted ion removal, continuous desalination system and its economic benefit. Finally, it highlights future perspectives, emphasizing the need to explore the role of amphoteric ions and AEMs in influencing effluent pH in order to develop more optimized strategies to limit mineral scaling, and to improve targeted removal of amphoteric ions.

Chapter 2. Unravelling pH changes during desalination with capacitive deionization

This chapter was published as:

Arulrajan, A. C., Dykstra, J. E., van der Wal, A. & Porada, S. Unravelling pH Changes in Electrochemical Desalination with Capacitive Deionization. *Environ. Sci. Technol.* **55**, acs.est.1c04479 (2021).

Abstract

Membrane Capacitive Deionization (MCDI) is a water desalination technology employing porous electrodes and ion exchange membranes. The electrodes are cyclically charged to adsorb ions and discharged to desorb ions. During MCDI operation, a difference in pH between feed and effluent water is observed, changing over time, which can cause the precipitation of hardness ions, and consequently affect the long-term stability of electrodes and membranes. These changes can be attributed to different phenomena, which can be divided in two distinct categories: faradaic and non-faradaic. In the present work we show that, during long-term operation, as the electrodes age over time, the magnitude and direction of pH changes shifts. We studied these changes for two different feed water solutions: a NaCl solution, and a tap water solution. Whereas we observe a pH decrease during regeneration of experiments conducted with a NaCl solution, we observe an increase during regeneration with tap water, potentially resulting in the precipitation of hardness ions. We compare our experimental findings with theory, and conclude that, with aged electrodes, non-faradaic processes are the prominent cause of pH changes. Furthermore, we find that, for desalination with tap water, the adsorption and desorption of HCO_3^- and CO_3^{2-} ions affects the pH changes.

2.1. Introduction

Increasing demand for surface water and ground water has resulted in water stress and scarcity in many countries.[4] To overcome water scarcity, technologies can be employed to produce potable water from brackish or saline sources.[79] Capacitive deionization (CDI) is one such technology for water desalination employing porous electrodes, which are cyclically charged and discharged. In conventional CDI, during charging, ions are adsorbed in electrical double layers (EDLs) in the micropores of the porous electrodes, and feed water is desalinated. During discharge, ions are desorbed, resulting in a concentrated effluent stream.[37,38]

Although CDI is a promising technology for brackish water desalination, stable long-term operation remains a challenge.[37,80] In addition to capacitive ion storage in EDLs, undesirable faradaic processes also occur.[73,81] These faradaic processes are considered to be the main reason for a decrease in desalination performance over time. Furthermore, these processes can cause pH changes during desalination,[66,82,83] which can result in the precipitation of salt when hardness ions (Mg^{2+}, Ca^{2+}, Fe^{2+}/Fe^{3+}) and carbonate ions (HCO_3^- and CO_3^{2-}) are present in solution, and consequently affect the desalination performance and long-term stability of the CDI cell.[66,82,83] Non-faradaic processes, including different ion mobilities, acid-base reactions between ionic species, and the protonation or deprotonation of chemical surface groups present on the electrode material, can also result in pH changes during CDI operation.[84]

Several possible faradaic reactions that can occur, either at the anode or cathode, have been studied to identify the mechanisms resulting in pH changes and CDI performance stability issues. While at the anode, reactions such as carbon, chloride, and water oxidation are mostly considered, at the cathode, the reduction of dissolved oxygen and water are relevant.[73,81,85,86] Among these reactions, carbon oxidation and dissolved oxygen reduction have been shown to significantly destabilize the desalination performance. At the anode, carbon oxidation results in the formation of oxygen containing

chemical groups. The direct consequence of these oxygenated surface groups is the occurrence of "inversion peaks" during operation which lowers the desalination efficiency by enhanced co-ion expulsion from the electrodes.[87] At the cathode, oxygen reduction has experimentally been confirmed by measuring the dissolved oxygen and hydrogen peroxide concentration changes in the effluent water during CDI operation.[88] Other faradaic processes that can occur during operation are chloride oxidation (formation of Cl_2 gas) at the anode, and water reduction (formation of H_2 gas) at the cathode. Formed Cl_2 gas can immediately dissociate in water to form HOCl, resulting in a decreased effluent pH.[73] Faradaic reactions related to carbon oxidation occur mainly on pristine electrodes, which are electrodes that have only been used for a limited number of cycles before the study was conducted.[80]

In order to mitigate negative effects of faradaic processes in CDI, three main strategies have been proposed. Firstly, different operational modes have been investigated to limit the cell voltage, to optimize the operational voltage window,[89–91] or to invert the cell voltage applied during charging and

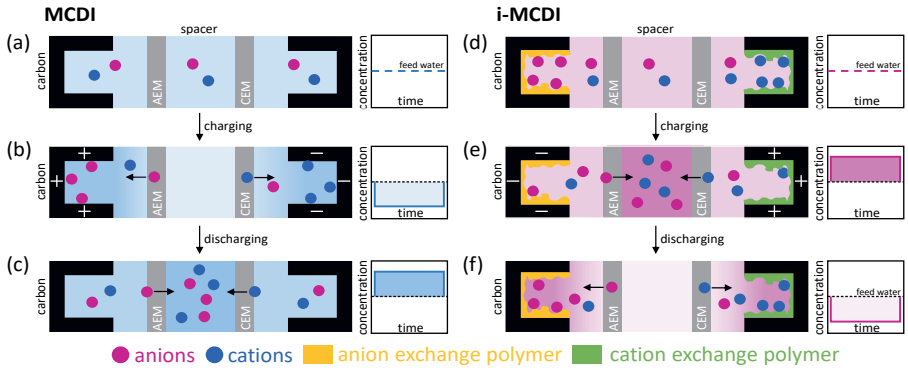

Figure 2.1. MCDI (a-c) and i-MCDI (d-f) for cyclic water desalination. In MCDI, water is desalinated during charging (b), and the electrodes are regenerated during discharge (c). In i-MCDI, the electrodes are modified with ion-exchange polymers which are located in the carbon pores, resulting in high counterion concentrations in the electrodes in uncharged state (d). During charging, these ions are expelled from the electrode compartments, and a concentrated salt solution (concentrate) is produced (e). During discharge, water is desalinated (f).

discharge.[92,93] Secondly, alternative CDI cell designs are considered, either by applying different flow patterns (i.e., flow by/flow through)[90,91] or by placing ion exchange membranes between the spacer channels and the porous electrodes, a cell design we refer to as membrane capacitive deionization.[94–96] Thirdly, electrode modifications, such as titania deposition on carbon to prevent carbon oxidation, have been proposed.[97,98]

One of the most effective strategies to keep a high desalination performance is the inclusion of ion-exchange membranes in the CDI cell, a cell design we refer to as membrane CDI (MCDI). These ion exchange membranes are placed in front of the electrodes, and contribute to maintaining the desalination performance in two ways: the membranes effectively slow down the transport of dissolved oxygen to the electrodes, and consequently limit the rate of carbon oxidation and the related pH changes.[99,100] However, during long-term operation, dissolved oxygen will eventually oxidize the electrically positively polarized electrode (anode), and oxygen containing surface groups will form.[95,101] Whereas these groups would have negatively affected the desalination performance in CDI (without membranes) due to enhanced co-ion expulsion during desalination, in MCDI the desalination performance does not decline, because ion exchange membranes prevent co-ions from leaving the electrode region.[95,101] Furthermore, faradaic reactions during MCDI operation were also confirmed in our previous work by microscopic physics-based modelling of pH changes.[84] This study predicted only minor pH changes during desalination in MCDI when non-faradaic processes, including the effect of different mobilities of various ions on transport rates, combined with acid-base reactions, and the presence of chemical surface groups in the micropores are taken into account. In order to match theoretical predictions of pH changes with experimental data, this study concluded that faradaic reactions in the micropores must be considered.[84]

MCDI has successfully been applied in industry and systems have been running for many consecutive cycles.[102] In these systems, pH changes are still observed, and although these changes do not directly affect the salt adsorption performance, they can still be problematic.

Experimentally and theoretically, many studies have reported a pH decrease during desorption if the feed water only contains sodium chloride. However, present work shows that with real brackish water (tap water), which contains a mixture of different ions, a pH increase is observed during desorption. This pH increase during desorption is problematic, especially when we operate at high water recoveries, resulting in high salt concentrations in the spacer channel during desorption. These conditions, with high salt concentrations combined with high pH values, can lead to precipitation of salts like calcium carbonate (scaling) on membranes or other components of the CDI cell. Furthermore, if the aim is to remove amphoteric ions, which are ions that can protonate and deprotonate based on solution pH, such as phosphate, ammonium, carbonate and boron, the local pH affects the charge of the ion and thus the removal performance.

To improve our understanding of these pH fluctuations, we conducted experiments with aged electrodes. These aged electrodes have been used in MCDI for more than 2000 desalination cycles, and are therefore (partly) oxidized. Furthermore, we conduct experiments both with a NaCl solution and with tap water, and we perform experiments with different water recoveries, to be close to practical desalination conditions. We study these fluctuations in conventional MCDI operation, and in inverted MCDI (i-MCDI) operation. In i-MCDI, electrodes are chemically modified: we synthesized an electrode with positive chemical groups and an electrode with negative chemical groups. A cation exchange membrane (CEM) was placed in front of the electrode modified with negative chemical groups and an anion exchange membrane (AEM) was placed in front of the electrode modified with positive chemical groups. Fritz et.al., (2019) demonstrated that this configuration can be successfully employed for water desalination, and that water is desalinated during discharge (adsorption), and that a concentrated effluent stream (desorption) is produced during charging.[103]

This study reports pH fluctuations with aged electrodes in MCDI and i-MCDI operation, at different water recoveries. Furthermore, we compare our experimental findings of the NaCl experiments with theory that only includes

non-faradaic processes, and we find that the theory describes the trends of the experimental data well.

2.2. Materials and Methods

2.2.1. Electrode modification and desalination experiments

Desalination experiments were conducted using an MCDI and an i-MCDI stack. The MCDI stack consisted of two cells, each with two activated carbon electrodes (PACMM^{TM} 203, $\delta_e \sim 250$ μm, Materials and Methods, Irvine, CA, USA) two ion exchange membranes (IEMs) and a nylon spacer for an evenly distributed water flow. A cation exchange membrane (CEM, Neosepta CMX, ASTOM Corporation, Tokyo, Japan) was placed in front of one electrode, and an anion exchange membrane (AEM, Neosepta AMX, ASTOM Corporation, Tokyo, Japan) was placed in front of the other, and a nylon spacer was placed between the membranes. The i-MCDI stack consisted of two cells with chemically modified electrodes, which were activated carbon electrodes modified with ion exchange polymers. Anion exchange polymer modified electrodes (AEPE) were prepared by immersing activated carbon electrodes in an ionomer solution (FAS solution, 24 wt% of polymer dissolved in N-Methyl-2-Pyrrolidone (NMP); Fumatech, Bietigheim-Bissingen, Germany) that was diluted six times using NMP. Immersed electrodes were then placed inside a vacuum chamber for 30 min and then dried for 24 hr at 100 °C. Similarly, the cation exchange polymer modified electrodes (CEPE) were prepared by immersing the activated carbon electrode in a six times diluted (using NMP) ionomer solution (FKS solution, 16 wt% of polymer dissolved in NMP; Fumatech, Bietigheim-Bissingen, Germany). After modification, the electrodes were washed with ultrapure water before placement in the i-MCDI stack. The i-MCDI stack consisted of two cells, each with an AEPE and a CEPE. In front of each CEPE electrode a CEM was placed, and in front of each AEPE an AEM, and a nylon spacer was placed between the CEM and AEM. Graphite sheets were used as current collectors to electrically connect the porous carbon electrodes with the external electrical circuit, which connects the stack to a potentiostat (Iviumstat, Ivium Technologies, The Netherlands).

All desalination experiments were conducted using aged electrodes and NaCl solutions prepared using ultrapure water (resistivity of 18.2 Ω.cm at 25ºC) or tap water. The electrodes were aged by charging and discharging the MCDI stack for more than 2000 and the i-MCDI stack for more than 3000 desalination cycles using constant current operational mode with a fixed current density (11.1 A/m^2), and a 5 mM NaCl solution, which was constantly purged with compressed air, was pumped through the MCDI or i-MCDI stack at 12.5 ml/min flow rate (effluent pH changes during aging processes of an MCDI stack are shown in figure S2.1. After the aging process, to compare experimental data with theoretical calculation, desalination experiments were conducted with 5 and 20 mM NaCl solutions which were purged with N_2. Thereafter, further desalination experiments were conducted, either with a 5 mM NaCl solution purged with air, or with tap water (not purged with air, neither with N_2), for 80-100 desalination cycles. All desalination experiments were conducted in constant current operational mode with same current density and flow rate used during aging process. Desalination experiments were conducted for different values of water recovery. To increase water recovery, the flow rate during desorption was reduced. During desalination experiments with NaCl solution, the feed water was pumped from a 50 L tank which was purged with compressed air to the MCDI or i-MCDI stack and the effluent water was recycled to the same tank. In the tap water experiments, the feed water was pumped from a 20 L tank to the MCDI or i-MCDI stacks and the effluent water was not recycled. The tap water feed tank was constantly refilled to maintain the water level. During desalination experiments the feed water pH was continuously measured using a pH sensor connected to the stack inlet. Similarly, the effluent pH and conductivity were continuously measured.

For the desalination experiments conducted with a NaCl solution, the salt concentration was calculated from the measured conductivity using a calibration curve. For the tap water experiments, in addition to the online conductivity and pH measurements, the effluent water during adsorption and desorption (from the last 3 cycles of each experiment) were collected separately and the pH was measured immediately after sampling. Also, the

concentrations of cations (Na^+, K^+, Ca^{2+} and Mg^{2+}) and anions (Cl^-, NO_3^-, PO_4^{3-} and SO_4^{2-}) present in the samples were analyzed using inductively coupled plasma-optical emission spectroscopy (ICP-OES, Optima 5300 DV, Perkin Elmer) and ion-chromatography (IC, Dionex Aquion, Thermo scientific) which are shown in Table S1.1 in the Annex A. The concentration of dissolved inorganic carbon (DIC) i.e., the total concentration of the ionic species H_2CO_3, HCO_3^- and CO_3^{2-}, and the effluent pH (during adsorption and desorption) were calculated using Visual MINTEQ 3.1 software, as discussed in the next section.

2.2.2. pH and ionic speciation calculations using Visual MINTEQ

Visual MINTEQ 3.1 is a software tool that uses a chemical equilibrium model to calculate, in water, the ionic speciation, the solubility, and several parameters related to the water chemistry, including pH and DIC, which are calculated based on charge and mass balances of the different (ionic) species in solution. In our study, we used MINTEQ to calculate the pH and DIC of water samples by including the experimentally determined concentrations of all other ions from ICP-OES and IC analysis (Annex A, Table S2.1). Furthermore, we specify the partial CO_2 gas pressure in air, which is in equilibrium with the aqueous phase. With these inputs, the pH, the total concentration of DIC, and the speciation thereof (concentrations of H_2CO_3, HCO_3^- and CO_3^{2-}), were calculated by MINTEQ, for tap water, and for effluent water during adsorption and desorption.

2.3. Results and discussion

2.3.1. Comparing data and theory: desalinating a NaCl solution

Desalination experiments were conducted using an MCDI stack with aged electrodes and a N_2 purged NaCl solution for 100 desalination cycles. With aged electrodes, the average concentration reduction during a desalination step, Δc, and charge efficiency, were stable for all 100 cycles (see annex.

figure S2.2). During the adsorption step, the effluent pH is higher than the feed pH, whereas during desorption, the effluent pH is lower than the feed pH, see figure 2.2. We compare experimentally observed and theoretically predicted effluent pH changes by employing the theoretical framework as described in previous work,[84] which considers the effect of non-faradaic phenomena, including the effect of different diffusion coefficients of the ions present in solution, and the presence of chemical surface groups.[84] The theoretical pH changes are calculated for a feed solution with a NaCl concentration of 20 mM, whereas the experiments were performed with feed concentrations of 5 mM and 20 mM. Interestingly, we observe, considering the trend, a good description of the effluent pH changes by theory, i.e., we observe a pH increase during adsorption and a pH decrease during desorption. The dynamics of experimentally observed pH changes with a 5 mM NaCl solution, both for a solution purged with N_2 (figure 2.2a) and with air

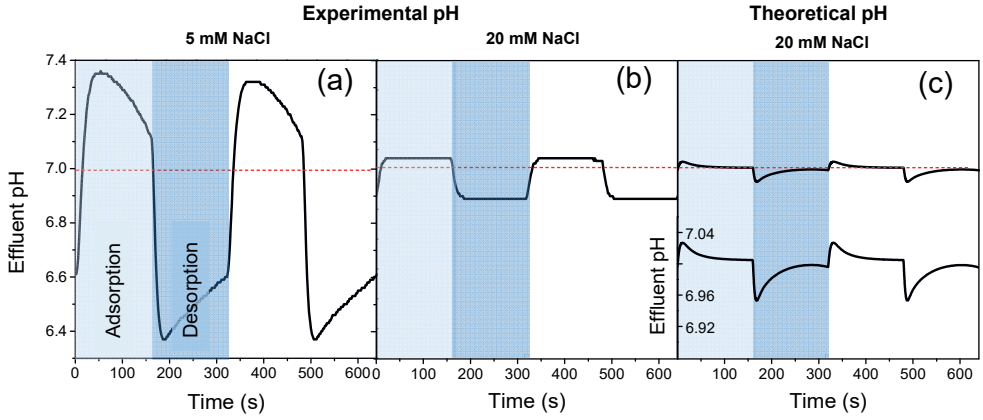

Figure 2.2. Experimentally observed effluent pH (a and b) and theoretically calculated effluent pH (c) for MCDI in a N2 purged NaCl solution. The inset in panel c shows the theoretically calculated zoomed effluent pH change.

(figure 2.3a), are similar to the theoretically calculated pH changes for a 20 mM NaCl solution, but the magnitude of the experimentally observed pH changes is larger than predicted by theory. For the 20 mM NaCl feed solution, the magnitude of experimentally observed pH changes is similar to the theoretical predictions for the adsorption step, whereas, for desorption step, the magnitude is slightly larger than predicted by theory. But, the dynamics

are not similar to the predictions, which could possibly be explained by the limited sensitivity of the pH sensor (<0.1 pH unit). Clearly, the theory, which only includes non-faradaic phenomena, such as the effect of different diffusion coefficients of the ionic species present in solution, describes the data well compared to our previous study where the theory could not describe pH data well.[84] In our previous study, we compared theory with experiments conducted with pristine electrodes, and we concluded that faradaic phenomena must be considered to explain the experimental data. In the present work, however, we used aged electrodes, and the agreement of theory with data indicates that, with aged electrodes, non-faradaic phenomena are the prominent cause of pH changes.

2.3.2. Effluent pH changes with MCDI and i-MCDI

Furthermore, we studied pH changes with an air purged NaCl containing solution and with tap water (see Table S2.1 for exact composition of the tap water). The pH of the NaCl solution purged with air is reduced to 5.6 as CO_2 from air dissolves in water, resulting in the formation of carbonic acid (H_2CO_3) which then dissociates into protons, bicarbonate and carbonate ions. The pH of tap water is 7.72 due to the presence of carbonate and bicarbonate ions in the solution. The sum of the concentrations of hardness ions, i.e., calcium and magnesium, and of bicarbonate/carbonate ions present in the tap

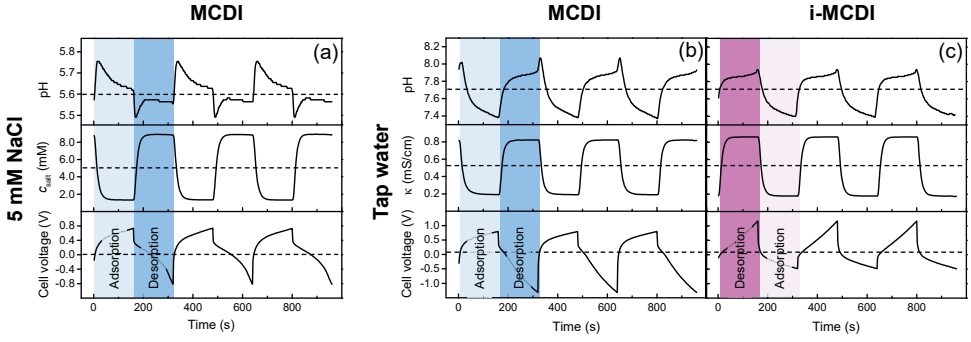

Figure 2.3. Cell voltage, effluent concentration (or conductivity in case of tap water), and effluent pH changes of MCDI experiments with a NaCl solution (a) and with tap water (b), and i-MCDI experiments with tap water (c) after reaching dynamic steady state.

water studied in this work, is in the range of moderately hard water. The desalination experiments were done for 80-100 cycles to reach dynamic steady state, which means that the cell voltage, salt adsorption and effluent pH of a particular cycle are the same as of the previous cycle (see figure S2.3 for averaged pH and peak cell voltage for 80-100 cycles). These results are shown in figure 2.3a and 2.3b. Interestingly, for the MCDI experiments conducted with tap water, the pH changes are reversed compared to the case of NaCl, i.e., the pH value decreases during adsorption and increases during desorption (figure 2.3b). As the observed pH increase during desorption with tap water can result in scaling, strategies have to be developed and explored to invert these changes. To that end, tap water desalination experiments were conducted with an inverted-MCDI (i-MCDI) stack. Figure 2.3c, shows that

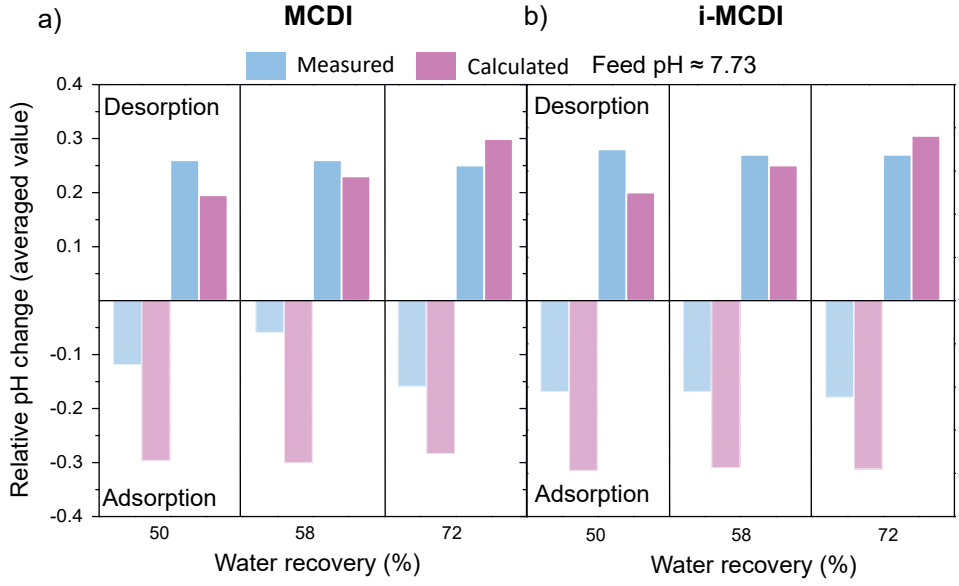

Figure 2.4. Comparison between experimentally measured and theoretically calculated effluent pH changes in MCDI and i-MCDI during tap water desalination.

the effluent pH changes observed in i-MCDI are, for tap water desalination, similar to that of MCDI: the effluent pH decreased during adsorption and

increased during desorption. This finding suggests that the pH changes in tap water are independent of cell operation during adsorption and desorption. s

After steady state is reached in tap water desalination experiments, the effluent water during adsorption and desorption is collected (after 90 desalination cycles) and the pH and ionic concentrations are measured (composition is reported in Table S2.3 and S2.4 in Annex A). Table S3 and S4 show that, during tap water desalination, the HCO_3^- ion is the dominantly adsorbed anion while Na^+ is the dominantly adsorbed cation. Since the HCO_3^- ion is an amphoteric ion (i.e., an ion which can act both as acid and base), which is in local chemical equilibrium with dissolved CO_2, any change in the concentration can result in a local shift of acid-base equilibria, which can affect the pH. This finding further supports the argument that, for tap water desalination, pH changes are mainly due to the adsorption and desorption of HCO_3^- ions during operation.

In figure 2.4, we compare the experimentally measured relative effluent pH change for tap water desalination during adsorption and desorption with calculated pH values using Visual MINTEQ 3.1. The calculated pH follows a similar trend as the measured pH, i.e., the effluent pH decreases during adsorption and increases during desorption. The calculated values are based on the experimentally determined ionic composition of the water collected during adsorption and desorption, and MINTEQ adjusted the concentration of DIC to maintain the charge and mass balance. Though there is a difference between measured pH and calculated pH at different water recovery conditions, the direction of pH changes is in agreement. This shows that the pH changes observed during tap water desalination are due to a change in the concentration of DIC (mainly HCO_3^- ions, considering the pH and composition of the analyzed water) during adsorption and desorption. The preferential adsorption of HCO_3^- ions during tap water desalination could mainly be due its high concentration over other anions present in the tap water.

2.3.3. Effect of HCO_3^- ion concentration on effluent pH changes

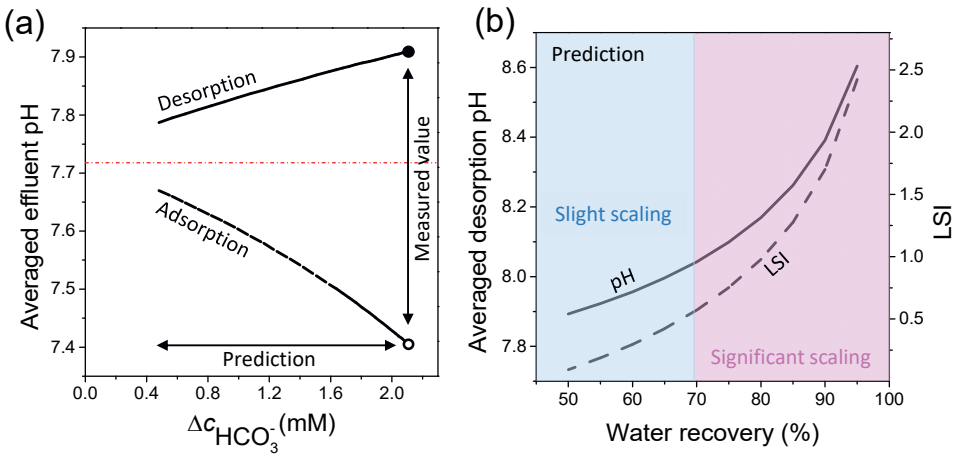

Figure 2.5. (a) Effluent pH prediction as function of bicarbonate ion removal ($\Delta cHCO_3^-$), (b) Prediction of effluent pH during desorption for different water recoveries, (c) Prediction of Langelier saturation index (LSI) as function of the water recovery.

In order to obtain more insight into the effect of DIC on the effluent pH, we have performed an analysis where we changed the concentration reduction of HCO_3^- ($\Delta c_{HCO_3^-}$) during the desalination step, see figure 2.5a. For this analysis, we used the ionic composition of the water during adsorption and desorption of the 50% water recovery experiment (Annex A, Table S2.3). In order to maintain the charge balance, we adjusted the concentration of Na^+ ions accordingly. Fig 2.5a shows that the pH changes are dependent on $\Delta c_{HCO_3^-}$, and that an increased removal of HCO_3^- ions during the adsorption step results in more pronounced pH changes.

Next, we predicted the scaling potential as function of the water recovery. To do this, we calculated the pH of the water collected during desorption using Visual Minteq software for the 50% water recovery experiment, based on the measured ionic composition. To calculate the pH of the effluent water during desorption at higher water recoveries, the ionic composition of the solution

was calculated by decreasing the volume during desorption, while maintaining the total amount of ions desorbed during discharge. Using these calculated ionic compositions, the pH of water during desorption is predicted using Minteq, as well as the Langelier Saturation Index (LSI). The LSI is a measure to express the scaling potential based on pH, total dissolved solids (TDS), alkalinity and the concentration of Ca^{2+} ions. Figure 2.5b shows that, for water recoveries higher than 70%, we observe a significant scaling potential (LSI > 0.5), and the scaling potential increases with water recovery.

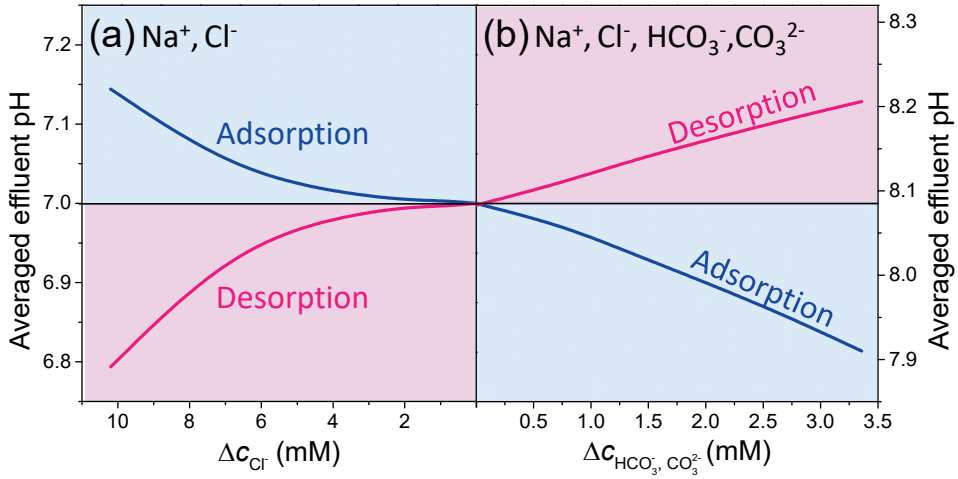

Figure 2.6. (a) Effluent pH calculated for different values of the concentration reduction of NaCl (i.e., Δc_{Cl^-}) (b) Prediction of the effluent pH at fixed concentration reduction ($\Delta c = 3.45$ mM) with different concentration reduction of carbonate species ($\Delta c_{HCO_3^-,CO_3^{2-}}$) over Cl^-.

As shown in figure 2.5a, during tap water desalination, pH changes are mainly caused by the adsorption and desorption of carbonate species. If carbonate species are not present, however, pH changes are attributed to the effect of the difference in mobilities of Na^+, Cl^-, H^+, and OH^- ions on individual ion transport rates. These two different phenomena result in the inversion of the direction of pH changes experimentally observed (figure 2.3a and b). To get more insight, we have calculated the average effluent pH change for a 20 mM NaCl solution based on the theory as previously described, and also for an artificial water solution with a total concentration of salts equal of 20 mM, with equimolar concentrations of NaCl and $NaHCO_3$,

using Visual Minteq 3.1. Figure 2.6a shows the calculated pH changes for a NaCl solution as function of the concentration reduction of NaCl during desalination, Δc_{Cl}, whereas in figure 2.6b we show pH changes for the case of overall $\Delta c = 3.45$ mM, but here the ratio between the adsorption of Cl^- and HCO_3^-/CO_3^{2-} is varied. Figure 2.6 clearly shows that the direction of the average pH changes during adsorption and regeneration are exactly opposite for these two cases. Increasing Δc_{Cl^-} results in more notable pH changes, with an average pH above the feed water pH during the adsorption step, and below during the desorption step. For the case of artificial tap water, pH changes become more notable with increasing adsorption of carbonate species (HCO_3^-, CO_3^{2-}), resulting in a pH decrease during adsorption and increase during desorption. This result highlights the importance to study pH changes in practical desalination conditions and the need control effluent pH changes, for example by reducing HCO_3^- adsorption, in order to mitigate scaling problems.

2.4. Conclusion

In conclusion, we studied pH changes in MCDI and i-MCDI using aged electrodes, with a NaCl solution and with tap water. When dynamic steady state is reached, the observed effluent pH does not significantly change during desalination. The trend of these pH changes with a NaCl feed water purged with N_2 is in agreement with our theory that only considers the differences in diffusion coefficients of the ions, which indicates that non-faradaic processes are the main cause of pH changes with aged electrodes in MCDI. This finding is significantly different from the existing understanding that faradaic processes are the major cause of pH changes in MCDI. In addition, we showed that pH changes observed for tap water desalination show different dynamics than for NaCl: the effluent pH increases during desorption. We explain this inversion of the direction by the adsorption of bicarbonate ions (HCO_3^-) during desalination, and by the desorption during regeneration. This study also shows that aged electrodes are preferable to be used to study pH changes in CDI.

Annex A

Table S2.1. Concentrations of various ions in tap water and effluent water during adsorption and desorption of tap water desalination using MCDI and i-MCDI operation at 50% water recovery conditions. Cations were quantified using ICP-OES and anions were quantified using IC. The concentrations of ions in effluent water during adsorption and desorption are average of three measurements from three different samples collected from three adsorption and desorption steps.

*All values are reported in mg/l

Ions	Tap water (Feed)	MCDI (50% WR)		i-MCDI (50% WR)	
		Adsorption	Desorption	Adsorption	Desorption
Na^+	72.50	36.77	111.40	34.44	112.67
K^+	2.46	0.82	3.68	0.89	3.92
Ca^{2+}	25.80	7.48	45.65	8.40	48.07
Mg^{2+}	8.94	2.53	14.69	2.84	15.40
Cl^-	35.60	8.87	60.80	8.60	59.40
NO_3^-	11.00	2.73	18.13	2.90	18.80

Table S2.2. Diffusion coefficients of ions used in theory to calculate effluent pH changes during desalination of NaCl solution purged with N_2, using MCDI. Diffusion coefficients in 5 mM solution are increased 10 times to increase mixing of ions in the spacer channel during calculations.

Ions	Diffusion coefficient (D_i)
Na^+	$1.33 \cdot 10^{-9}$ m^2/s
Cl^-	$2.02 \cdot 10^{-9}$ m^2/s
H^+	$9.13 \cdot 10^{-9}$ m^2/s
OH^-	$5.16 \cdot 10^{-9}$ m^2/s

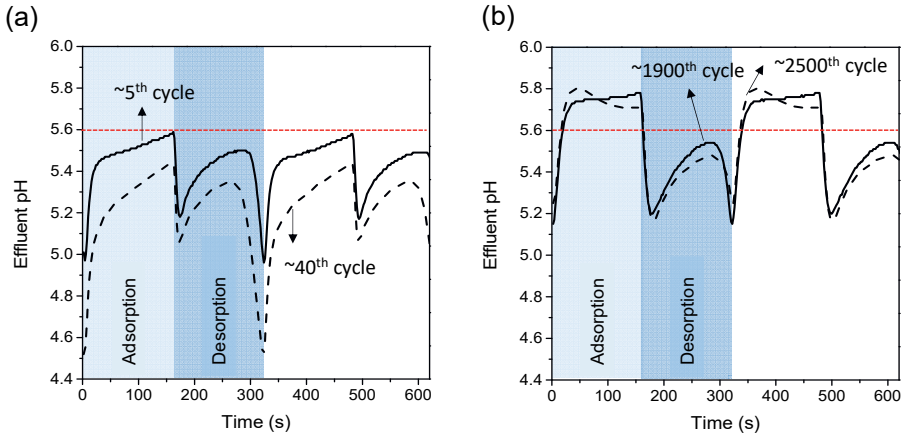

Figure S2.1. Aging of MCDI electrodes in air purged 5 mM NaCl solution. Aging process is conducted until there is no change in the dynamics of pH changes observed (ca. 2500 desalination cycles). Early desalination cycles had significantly different pH changes (a) compared to desalination cycles after~1800 cycles (b).

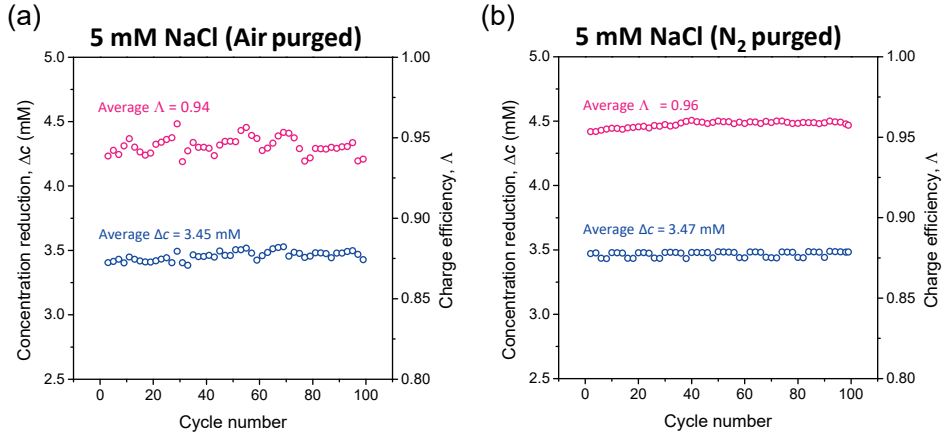

Figure S2.2. Concentration reduction and charge efficiency of aged electrodes in air purged NaCl solution and in nitrogen purged NaCl solution. In both cases, the charge efficiency and the concentration are in (dynamic) steady state.

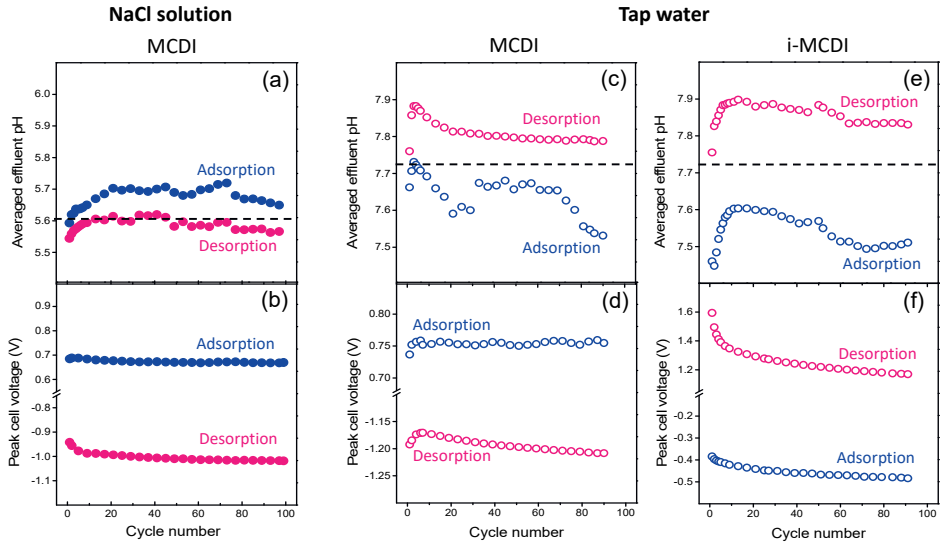

Figure S2.3. Averaged effluent pH (i.e., integrated pH value of each adsorption or desorption step), and peak cell voltage for ~100 desalination cycles of MCDI experiments with an NaCl solution and with tap water, and of i-MCDI experiments with tap water purged with air.

pH and ionic speciation calculations using Visual MINTEQ for tap water desalination

The experimentally measured pH of freshly collected tap water was 7.72. However, when the collected water sample was allowed to equilibrate with atmospheric air for sufficient time (approximately 1 day), the pH increased to 8.6. This pH increase is the result of a new equilibrium established between tap water and atmospheric air, of which the partial CO_2 gas pressure is lower. In order to confirm this, we calculated the pH of tap water, of which we experimentally determined the ionic composition, in Visual MINTEQ 3.1 using two different values for the partial pressure of CO_2. The calculated pH of a solution of which the CO_2 partial pressure is 0.289 mmHg (which is the partial pressure of CO_2 in atmospheric air) was 8.7, which is the same as the experimentally measured pH value of tap water equilibrated with air. The calculated pH decreased to 7.72 (same value as experimentally measured for

fresh tap water) when the CO_2 partial pressure was increased to 3.496 mmHg in the calculation. This observation confirmed that the partial pressure of CO_2 in fresh tap water is higher than the air equilibrated tap water. This increased value of the partial CO_2 pressure is used to calculate the pH of tap water (feed), and effluent water collected during adsorption and desorption.

Table S2.3. Ionic concentrations in feed water and effluent water during adsorption and desorption tap water desalination using MCDI at different water recovery conditions. The concentrations of bicarbonate and carbonate ions are calculated using VISUAL Minteq 3.1 software as mentioned above.

*All values are reported in mg/l

Ions	Tap water	50% WR		58% WR		72% WR	
		Adsorption	Desorption	Adsorption	Desorption	Adsorption	Desorption
Na^+	72.50	36.77	111.40	36.50	124.20	36.50	164.40
K^+	2.46	0.82	3.68	0.81	4.27	1.38	5.70
Ca^{2+}	25.80	7.48	45.65	7.68	51.30	8.62	41.33
Mg^{2+}	8.94	2.53	14.69	2.61	16.70	2.81	21.87
Cl^-	35.60	8.87	60.80	9.41	71.83	9.25	84.67
NO_3^-	11.00	2.73	18.13	2.75	20.25	3.10	27.97
HCO_3^- (calculated)	242.6	115.56	376.30	114.89	415.96	119.4	486.82
CO_3^{2-} (calculated)	0.75	0.16	1.91	0.16	2.33	0.17	3.24

Table S2.4. Ionic concentrations in feed water and effluent water during adsorption and desorption of tap water desalination using i-MCDI at different water recovery conditions. The concentrations of bicarbonate and carbonate ions are calculated using VISUAL Minteq 3.1 software as mentioned in the methods section.

*All values are reported in mg/l

Ions	Tap water	50% WR		58% WR		72% WR	
		Adsorption	Desorption	Adsorption	Desorption	Adsorption	Desorption
Na^+	72.50	34.44	112.67	34.6	126.67	34.40	163.67
K^+	2.46	0.89	3.92	0.85	4.58	0.89	6.16
Ca^{2+}	25.80	8.40	48.07	8.88	54.30	9.68	54.80
Mg^{2+}	8.94	2.84	15.40	2.98	17.57	3.15	22.73
Cl^-	35.60	8.60	59.40	9.10	65.30	10.9	96.30
NO_3^-	11.00	2.90	18.80	3.10	21.70	3.2	27.50
HCO_3^- (calculated)	242.6	114.00	393.27	115.55	443.90	115.14	507.35
CO_3^{2-} (calculated)	0.75	0.16	2.07	0.16	2.66	0.16	3.54

Calculation of Langelier saturation index

LSI for 50% WR is calculated based on the difference between the measured pH during desorption (pH) and the saturation pH (pH_s) of calcium carbonate saturation based on the concentration of Calcium ion and carbonate ion present in the solution. For other water recovery conditions, LSI is calculated as the difference between the predicted effluent pH during desorption and the saturation pH_s.

$$LSI = pH - pH_s$$

The saturation pH_s is calculated based on following formula,

$$pH_s = (9.3 + A + B) - (C + D)$$

where,

$$A = (Log_{10}[TDS] - 1) / 10$$

$$B = -13.12 \times Log_{10}(\text{Temperature in K}) + 34.55$$

$$C = Log_{10}[Ca^{2+} \text{ as } CaCO_3] - 0.4$$

$$D = Log_{10}[\text{alkalinity as } CaCO_3]$$

In LSI calculation for 50% WR, TDS is calculated as the sum of all ionic concentrations measured (all cations and anions including calculated carbonate and bicarbonate ionic concentrations). Temperature is considered to be 296 K. Alkalinity of the effluent during desorption is calculated as the sum of the concentrations of bicarbonate and carbonate ions calculated for 50% WR. For higher water recoveries, the TDS and alkalinity is calculated based on the predicted concentrations of ions.

Chapter 3. Mitigation of mineral scaling in membrane capacitive deionization – understanding the role of pH changes and carbonates

This chapter was published as:

Arulrajan, A. C. *et al.* Mitigation of mineral scaling in membrane capacitive deionization – Understanding the role of pH changes and carbonates. *J. Water Process Eng.* **60**, 105094 (2024).

Abstract

Mineral scaling in water desalination is caused by the precipitation of salts, which is affected by various factors such as the presence of specific ions, solution pH, and temperature. While extensively researched in technologies like reverse osmosis (RO), understanding mineral scaling in membrane capacitive deionization (MCDI) remains limited. During MCDI operation, the pH of the effluent fluctuates, potentially triggering mineral scaling. The present study investigates how the adsorption and desorption of HCO_3^- ions and the distribution of dissolved inorganic carbon (DIC) species (H_2CO_3, HCO_3^-, and CO_3^{2-}) drive pH changes. We examine mineral scaling formation at various water recoveries during MCDI operation using different thicknesses of the anion exchange membrane (AEM). Our findings indicate that pH changes increase with higher water recoveries and that increasing the AEM thickness provides a pathway to enhance MCDI stability, consequently lowering the need for anti-scaling agents.

3.1. Introduction

The Desalination technologies play a vital role in addressing water scarcity issues by producing fresh water, particularly in regions with limited access to natural freshwater sources.[2,4,79] Desalination processes remove salt ions from the source water employing various driving forces such as temperature, pressure, or electrical potential differences.[34,37,104–107]. For instance, in thermal desalination methods like multi-effect distillation (MED), the feed water undergoes vaporization, and upon condensation, purified water is obtained, while the salt is left behind in the concentrate [107,108] Reverse osmosis (RO) and nanofiltration (NF) techniques involve the passage of water through semi-permeable membranes under pressure, separating desalinated water from a concentrated stream rich in salt ions.[51,60,64,104,109,110] In membrane capacitive deionization (MCDI) and electrodialysis (ED), an electrical potential difference is applied to extract salt ions from saline water, generating desalinated water and concentrate.[34,37,111] Despite their differences, all these technologies share a common challenge: the concentration of ions in the concentrate is higher than in the feed water, posing a potential risk of mineral scaling.

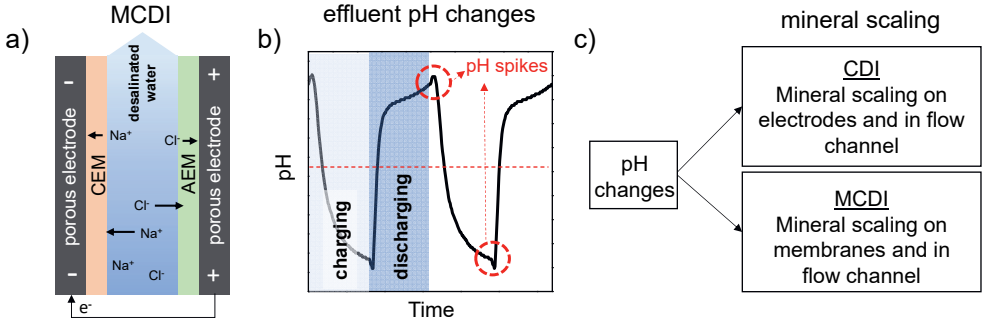

Figure 3.1. (a) MCDI operation during the charging step and (b) the effluent pH during the desalination of a $NaHCO_3$ solution, (c) the impact of pH changes in CDI and MCDI.

In the context of MCDI, various factors influence mineral scaling, including salt solubility limits, ion types, and solution pH.[83,105,108,112] Particularly noteworthy is the impact of hardness ions such as Ca^{2+} and Mg^{2+}, as they tend to precipitate as carbonate, sulfate, or phosphate salts, resulting in mineral

scaling in MCDI systems. Mineral scaling in MCDI can impact long-term salt removal efficiency and energy consumption, leading to increased operational costs and greater reliance on anti-scaling agents.[37,64,74,109,113] Despite numerous strategies proposed to mitigate scaling in conventional desalination methods such as RO and MED, understanding and controlling scaling in MCDI remain limited.[51,112]

An MCDI cell consists of two porous carbon electrodes (an anode and a cathode), two ion-exchange membranes (IEMs) (an anion exchange membrane (AEM) positioned in front of the anode and a cation exchange membrane (CEM) in front of the cathode), and a porous spacer material used to separate the electrodes and facilitate water flow during operation. The MCDI cell is alternatingly charged to adsorb ions, resulting in the production of desalinated water, and discharged to desorb ions, resulting in the production of a concentrate solution (figure 3.1a). Throughout MCDI's cyclic operation, noticeable pH fluctuations are observed in the effluent, as shown figure 3.1b. Notably, the discharge phase yields a higher pH than the feedwater. This pH elevation during discharge triggers mineral scaling, underscoring the importance of understanding the underlying mechanisms behind these pH changes. Such insights are essential for improving the long-term stability of MCDI systems.

Earlier studies of pH fluctuations in MCDI systems postulated that such changes originated from faradaic processes like water splitting, carbon oxidation, and the generation of Cl_2 gas. However, there are also studies indicating theoretically and experimentally that non-faradaic processes, such as water dissociation because of disparities in ion transport rates, can also contribute to pH alterations.[38,84,88,99] As MCDI cells undergo numerous desalination cycles, the electrodes gradually age, diminishing the significance of faradaic reactions like carbon oxidation due to the depletion of available carbon groups for oxidation. Consequently, non-faradaic processes emerge as the primary cause of pH changes. [114]

In the previous chapter, using aged electrodes, we have shown that pH fluctuations in brackish water desalination stem from the adsorption and desorption of bicarbonate ions (HCO_3^-). During charging, HCO_3^- ions are adsorbed, resulting in a decrease in effluent pH. Conversely, discharge results in the desorption of HCO_3^- ions, leading to a rise in effluent pH. When the concentrations of ions such as Ca^{2+} and HCO_3^- increase, mineral scaling may also exacerbate as these ions can precipitate as $CaCO_3$ salt.[114]

Previous studies on mineral scaling in MCDI have clarified that scaling primarily occurs on the membranes and the spacer channel, with minimal impact on the electrode surfaces compared to CDI, where scaling occurs in spacers and electrodes as depicted in figure 3.1c. This is attributed to the IEMs effectively hindering the movement of co-ions. Specifically, the AEM serves as a barrier to the transport of Ca^{2+} and Mg^{2+} ions towards the anode. Meanwhile, anions (HCO_3^-, PO_4^{3-}, and SO_4^{2-}) are hindered by the CEM from transporting towards the cathode, where Ca^{2+} and Mg^{2+} ions are electrosorbed.[66,115] In addition to Ca^{2+} and Mg^{2+}, other ions such as Fe^{2+}/Fe^{3+} and Ba^{2+} can also precipitate, contingent on their concentrations, the presence of different counterions, and the pH of the feed water. Wang et al. examined Fe^{2+} scaling in MCDI, observing Fe^{2+} precipitation on both the AEM, CEM, and the spacer.[115] Despite this advancement, a comprehensive understanding of how changes in pH affect mineral scaling remains an unresolved aspect.

To address the challenges associated with mineral scaling in MCDI, this study systematically conducts desalination experiments using tap water and synthetic water. Effluent pH changes are recorded at various water recovery (WR) levels. These pH changes are elucidated by the removal of HCO_3^- ions and subsequent changes in the distribution of dissolved inorganic carbon (DIC) species. Furthermore, a mitigation strategy is devised to mitigate mineral scaling by adjusting the thickness of the AEM.

3.2. Materials and methods

3.2.1. MCDI stack construction

The MCDI stack consisted of three cells, each comprising two graphitic current collectors, two activated carbon electrodes (PACMM 203, δe ~ 250 μm, Material Methods, Irvine, CA, USA), a cation exchange membrane (CEM), an anion exchange membrane (AEM), and a porous spacer. The CEM (140 μm thick, Neosepta CMX, ASTOM Corporation, Tokyo, Japan) was positioned in front of the cathode, while the AEM (140 μm thick, Neosepta AMX, ASTOM Corporation, Tokyo, Japan) was in front of the anode. A nylon spacer (160 μm thick) was placed between the membranes. The graphite current collectors were situated behind each activated carbon electrode. To augment the thickness of the AEM within the stack, an extra AEM was placed in each cell.

3.2.2. Desalination experiments

Desalination experiments were conducted using three types of feed water: tap water (sourced from Wetsus, Leeuwarden, The Netherlands), synthetic water (prepared by dissolving NaCl, $CaCl_2$, $NaHCO_3$ and $CaCO_3$ salts in deionized water), and a $NaHCO_3$ salt solution (prepared by dissolving $NaHCO_3$ salt in deionized water). Detailed ionic compositions are provided in Table S3.1. Water was circulated through the stack at a rate of 17 ml/min, achieving a productivity (P) of 55 L/h/m^2 at 50% WR. To increase water recovery, the flow rate during discharge was reduced. Experiments were conducted in constant current (CC) mode using an Ivium-n-stat potentiostat (Ivium technologies, The Netherlands) with a current density of 11.1 A/m^2 during charging and reversed current during discharging. The half cycle time was 160 seconds, except for asymmetric experiments (See section 2.2.3). Desalination experiments were performed at various water recovery conditions (WR, the ratio of desalinated water over the total volume of water treated) in single-pass mode (i.e., effluent water was drained). The pressure difference (Δp) between the stack inlet and outlet was continuously monitored using a differential pressure meter (EJA110E, Yokogawa Electric

Corporation, Japan). Effluent pH and conductivity were also continuously recorded with 2-second data intervals using pH and conductivity sensors.

3.2.3. Feed water pH adjustment

In experiments involving tap water, the feed pH was measured at 7.73 ± 0.05. However, in the case of the $NaHCO_3$ solution and synthetic tap water, the initial feed pH was higher than that of tap water and exhibited variability over time due to interactions with atmospheric CO_2. To ensure a consistent comparison of pH changes during MCDI operation across different feed water compositions, we purged the $NaHCO_3$ solution and synthetic water with CO_2 to establish and maintain a stable feedwater pH of 7.73. Once pH=7.73 was attained, it remained relatively stable (7.73 ± 0.03) throughout the experimental duration.

3.2.4. Sample collection and ionic composition analysis

In addition to continuous pH monitoring, we employed two methods for collecting desalinated water and concentrate samples. The first method involved sample collection throughout the entire charging or discharging step (i.e., 160 seconds), while the second method focused specifically on samples collected during the final 50 seconds of the charging or discharging step, representing the steady-state period. Following sample collection, we measured the pH and conductivity of each sample (within approximately 5 minutes). For the determination of cationic and anionic concentrations, we used inductively coupled plasma-optical emission spectroscopy (ICP-OES, Optima 5300 DV, PerkinElmer) and ion chromatography (IC, Dionex Aquion, Thermo Scientific), respectively. The bicarbonate ion concentration was calculated using Aqion software, employing charge and mass balance calculations involving all other measured ions.

3.2.5. Asymmetric desalination experiments

Experiments involving asymmetric desalination conditions, where variations occur between the charging and discharging steps, are conducted. In each

experiment, parameters during the charging step, such as flow rate (17 ml/min for the stack), charging time (160 seconds), and current density (11.1 A/m^2 for the stack), remained constant. However, during the discharging step, only the flow rate remained constant, while the discharging time and current density were adjusted to ensure that the total charge transferred during the discharging step matched that of the charging step. Specific discharge conditions employed in asymmetric experiments are outlined in detail in Table S3.2.

3.2.6. Mineral scaling experiments

Mineral scaling experiments were conducted using two configurations of the MCDI stack: one with a single AEM (Single-AEM MCDI) and the other with double AEM (Double-AEM MCDI), as described in section 2.1. For tap water, scaling experiments were conducted continuously for over 100 hours of operation, while for synthetic water, they were carried out for a duration of 17.8 hours (200 cycles). Throughout the scaling experiments, continuous measurement of the pressure difference (Δp) across the MCDI stack inlet and outlet was performed. Following each experiment, the stack underwent a cleaning process involving the circulation of a 0.1 M HCl solution through the stack until Δp returned to its initial value (+/- 10 mbar). This cleaning procedure, typically lasting 2-4 hours, aimed to remove any scale formation and prepare the cell for subsequent experiments. After acid cleaning, the feed water was pumped through the cell until both the feed pH and effluent pH were equal.

3.2.7. Calculation of ionic composition, saturation index, DIC, and titration

Aqion Pro 8.1.5 software was used to compute the concentrations of the DIC species (H_2CO_3, HCO_3^-, and CO_3^{2-}), as well as the Langelier saturation index (LSI) in both the feed water and the samples collected during charging and discharging. Additionally, titration curves for $NaHCO_3$ titration with an acid were generated using the software. These calculations were performed by

taking into account charge and mass balance principles. The calculations were conducted within a closed CO_2 system, meaning there was no interaction with the atmosphere.

3.2.8. Ionic composition calculations for feed water

In the feed water, all ions except for carbonates are experimentally measured, along with pH. These measured concentrations and pH values are then input into the software to calculate the DIC concentration, including HCO_3^- and CO_3^{2-}. The calculations were performed using the software, employing charge and mass balance principles, while assuming a closed CO_2 system.

3.2.9. Ionic composition & LSI calculations for collected samples

In analysing the ionic composition of collected samples, we used both the measured ionic concentrations and pH as fixed parameters to compute the concentrations of dissolved inorganic carbon (DIC). The pH measured experimentally in these collected samples represents the average pH of the total volume of desalinated or concentrate water collected during the entire step. Hence, the calculated DIC concentrations reflect the concentrations for the entire adsorption or desorption cycle, based on the measured pH. To account for varying pH values and their impact on ionic composition, different pH inputs were used, and a charge balance was conducted for each pH value to ascertain the corresponding ionic composition, including DIC concentrations. Additionally, these calculations facilitated the extraction of the Langelier Saturation Index (LSI) values for each sample from the software. The detailed calculation method of LSI is outlined in chapter 2.

3.2.10. DIC calculation for $NaHCO_3$ desalination

The DIC concentration during $NaHCO_3$ desalination was calculated by using the effluent Na^+ concentration (calculated from effluent conductivity) and the

effluent pH as inputs. With these inputs, the DIC concentration is calculated through charge and mass balances considering a closed system.

3.2.11. Titration calculations

To predict the titration curves in Aqion Pro, we input the concentrations of NaHCO3, and the charge balance is adjusted based on the DIC concentration before titrating against HCl (50 mM). The titration predictions take into account a closed CO2 system, mirroring the conditions of the experimental titrations conducted in a closed vessel.

3.3. Results and Discussion

3.3.1. pH changes in MCDI

We conducted desalination experiments using tap water, a synthetic solution containing a limited set of salts (consisting of Na^+, Ca^{2+}, Cl^-, and HCO_3^-), and a single salt solution (only Na^+ and HCO_3^-) to elucidate the underlying mechanisms for pH changes. As depicted figure 3.2(a-c), the charging step induces a decrease in pH, while discharging leads to an increase in pH across all feed waters. Notably, the effluent pH changes demonstrate consistent trends in terms of both direction and dynamics for both the $NaHCO_3$ (single salt) solution and multi-ionic salt solutions (tap water, multi-ionic synthetic water). However, in chapter 1 we have demonstrated that for single salt solutions, when the anion present is Cl^- instead of HCO_3^-, the resulting pH changes differ in terms of direction and dynamics, as demonstrated by the desalination of NaCl solution instead of $NaHCO_3$, as shown figure 3.2d.

This finding suggests that the presence of different anions in the water impacts the changes in effluent pH. The diverging trends in pH may stem from variations in anion compositions; specifically, the amphoteric nature of HCO_3^- allows it to function as both an acid and a base, influencing pH, whereas Cl^- does not buffer the solution pH. Chapter 1 has shown that, under identical experimental conditions (11.1 A/m^2 current density, feed water equilibrated with the atmosphere, and voltages below 0.95 V), faradaic

reactions occur solely at pristine electrodes, and as electrodes age, pH changes are predominantly attributed to non-faradaic processes.[114] Hence, faradaic reactions can be discounted as a potential cause of pH changes, with focus instead on HCO_3^- ion adsorption and desorption as the primary driver in feed waters where these ions are present.

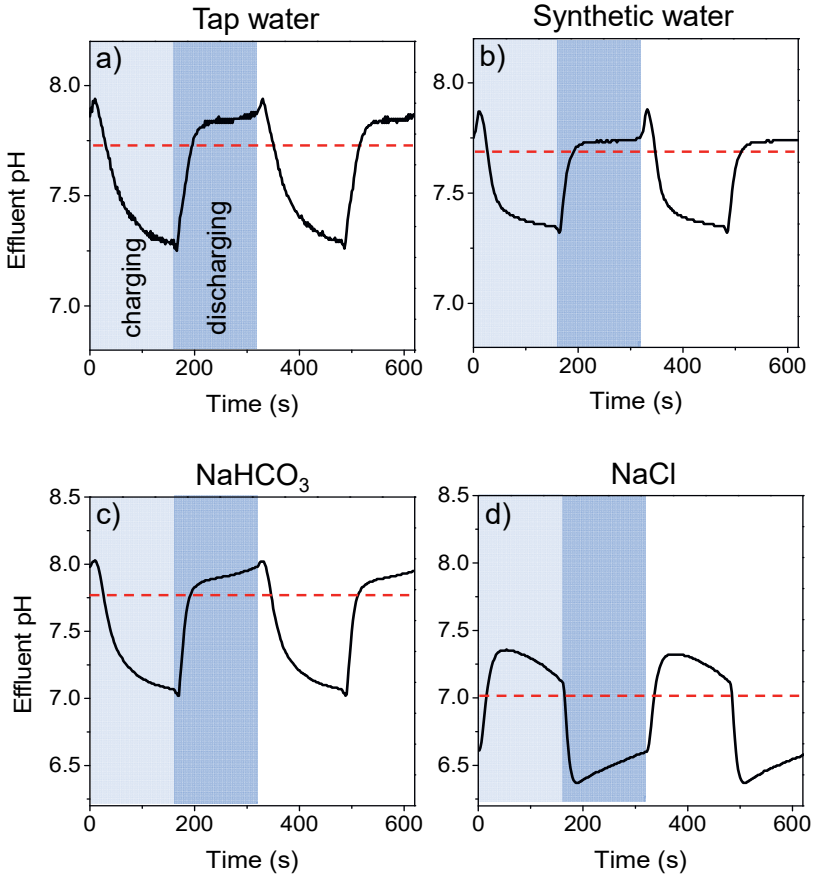

Figure 3.2. Effluent pH changes observed during desalination of a) tap water, b) synthetic water, c) a $NaHCO_3$ solution and d) an NaCl solution (adapted from our previous study, Arulrajan et al. (2021)). The feed pH of the NaCl solution is 7, while for all other feed waters the pH is 7.72.

To investigate the impact of effluent concentration on pH changes, we conducted additional desalination experiments using freshly prepared $NaHCO_3$ with an initial feed pH of 8.35. By adjusting the applied current

density to the MCDI stack, we adjusted the ion concentration in the effluent water (Δc). Figure 3.3a presents the mean effluent pH during adsorption and desorption steps relative to the applied current density. As the charging current density increases from 4.95 A/m^2 to 8.9 A/m^2, the effluent pH decreases from 8.31 to 8.26. Conversely, during discharge, the effluent pH rises from 8.41 to 8.46. This observation indicates that modifying the applied current density to alter ion concentrations in the effluent directly influences the magnitude of pH variations in tap water.

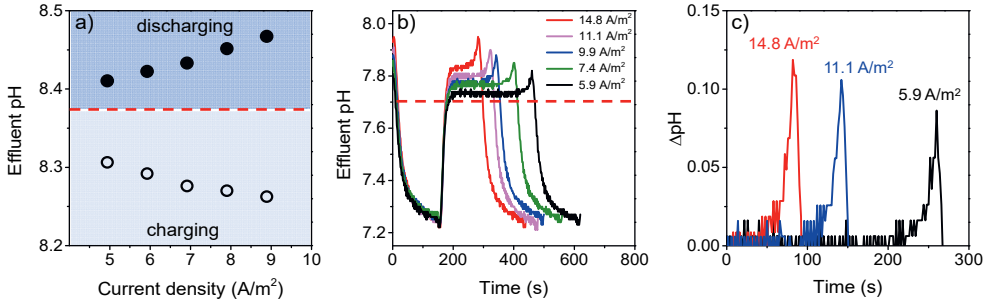

Figure 3.3. (a) Averaged effluent pH of the experiment with the $NaHCO_3$ solution during charging and discharging, (b) the effluent pH changes during asymmetric desalination experiments, and (c) the magnitude of pH spikes at the beginning of the charging step.

To understand the effect of operational parameters such as current density, which can affect the effluent concentration and subsequently pH changes, particularly for concentrates, we conducted asymmetric desalination experiments using tap water. Throughout these experiments, the conditions (i.e., flow rate, current density, and charging time) during the charging step remained the same across all experiments, but the conditions during the discharging step were varied (maintaining a constant flow rate while altering the current density and discharging times). In these asymmetric experiments, the change in effluent concentration during charging remained consistent across all cycles due to the uniformity of experimental conditions, whereas the effluent concentration during discharging is affected by the applied current. The cell voltage during asymmetric experiments is presented in figure S3.1. When the current was increased during discharging, the discharging time was proportionally reduced to keep the total charge

transferred during discharge the same for all applied currents. Figure 3.3b shows the effluent pH during asymmetric desalination. The pH changes observed in different asymmetric experiments overlapped during the charging step, while during the discharging step, the magnitude of effluent pH changes increases with increasing current density. A noteworthy aspect of pH changes is the distinct pH spike at the beginning of the charging step, followed by a smaller yet inverted pH spike at the beginning of the discharging step, as shown figure 3.2a-c. As illustrated figure 3.3b, the magnitude of the pH spike during the charging step was influenced by the current density applied during charging, with higher current densities resulting in larger pH spikes. These pH spikes can induce mineral scaling, particularly when hardness ions are present at elevated concentrations.

3.3.2. pH changes with high DIC concentrations

To investigate the mechanisms causing pH changes, we focussed on a simpler solution than tap water, i.e., a $NaHCO_3$ solution. Despite the effluent pH fluctuations during charging and discharging, the effluent concentration stabilizes at a steady plateau value shortly after the start of a charging or discharging step (figure 3.4a), characteristic of constant current operation. The HCO_3^- ions, being amphoteric, participate in the carbonic acid equilibrium expressed as: $H_2O + CO_2(g) \rightleftharpoons H_2CO_3^* \rightleftharpoons HCO_3^- + H^+ \rightleftharpoons CO_3^{2-} + 2H^+$ (apparent H_2CO_3* represents the combined concentrations of H_2CO_3 and aqueous CO_2). This equilibrium governs the concentration of each species involved, including $CO_2(g)$, DIC ($H_2CO_3^*$, HCO_3^-, and CO_3^{2-}), along with pH.[116] Throughout charging and discharging, the adsorption and desorption of charged DIC species affect the carbonic acid equilibrium, leading to a shift in pH.[114]

We used Aqion Pro software to compute the DIC concentration from the effluent pH and Na^+ concentration, employing the methodology outlined in the materials and methods section. This analysis aims to elucidate changes in DIC species (CO_2, H_2CO_3, HCO_3^-, and CO_3^{2-}) concentrations. Notably, we calculated the concentrations of apparent H_2CO_3*, HCO_3^-, and CO_3^{2-} while

treating the MCDI stack as a closed system (i.e., no CO_2 exchange with atmospheric air). In the pH range between 7 and 8, H_2CO_3* and HCO_3^- emerge as the dominant DIC species, while the concentration of CO_3^{2-} is negligible, as shown in figure S3.2 and S3.3.

Figure 3.4a displays the effluent pH and the $NaHCO_3$ concentration, while figure 3.4b shows the concentrations of H_2CO_3* and HCO_3^- over time. Clearly, due to the adsorption and desorption of charged DIC in the porous

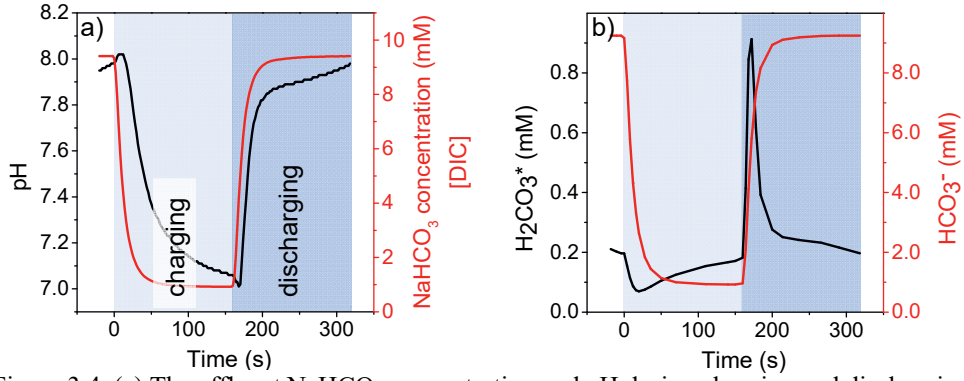

Figure 3.4. (a) The effluent $NaHCO_3$ concentration and pH during charging and discharging of MCDI. (b) The calculated concentrations of two primary DIC species, namely HCO_3^- and H_2CO_3*, during charging and discharging.

carbon electrodes, the equilibrium between H_2CO_3* and HCO_3^- is shifted. This shift in chemical equilibrium impacts the solution pH, as shown in figure 3.4a. Specifically, during charging, the H_2CO_3* concentration experiences a sharp initial decline from the feed concentration (~200 µM to ~60 µM), followed by gradual increase, ultimately returning to the initial feed water concentration (200 µM) by the end of the charging step. Similarly, during discharge, the H_2CO_3* concentration undergoes a sharp increase (from ~200 µM to ~1 mM), followed by a gradual decline, once again reaching the initial feed concentration (200 µM) by the end of the discharging step. The sharp changes in H_2CO_3* concentration coincide with the pH spike at the onset of the charging step, while the sharp decrease aligns with the inverted pH spike at the beginning of the discharging step.

Figure 3.4b shows that the rapid H_2CO_3* concentration change at the beginning of discharging (~0.75 mM) is approximately sixfold higher than the corresponding change during charging (~0.13 mM). However, this notable concentration increase does not translate into a proportionately amplified pH spike during discharge. As $NaHCO_3$ solution is a buffered solution, it is important to consider the buffer range of this solution to evaluate the reason for the magnitude in pH changes. At the beginning of the discharging step, the effluent pH is 7.1, which is close to the pK_a (6.37) of the carbonic acid-bicarbonate equilibrium,[117] indicating that the pH is minimally impacted by changes in the concentration of DIC species.. At the beginning of the charging step, however, the effluent pH is 7.9, which is further away from the pK_a of 6.37, and is therefore in the poorly buffered pH range. This lower buffer capacity could be the reason for the more pronounced pH spike at the beginning of the charging step. This argument is supported by the calculation conducted for the titration of $NaHCO_3$ composition measured during discharge, see figure S3.7.

3.3.3. Mineral scaling in MCDI

The pH changes in MCDI can induce scaling, especially noticeable under high water recovery conditions (WR > 50%).[67] During the investigation of mineral scaling, we examined various water recovery conditions. Our focus was on assessing the impact of AEM thickness on mineral scaling, as membrane thickness can influence the flux ratio of different species.[32] Two configurations of MCDI stacks were employed: one with a single-AEM MCDI cell and the other with a double-AEM MCDI cell setup. Desalination experiments were conducted for durations exceeding 100 hours for each water recovery condition. To enhance water recovery, the flow rate during discharge was reduced. Mineral scaling in the spacer channel was monitored by continuously measuring the pressure difference (Δp) across the spacer channel during experiments.[67]

The Δp measured between the inlet and outlet of the MCDI cell represents the pressure difference across the spacer channel connecting the inlet and outlet.

Mineral scaling occurs when minerals precipitate, blocking pores in the spacer. This blockage leads to an increase in Δp. In MCDI systems, Δp values often serve as indicators prompting cleaning cycles for mineral scale removal. Typically, cleaning cycles commence just before Δp begins to rise exponentially; however, specifics vary between systems, lacking a standardized protocol for cleaning cycle initiation. In this study, a threshold of 100 mbar was set to compare mineral scaling across operational conditions.

Figure 3.5 shows that, for tap water desalination, an increase in Δp with time is observed, which is an indicator of mineral scaling. Notably, at 50% and 75% WR conditions, Δp remains relatively stable, with values below 20 mbar even after 110 hours of operation. At 85% WR, although scaling causes a more pronounced increase in Δp, it does not reach the threshold of 100 mbar during the experiment. Only at WR of 90%, substantial Δp changes occur over time in both MCDI configurations. For the single-AEM MCDI, 100 mbar is reached in 35 hours; whereas, with double-AEM MCDI, it takes ~80 hours. This observation gives experimental support that increasing AEM thickness reduces mineral scaling, and therefore the consumption of cleaning in place chemicals. Experiments with tap water were poorly reproducible. Subsequent examination upon MCDI stack disassembly revealed pronounced mineral scaling exclusively on the spacer as visibly depicted in figure S3.4, whereas IEMs remained largely unaffected. The precipitated salt in the spacer was subjected to Raman spectral analysis. The Raman analysis shows 4 distinctive peaks at 153, 280, 712 and 1085 cm-1 which are in line with the peaks for calcite (CaCO3) revealing that the precipitated mineral is calcite, figure S3.5.[118] Interestingly, the initially transparent AEMs exhibited a brown hue (as seen in figure S6), potentially attributable to organic adsorption (e.g., humic/fluvic acid substances).This membrane fouling could impair experimental reproducibility. Therefore, we studied scaling in synthetic water containing only Na^+ and Ca^{2+} cations, and Cl^- and HCO_3^-/ CO_3^{2-} anions, with increased Ca^{2+} ion concentrations to accelerate mineral scaling (Table S3.1). These synthetic water scaling experiments were carried out for 200 desalination cycles (equivalent to ~18 hours), repeated three times for 85% and 90% WR to ensure replicability.

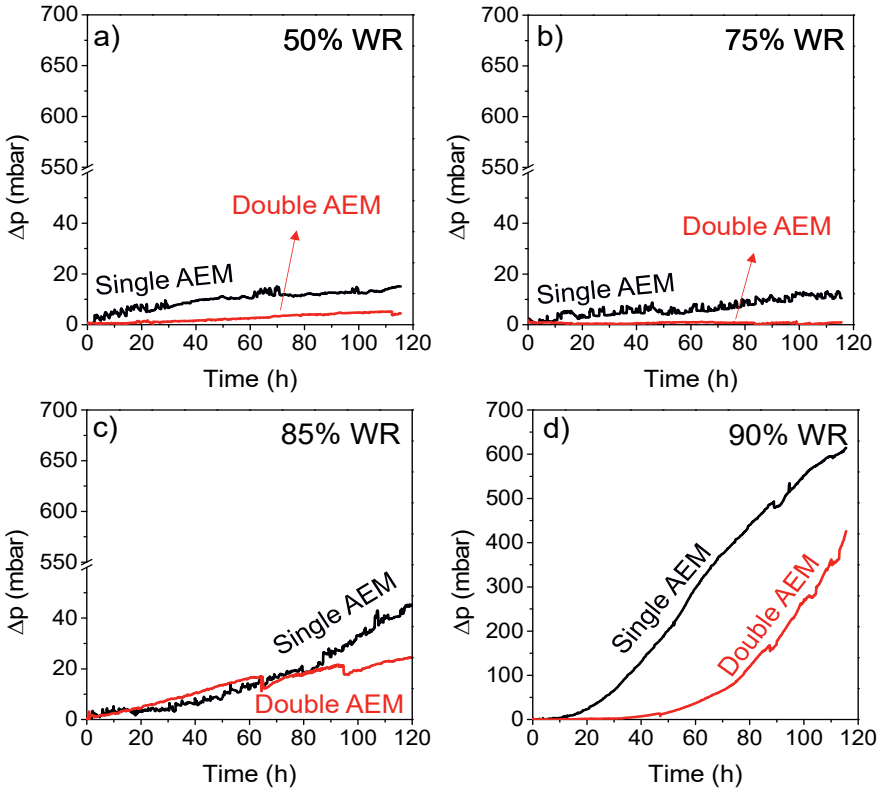

Figure 3.5. Pressure difference, an indication for mineral scaling, across the MCDI cell against operational time during tap water desalination at water recoveries a) 50%, b) 75%, c) 85%, d) 90%.

figure 3.6 shows Δp changes over operational time for synthetic water. Similar to the trends observed in tap water mineral scaling, experiments with synthetic water also demonstrate an increasee in scaling with rising WR. However, at 50% and 75% WR, though Δp increases it does not reach the 100 mbar threshold within the ~18-hour operational timeframe. At 85% WR, the single-AEM MCDI stack reaches 100 mbar Δp in 14 hours, while the double-AEM MCDI stack does not reach the 100 mbar threshold within the operational timeframe. Upon increasing the WR to 90%, the single-AEM MCDI achieves a 100 mbar Δp in 10 hours, whereas the double-AEM MCDI stack takes 13.5 hours, displaying that scaling is approximately 1.35 times slower. In experiments with tap water and synthetic water, mineral scaling is primarily influenced by two factors: the hardness ion concentration (Ca^{2+},

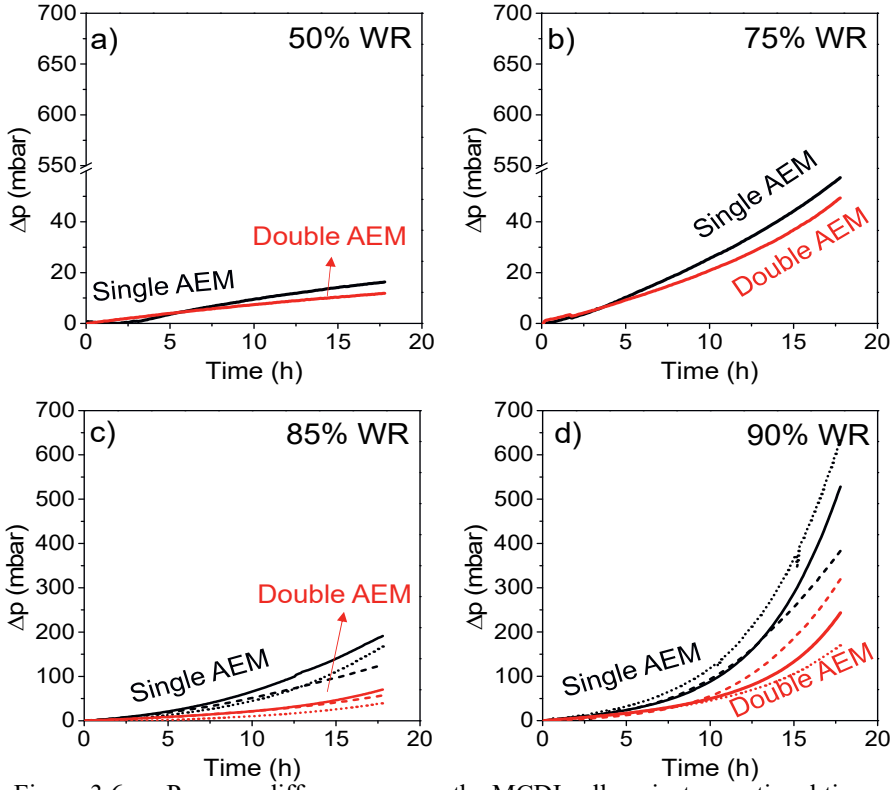

Figure 3.6. Pressure difference across the MCDI cell against operational time as an indication for mineral scaling during synthetic water desalination at water recoveries a) 50%, b) 75%, c) 85%, d) 90%. The dotted and solid lines of the same colour show data from replicate experiments.

Mg^{2+}) and pH. Analysis of ionic composition in tap water experiments shows no significant difference between single AEM and double AEM configurations. Effluent pH data from tap water and synthetic water experiments alone cannot explain pH variations by the AEM thickness, as simultaneous scaling can impact the measured effluent pH. To address this, we conducted theoretical calculations of the Langelier Saturation Index (LSI). The LSI is an indicator that shows the extent of scaling potential of a solution based on pH, TDS (total dissolved solids), temperature, Ca^{2+} concentration and alkalinity. While desalinating tap water or artificial tap water, at higher WR, the concentration of Ca^{2+} ions (together with all other ions) and pH in the effluent increases. This results in the precipitation of $CaCO^3$ (calcite) on the spacer. When the LSI values are above 0.5, the potential for scaling is

significantly high. We calculated the LSI for the concentrate composition of 90% water recovery under two conditions: firstly, varying the Ca^{2+} concentration (and Na^{+} concentration to maintain the charge balance) with constant pH, and secondly, varying pH and the total DIC concentration while the other ionic concentrations are constant, see figure S3.8. The initial LSI value for the concentrate is 1, and to raise the LSI to 1.2, the Ca^{2+} concentration must increase by 73% (i.e., from 3.42 mM to 5.92 mM) when pH is fixed, while a 2.9% increase in pH (i.e., from 8.02 to 8.25) results in the same LSI with fixed concentrations of Ca^{2+} and of the other ions except DIC. As the difference in the Ca^{2+} concentration between single AEM and CEM experiments is not significant (i.e., only 8.75%), the difference in effluent pH between single and double AEM is probably the most important cause of the observed differences in scaling, as shown in figure 3.5 and 3.6.

3.4. Conclusion

We conducted a series of experiments to understand the mechanisms driving pH changes during desalination processes, focusing on solutions containing HCO_3^- ions (such as tap water, synthetic water and $NaHCO_3$). Our empirical findings demonstrate that pH changes observed in $NaHCO_3$ experiments directly result from HCO_3^- removal, which we identify as a significant mechanism driving pH changes in tap water. Through systematic experiments and calculations, we determined that HCO_3^- removal, along with changes in concentrations of other dissolved inorganic carbon (DIC) species, can lead to pH changes by altering the carbonic acid equilibrium. Furthermore, we observed that desalination of tap water or synthetic water containing hardness ions at higher WR conditions results in elevated pH levels, contributing to increased mineral scaling. Raman spectral analysis revealed that during tap water desalination, scaling primarily occurs due to the precipitation of calcite mineral. Our findings also demonstrate that increasing the thickness of the AEM can reduce mineral scaling in MCDI, consequently decreasing the need for anti-scaling agents.

Annex B

Table S3.1. Composition of different feed water solutions at pH 7.73 with experimentally measured ionic compositions. The concentrations of HCO_3^- and CO_3^{2-} are calculated using Aqion Pro software as mentioned in the method section.

Ion	Concentration (mM)		
	Tap water (pH 7.72)	Synthetic water (pH 7.73)	$NaHCO_3$ water (pH 7.73)
Cations			
Na^+	3.08	1.97	4.93
Ca^{2+}	0.79	1.92	-
K^+	0.08	-	-
Mg^{2+}	0.40	-	-
Anions			
HCO_3^-	4.43 (calculated)	4.63 (calculated)	4.89 (calculated)
CO_3^{2-}	0.014 (calculated)	0.015 (calculated)	0.015 (calculated)
Cl^-	1.05	1.02	-
NO_3^{2-}	0.06	-	-
SO_4^{2-}	< detection limit	-	-
PO_4^{3-}	< detection limit	-	-

Table S3.2. Current and discharging time during the discharging step in asymmetric desalination experiments.

Current (A/m^2)	Discharging time (s)	Equivalent WR %
5.93	300	27
7.41	240	33.5
9.88	180	44.5
11.11	160	50
14.81	120	67

Charge and Mass balance calculations

The charge and mass balance calculations were carried out by Aqion Pro software as mentioned in the methods section. To calculate the concentration of each DIC species, the following equations are used by the software.

For a closed DIC system,

Mass balance: $[DIC] = [H_2CO_3^*] + [HCO_3^-] + [CO_3^{2-}] = \text{Constant}$

Charge balance: $[H^+] - [HCO_3^-] - 2\,[CO_3^{2-}] - [OH^-] = 0$

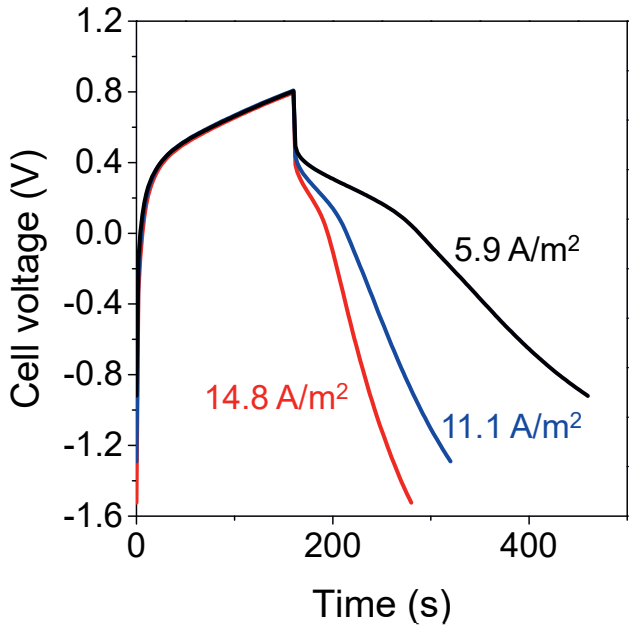

Figure S3.1. The cell voltage profiles during asymmetric desalination experiments.

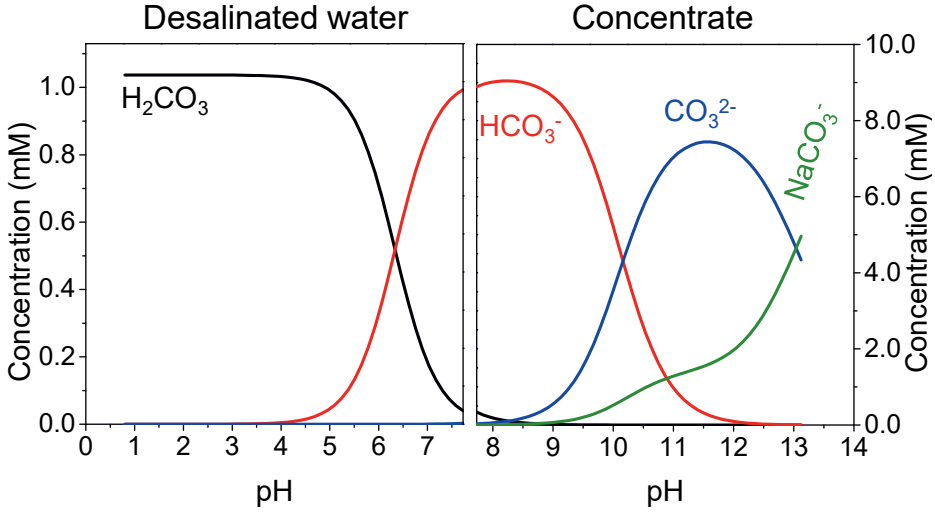

Figure S3.2. The carbonic species distribution for desalinated water and for concentrate with pH calculated using Aqion Pro software.

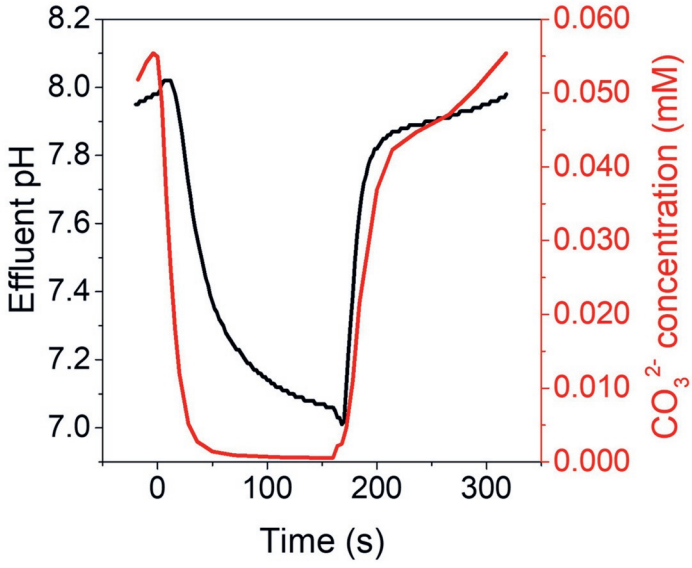

Figure S3.3. The carbonate concentration and the effluent pH changes during a complete desalination cycle.

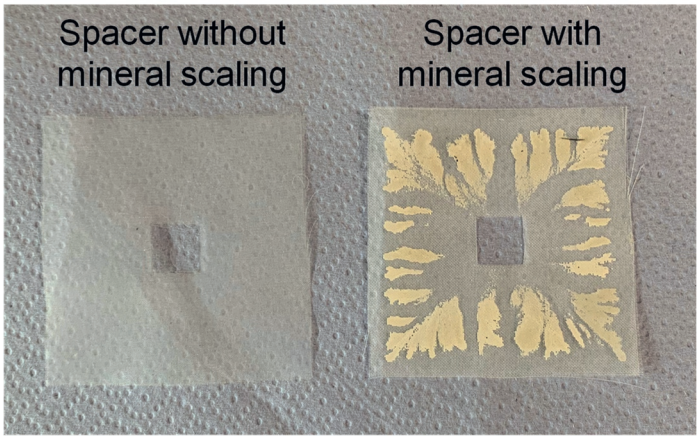

Figure S3.4. Unused and used spacer in tap water experiments; mineral scaling is observed on the used spacer.

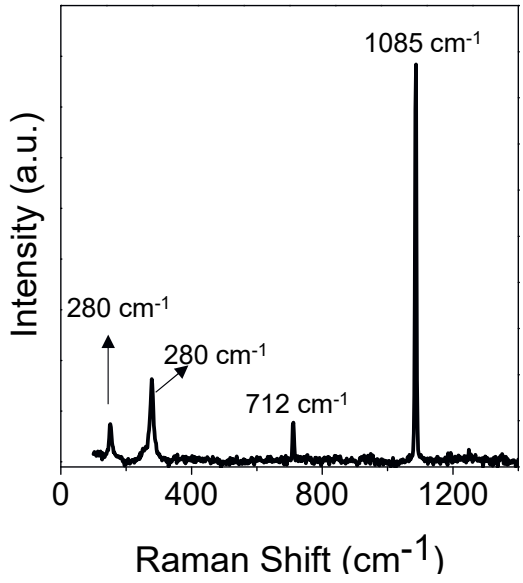

Figure S3.5. Raman spectra of precipitated salt collected from MCDI spacer

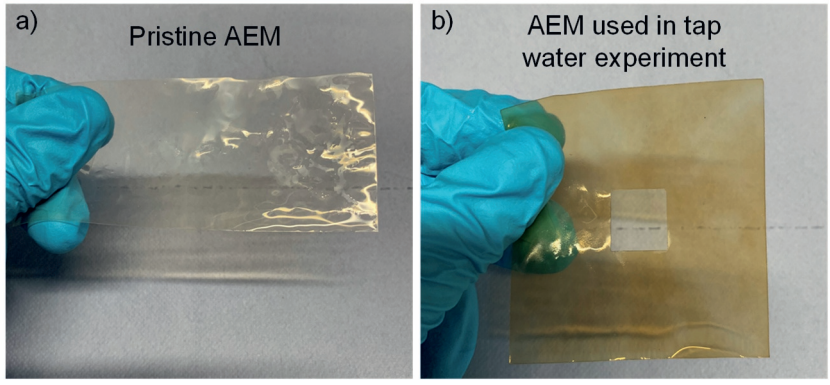

Figure S3.6. (a) A picture of a pristine AEM and (b) a used AEM in tap water experiments; the colour change is clearly visible.

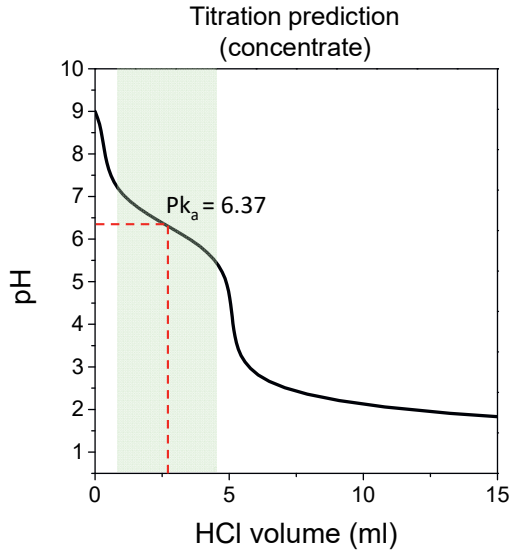

Figure S3.7. Predicted titration curve for the concentrate in $NaHCO_3$ desalination at 50% WR condition. The green highlighted area shows the buffer range with limited pH changes when HCl is dosed.

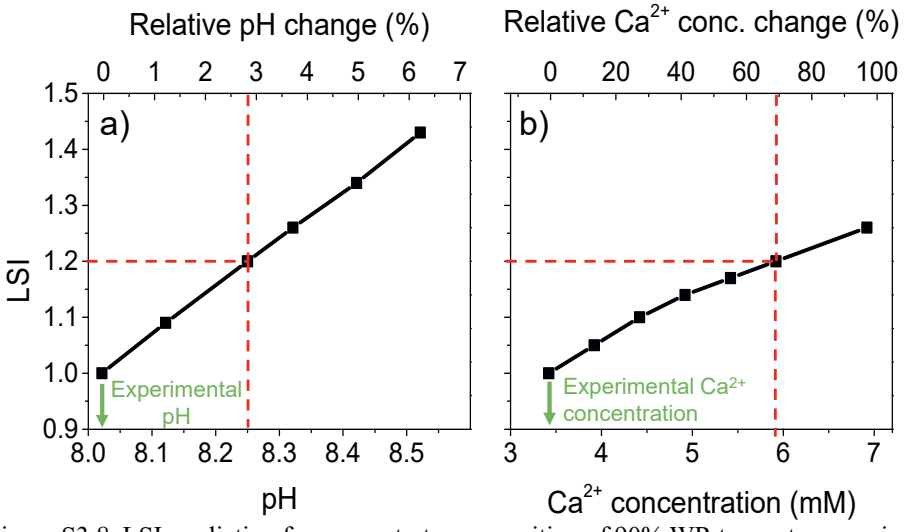

Figure S3.8. LSI prediction for concentrate composition of 90% WR tap water experiments as a function of (a) pH, and (b) of the Ca^{2+} concentration.

Chapter 4. Understanding pH changes in different compartments of the Membrane Capacitive Deionization cell

Abstract

Membrane capacitive deionization (MCDI) has emerged as a promising electrochemical method for desalinating brackish water. Despite its potential, MCDI systems encounter challenges such as low ion-selectivity and mineral scaling, which are influenced by pH changes during operation. Effluent pH changes cause mineral scaling while pH changes near electrodes can affect the removal efficiency of ions like carbonates and borates. Previous studies have shown the effluent pH changes during desalination of various feed waters. However, understanding pH changes at specific cell locations, such as the anode and cathode, is crucial for effective pH control strategies. This chapter investigates pH changes in different MCDI cell compartments using ultra-micro pH sensors under both faradaic and non-faradaic conditions. By comparing our findings with existing theoretical and experimental data, we aim to elucidate the pH changes within MCDI cells that can help to enhance operational strategies to mitigate mineral scaling and to improve ion-selective adsorption of pH sensitive ions.

4.1. Introduction

Increasing global demand for freshwater, coupled with diminishing natural water resources, necessitates water treatment. The need for water reuse in industries, environmental and health risks associated with effluents, and the need for potable water from brackish and seawater sources leads to the development of water treatment technologies.[2,4,6,79] Membrane capacitive deionization (MCDI) is an electrochemical water treatment technology for brackish water desalination.[37,119,120] Despite its potential, MCDI systems face challenges such as low selectivity towards the removal of specific ions and mineral scaling. In MCDI operation, pH is one of the factors that influences mineral scaling and ion-selectivity. A pH shift towards basic pH leads to hardness ion precipitation, causing mineral scaling especially in the spacer channel and on the membranes.[67,82,99] Similarly, pH changes near electrodes affect the removal of ions like carbonates and borates, emphasizing the importance of understanding pH changes to enable effective MCDI system development.[71]

The cyclic operation of MCDI, involving alternating charging and discharging, induces pH fluctuations in the effluent. The specific direction of these pH changes depends on the ion composition of the feed water. This variability poses a challenge, significantly impacting the efficiency and long-term stability of MCDI systems.[67,121] Addressing this challenge becomes important, prompting the need for strategies to mitigate pH changes. A comprehensive understanding of pH dynamics during MCDI operation is essential for developing effective strategies to control or minimize pH changes. Previous research has extensively investigated pH changes in CDI and MCDI, focusing on effluent streams using pristine activated carbon electrodes and NaCl feed water. Various operational modes, including single pass or batch mode operation, and diverse experimental conditions such as constant current or constant voltage operation, have been explored to study the mechanisms causing pH changes and to minimize the loss in stability.[73,74,88]

Most existing studies have identified faradaic reactions as the predominant factor behind observed pH variations during (M)CDI operation. Under certain (M)CDI operational conditions, faradaic reactions (as listed in Table 4.1), including carbon oxidation, oxygen reduction, water splitting, and chlorine formation can be induced.[73,84,88,99,122,123] These reactions exert a significant influence on pH changes in both CDI and MCDI. The incorporation of ion-exchange membranes (IEMs) in MCDI is expected to suppress faradaic reactions related to dissolved O_2 by limiting its transport into the electrode compartments.[99,124]

Table 4.2 Overview of possible faradaic reactions that can take place in MCDI

Reaction number	Reaction	Potential vs SHE
	Anode	
	Oxygen evolution reaction[88]	
1	$2H_2O \rightarrow O_2 + 4H^+ + 4e^-$	1.23 V
	Carbon oxidation reaction[88]	
2	$C + H_2O \rightarrow C{-}O_{ads} + 2H^+ + 2e^-$	0.21 V
	Chlorine oxidation reaction[88]	
3	$2Cl^- \rightarrow Cl_2 + 2e^-$ $Cl_2 + H_2O \rightarrow HClO + H^+ + Cl^-$	1.36 V
	Cathode	
	Hydrogen evolution reaction	
4	$2H^+ + 2e^- \rightarrow H_2$	0 V
	Oxygen reduction reaction[88]	

5	$O_2 + 2H^+ + 2e^- \rightarrow H_2O_2$	0.69 V

In addition to faradaic reactions, non-faradaic processes, such as differences in ion mobilities and the protonation/deprotonation of surface chemical groups can also cause pH changes during MCDI operation as shown in figure 4.1.[38,84] Theoretical evaluation conducted by Dykstra et al. (2017) demonstrated that differences in ion mobilities contribute to effluent changes during NaCl desalination with a pH increase during the charging and a subsequent decrease during discharge.[84] This theoretical framework is validated in chapter 2 of this thesis, where MCDI operation with aged electrodes revealed that pH changes during NaCl desalination are predominantly caused by non-faradaic processes.[114] This phenomenon becomes particularly pronounced when faradaic reactions, such as carbon oxidation, diminish as the electrodes age during long-term operation. Additionally, in tap water desalination, the presence of bicarbonate ions (HCO_3^-, an amphoteric ion) in the feedwater causes pH changes with inversed direction compared to NaCl due to the adsorption and desorption of HCO_3^-, representing another non-faradaic process.[114]

In literature, investigations on pH changes in (M)CDI have predominantly focused on effluent water.[99,114] While insights derived from studying effluent pH data contribute to addressing challenges like mineral scaling in the spacer channel, a comprehensive understanding of pH changes at specific locations within the MCDI cell, namely the anode, cathode, and ion-exchange membranes, is crucial to propose effective strategies for pH control. Despite the theoretical framework established by Dykstra et al. (2017)[84] elucidating pH dynamics at the cathode and anode during MCDI operation, experimental studies targeting near-electrode pH changes are limited. A recent study by London et al. (2021)[86] has undertaken an examination of pH changes in proximity to the electrode surfaces in CDI and MCDI cells under equilibrium desalination conditions. Their findings reveal that, with aged electrodes, CDI exhibits greater pH changes in comparison to MCDI. Notably, the pH near

the anode tends to be acidic, while near the cathode, the pH tends to be basic during the charging phase for both CDI and MCDI. During discharge, the pH in the MCDI anode and cathode stays acidic and basic, respectively, while in CDI the pH in the anode and cathode gradually reaches feed pH.[86] Further elucidation of near-electrode pH dynamics under conditions such as constant current operation holds significant promise for enhancing operational strategies aimed at controlling pH changes.

In a recent study, Shocron et al. (2021)[71] provided a comprehensive elucidation of how the pH close to the anode and cathode influences boric acid speciation and its subsequent efficient removal. In the context of a flow-through electrode capacitive deionization (FTE-CDI) system, the cell design with an anode placed upstream and cathode downstream has been demonstrated to be particularly effective in removing boric acid, a different observation from the less efficient removal observed when the cathode was

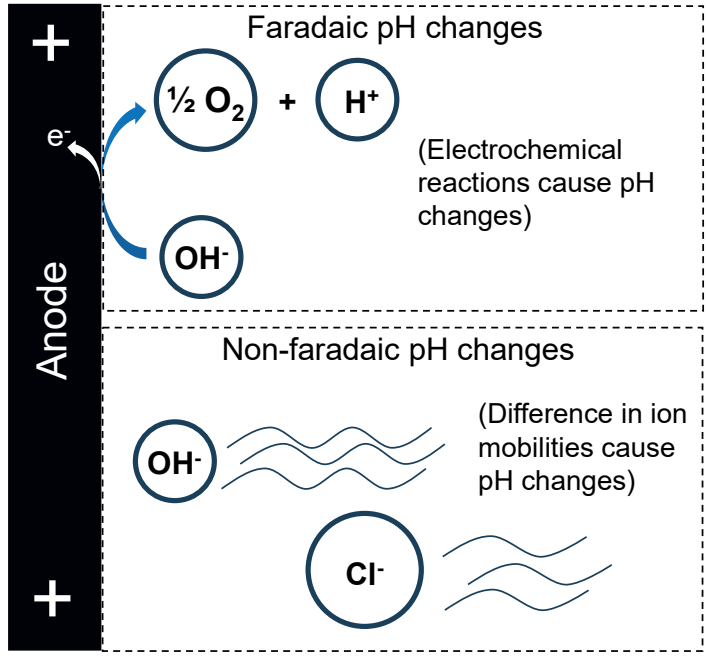

Figure 4.1. Graphical representation of faradaic reactions and non-faradaic processes that cause pH changes in MCDI, presented for the anode as an example.

positioned upstream. Theoretical pH calculations conducted by Shocron et al. underscore that maintaining a higher pH in the anode, especially at the spacer channel interfaces, plays a crucial role in facilitating the effective removal of boric acid. This is achieved by promoting its speciation under basic conditions. Translating this understand the potential to elevate its capacity for removing amphoteric ions.

In this chapter, we studied pH changes in different elements of an MCDI cell, namely at the effluent, near the cathode and the anode, to get better insights into pH dynamics during MCDI operation. By using an ultra-micro pH sensor which can be positioned with μm precision near the electrodes, we recorded pH changes under two different operational conditions, namely, a condition in which faradaic reactions are likely to run which we refer as faradaic condition, and a condition in which these are not likely to run, which we refer to as the non-faradaic condition. Finally, by comparing with existing theoretical and experimental studies, we explain the pH changes observed in the different compartments of the MCDI cell.

4.2. Materials and methods

4.2.1. MCDI Stack construction

The MCDI stack consisted of 3 cells. Each cell consisted of two graphitic carbon sheets, two activated carbon electrodes (PACMM 203, $\delta e \sim 250$ μm, Material Methods, Irvine, CA, USA), two ion exchange membranes and a porous nylon spacer. In each cell, a cation exchange membrane (CEM; Neosepta CMX, ASTOM Corporation, Tokyo, Japan) was placed in front of an activated carbon while an anion exchange membrane (AEM; Neosepta AMX, ASTOM Corporation, Tokyo, Japan) was placed in front of the other activated carbon electrode. The nylon spacer (160 micrometer thick) was placed between the membranes. Each cell was placed between two graphite sheets that acted as current collectors. There was a hole at the top of the cell to place micro pH sensors to measure pH near the electrodes (Section 2.5).

4.2.2. Aging of electrodes

Before starting desalination experiments to measure pH changes, the electrodes were aged by operating the MCDI stack for more than 3000 desalination cycles at constant current operational mode with a current density of 11.1 A/m^2, flow rate of 18.75 ml and half-cycle time (HCT) of 160 seconds. During aging, a 5 mM NaCl feed water purged with air was desalinated in order to have dissolved O_2 and CO_2 in the system. The electrodes are considered as aged once the effluent pH changes become minimal, the pH dynamics become consistent over cycles, the magnitude of pH changes for consecutive cycles are similar, and the overall pH changes fluctuate around the feed water pH.

4.2.3. Desalination experiment

After the electrodes are aged, the desalination experiments to measure pH changes were performed with a 20 mM NaCl feed solution prepared using

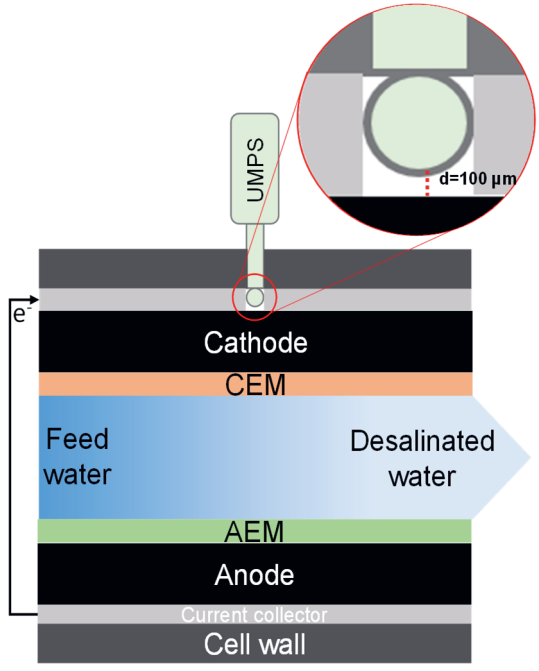

Figure 4.2. Graphical representation of MCDI cell and near electrode pH measurement using an ultra-micro pH

ultrapure water (resistivity of 18.2 Ω cm at 25 °C) and purged with nitrogen to eliminate dissolved O_2 and CO_2. The feedwater was pumped from a 50 L tank and the effluent was discharged. Constant current operational mode is used for desalination with an applied current density of 11.1 A/m^2 and with a flow rate of 18.75 ml/min. Two different operational schemes were used, i.e., one scheme to operate the cell under non-faradaic condition, and a scheme for faradaic condition. For non-faradic condition, the MCDI stack is charged until 0.65 V with a positive current and discharged until 0 V with a negative current. Whereas for faradaic condition, the MCDI stack is charged until 1.6 V and discharged until 0 V. All experiments were carried out for 40 to 100 cycles to reach dynamic steady state where pH changes of consecutive desalination cycles overlap.

4.2.4. Conductivity and pH experiments at the effluent

The pH and the conductivity of the effluent was measured continuously with a pH sensor and a conductivity sensor connected to the effluent. The pH and conductivity are recorded with a 2 second interval.

4.2.5. pH measurements near the electrode

To measure the pH near the electrode, a hole through the MCDI cell wall and current collector was made as shown in figure 4.2, with a 4 mm diameter hole through the cell and a 8 mm hole through the current collector. An ultra-micro pH sensor (Orion™ 8103BNUWP ROSS Ultra™ pH Electrode) with a 3 mm tip width that was attached to a homemade micro-positioning system, as shown in figure 4.2, was used to measure the pH near the electrode surface. The micro-positioning system has a stepper motor controlled vertically moving platform (Thorlabs' MTS50-Z8 (MTS50/M-Z8) in which the pH probe is mounted and the stepper motor was controlled by Thorlabs's APT software to make micro steps of 50 micrometers. Initially, the micro pH sensor was manually placed through the hole to touch the electrode surface, and thereafter the sensor was mounted to the vertically moving platform and lifted 100 micrometers above the electrode surface using two 50 micrometer

steps. The pH data were collected every 5 seconds. The provision for the near electrode pH measurement was only made on the top side of the MCDI stack. Therefore, two individual experiments, one with an anode at the top side of the stack and the other with a cathode at the top side, were carried out to measure cathode pH and anode pH individually.

4.2.6. pH measurements with pH indicators in CDI configuration

To measure pH near the electrodes using pH sensitive color indicators, a conventional CDI configuration is used. Two carbon electrodes separated by a 9 mm channel gap were placed inside a transparent cell. A camera was used to continuously record solution color between electrodes. A universal pH indicator (Merck, pH range 4-11) was mixed with 100 mM NaCl solution before measurements. pH visualization experiments were performed by applying a constant voltage for 600 s during charging and 0 V for 600 s during discharging. While charging, color changes of the pH indicator are filmed in the spacer channel between the electrodes. To correlate color changes with pH values, calibration was conducted across a broad pH range, spanning from 4 to 10.5. At each pH value a photograph is taken and processed using ImageJ software to determine the RGB (red, green, blue) color intensities. This calibration revealed that the red color can be used as an indicator of pH changes for the full pH range as shown in figure S4.3. After performing this calibration, a desalination experiment was conducted and photographs were taken during the charging step of the CDI cell. These photographs, taken at various times during the charging step, were processed and the red color intensity was used to determine the local pH inside the cell.

4.3. Results and discussion

4.3.1 Effluent pH changes: non-faradaic and faradaic conditions

In the present investigation, we conducted a series of experiments to measure pH changes in the effluent, anode, and cathode of an MCDI cell operating

under non-faradaic and faradaic conditions. Figure 4.3a shows the cell voltage and the effluent pH for both conditions. Under non-faradaic condition, charging the MCDI cell to 0.65 V and discharging to 0 V resulted in an effluent pH increase during charging and a subsequent decrease during discharging, with pH changes oscillating around the initial feed pH. Effluent pH changes oscillating around feed pH indicates the absence of faradaic reactions as we showed in chapter 2 that the effluent pH changes oscillate away from the feed pH when faradaic reactions are present (i.e., at the beginning of electrode aging), and oscillate around the feed pH when faradaic reactions are absent (i.e., after aging of the electrode).[114] Furthermore, our findings are also consistent with the theoretical predictions of Dykstra et al. (2017), where the predicted effluent pH changes during charging and discharging under non-faradaic condition oscillate around feed pH and the direction of pH changes are the same as observed in this study.[84]

In contrast, under faradaic condition, when the cell was charged to 1.6 V to induce faradaic reactions such as water splitting, and subsequently discharged to 0 V, the effluent pH changes deviated from the feed pH. The effluent pH changes oscillate around pH 5 after achieving dynamic equilibrium. Notably, the deviation in effluent pH from feed pH can be seen during the initial desalination cycles i.e., approximately the first 10 cycles, which then stabilizes around pH 5 during later desalination cycles, as shown in figure S4.1. In figure 4.3b, the pH sharply increases during charging, followed by a gradual decrease, while during discharge, the pH shows a gradual increase from the lower pH reached during charging. The observed pH decrease during charging signifies an elevated concentration of H^+ ions in the spacer, indicative of occurrence of faradaic reactions at the electrodes.

We conducted a qualitative comparison of our results with the theoretical predictions by Dykstra et al. (2017), who exclusively considered non-faradaic processes and faradaic reactions in their pH change assessments. Although a direct comparison is challenging due to the disparate experimental conditions employed in the two studies, a qualitative evaluation provides valuable insights. As depicted in figure 4.3c, the effluent pH under non-faradaic

condition in both cases consistently oscillates around the feed pH, displaying a pH increase during charging and a decrease during discharging.

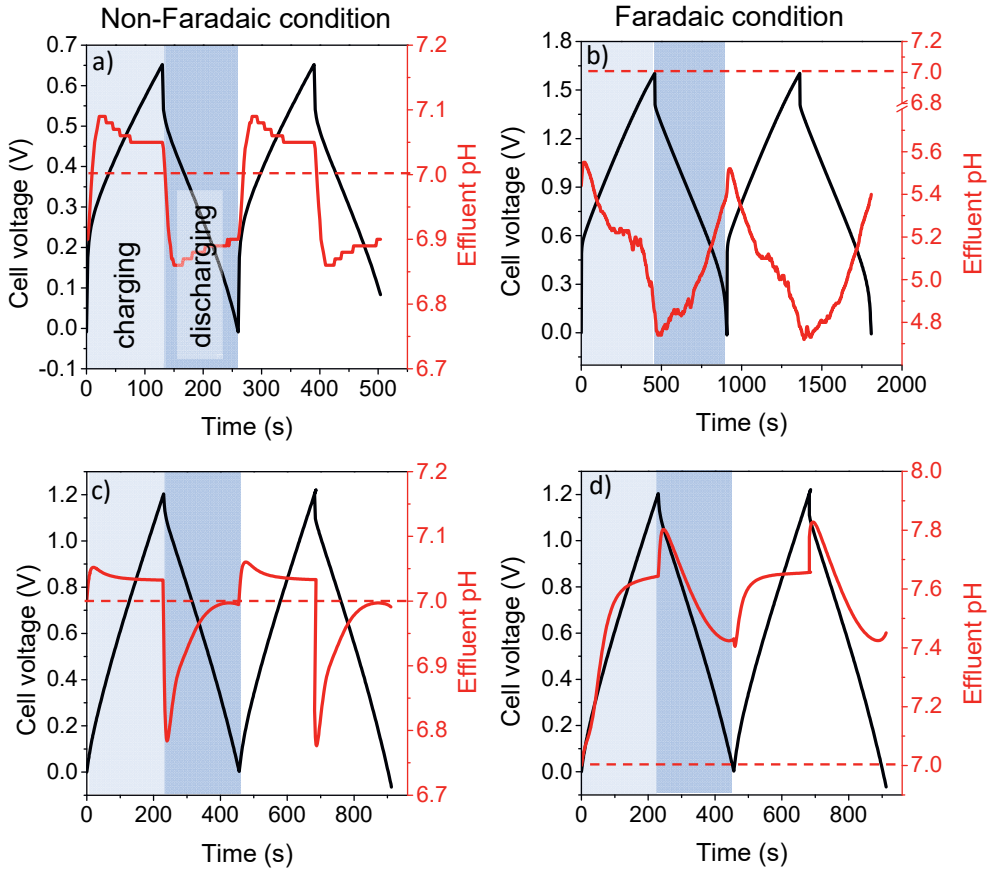

Figure 4.3. Cell voltage and effluent pH experimentally measured during non-Faradaic condition (a) and Faradaic condition (b) compared with the cell voltage and effluent pH predicted for non-faradaic condition (c) and faradaic condition (d) by Dykstra et.al (2017).

However, notable differences are observed when examining effluent pH changes under faradaic condition in the present study compared to the theoretical predictions by Dykstra et al (2017) as shown figure 4.3d. In their theoretical investigation, the effluent pH was shown to be basic during charging, whereas our experimental results indicate an acidic effluent pH. Additionally, the direction of pH changes during charging and discharging between these two studies are opposite to each other.

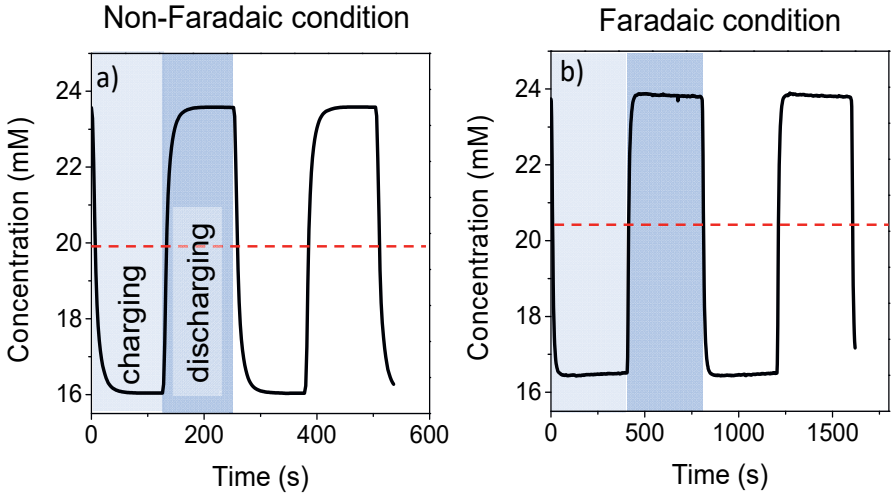

Figure 4.4. Effluent concentration change during charging and discharging under non-faradaic (a) and faradaic conditions (b), and the charge efficiency for both conditions (c).

The observed discrepancy between our experimental results and the predictions by Dykstra et al. (2017) may arise from their consideration of only the water reduction reaction ($2\ H_2O + 2e^- \rightarrow H_{2(g)} + 2\ OH^-$) in the cathode as the sole faradaic reaction influencing effluent pH changes. However, this theoretical finding may not be directly applicable when different faradaic reactions than water reduction occur, and when faradaic reactions occur both at the cathode and anode instead of only in the cathode. Therefore, the deviation of effluent pH changes in the current study could be due to the occurrence of different faradaic reactions at both electrodes. So, the measured effluent pH in the present study should not be directly compared with the predictions of Dykstra et al. (2017).

The charge efficiency, a key metric in MCDI, reflects the ratio of ions adsorbed to the applied charge. Figure 4.4 shows the effluent concentration change during non-faradaic and faradaic condition. Under ideal situation without faradaic reactions and co-ion expulsion, the theoretical maximum charge efficiency is 1, indicating complete utilization of charge for ion adsorption. Experimental charge efficiency in MCDI closely aligns with the

theoretical maximum as co-ion expulsion is minimized by the IEMs. However, when faradaic reactions or co-ion expulsion occur, part of the charge applied is utilized to drive faradaic reactions, or to expel co-ions resulting in reduction in charge efficiency. In our study, the MCDI cell under non-faradaic condition yields a charge efficiency of 0.96, nearing the theoretical maximum. Introducing faradaic condition reduces charge efficiency to 0.88. As co-ion expulsion is not significant in MCDI, faradaic reactions could be the reason for decreased charge efficiency. The desalination time figure 4.4b is slightly different from that of figure 4.3b due to different cell resistance when the cell is rebuilt between experiments.

4.3.2 Near electrode pH: non-faradaic condition

Next, we examined pH changes near the electrodes under both non-faradaic and faradaic conditions, which are shown figure 4.5. The pH measurements, conducted 100 micrometers away from the electrode surface, provide a representation of pH changes in the macropores of the carbon electrode.

We qualitatively compared our observations with the theoretical pH predictions by Dykstra et al. (2017) under non-faradaic condition, specifically comparing our experimentally measured pH with the pH predicted in the macropores of carbon electrodes by Dykstra et al. The comparison reveals that in the anode, the measured direction of pH changes aligns with the theoretical prediction for non-faradaic condition—indicating a pH increase during charging and a subsequent decrease during discharge (figure 4.5c). In contrast, in the cathode, the theoretical prediction shows a pH decrease during charging and an increase during discharge (figure 4.5d), exhibiting inverted behavior compared to the measured cathode pH in this study (figure 4.5b).

To confirm the accuracy of pH directions in cathode, we conducted an experiment in which the pH was measured a few millimeters above (approximately 4 mm) the cathode in a larger open cavity filled with NaCl solution (approximately 1.8 ml) as illustrated figure S4.1. The cavity was filled with an NaCl solution and purged with N_2. Before starting the MCDI operation, the pH measured in the cavity is the same as the feed pH. The N_2 purging was stopped just before the pH was measured to avoid disturbance during the measurement. Remarkably, the observed direction of pH changes during charging and discharging remained consistent with the direction measured at a distance of 100 µm, despite the minimal magnitude of pH changes due to the increased volume of NaCl as shown figure S4.1. This

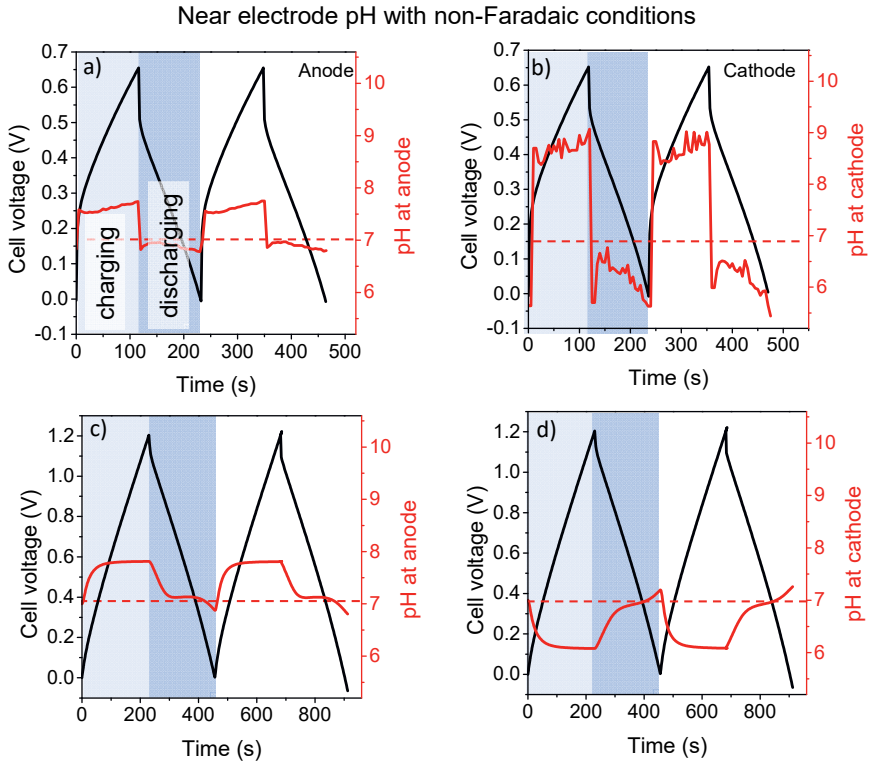

Figure 4.5. Cell voltage and experimentally measured pH under non-faradaic condition in anode (a) and cathode (b) compared with theoretically predicted effluent pH by Dykstra et.al (2017) for non-faradaic condition in anode (c) and in cathode(d).

observation confirms the reliability of the direction of pH changes measured in the cathode.

Additionally, we also carried out experiments with pH indicator using conventional CDI setup without membranes and using constant voltage mode to enable studying pH changes at electrode boundaries using color changes on the pH indicator containing feed water as mentioned in the methods section. The color change on the pH indicator at the electrode spacer boundaries can represent the pH changes in the electrode. Figure 4.6 shows the red color intensity and related pH from the anode boundary to the cathode

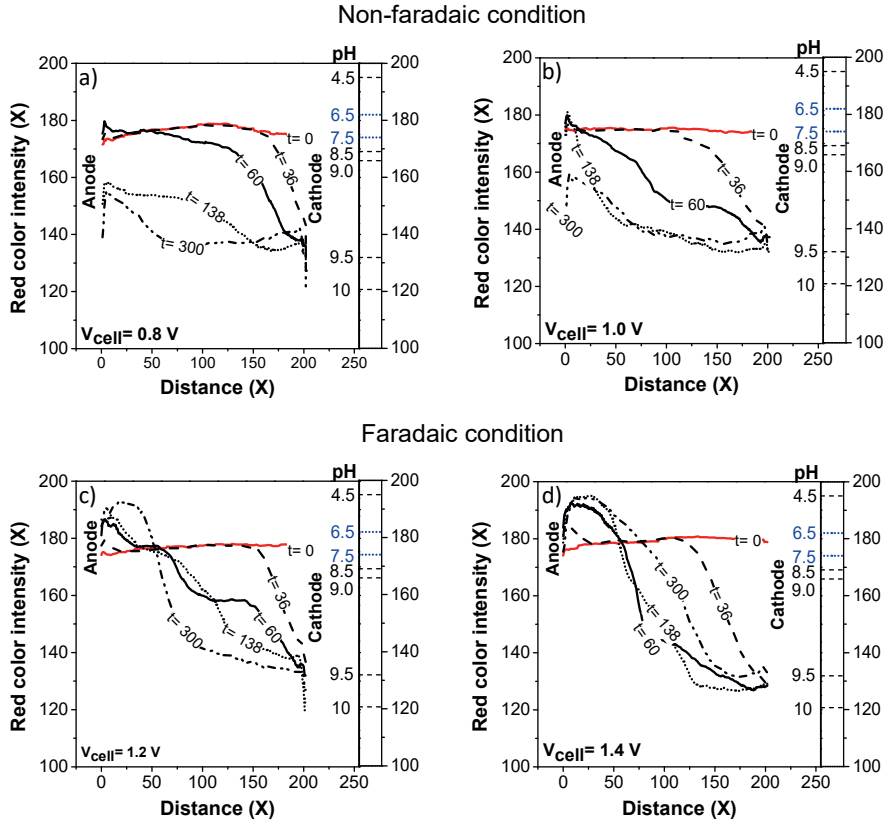

Figure 4.6. Red colour intensity from the captured pictures of pH indicating dye experiments under non-faradaic condition (a&b) and under faradaic condition (c&d)

boundary at various times during charging step. Multiple experiments were carried out with non-faradaic voltages (i.e., 0.8 and 1 V) and with faradaic voltages (1.2 and 1.4 V). The pH at t=0 is the feed pH which is around 7 in all cases.

Figure 4.6a and b shows that, when the cell is charged with the non-faradaic condition (cell voltage of 0.8 V), the pH in the anode and the cathode pH slowly shifts towards basic pH over time. Interestingly, the direction of pH changes in the anode and cathode (i.e., shift towards basic pH) is in line with experiments carried out using micro pH sensors. The pH directions observed at cathode from the experiment with MCDI using ultra micro pH sensor and the experiment with CDI using pH indicator should not be compared directly. However, the observation from both of these experiments indicates that the direction of the pH changes at cathode is different from what was predicted theoretically. The reason behind the difference between experiments and theoretical prediction is still unclear.

4.3.3 Near electrode pH: faradaic condition

We also conducted pH measurements near the electrode surface under faradaic condition. When faradaic condition is applied, the pH in the electrode compartments shifts from feed pH to acidic or basic pH over successive desalination cycles as shown figure S4.2. Under faradaic condition, all possible anodic reactions will result in acidic pH due to production of H^+ ion (or, consumption of OH^- ion) as described in table 4.1. Similarly, all cathodic reactions as described in table 4.1 will result in basic pH in the cathode due to consumption of H^+ ion (or production of OH^- ion). The H^+ ions produced in anode are effectively blocked by AEM resulting in the buildup of H^+ ion concentration in the anode making it acidic even during discharge. Similarly, the OH^- ions are blocked in the cathode by CEM resulting in basic pH at the cathode.

During faradaic condition, charging step has a non-faradaic regime i.e., cell voltage before the onset of faradaic reactions and a faradaic regime i.e., the

cell voltage after the onset of faradaic reactions. Discharging step also has both regimes. In the non-faradaic regime, the directions of the pH changes near the electrode should follow the trend observed for non-faradaic condition figure 4.5. In the faradaic regime, the pH behavior should deviate due to the faradaic reactions.

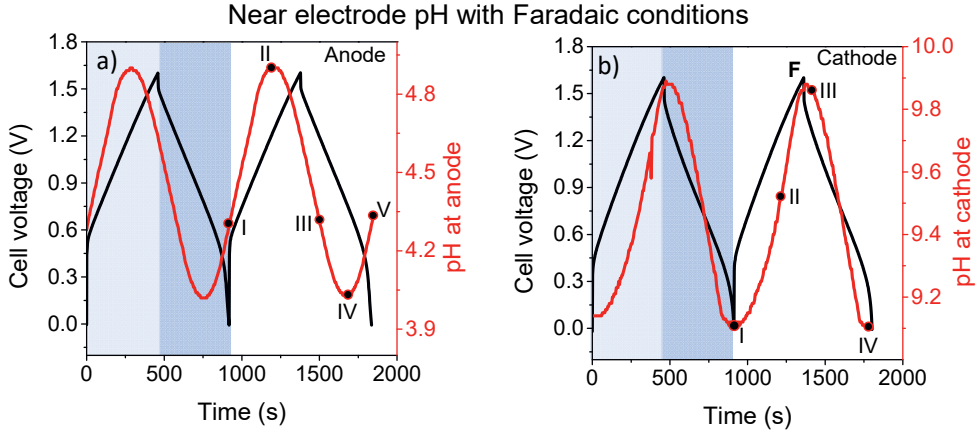

Figure 4.7. Cell voltage and experimentally measured pH changes near anode (a) and cathode (b) under faradaic conditions

Figure 4.7 shows pH changes in the anode and cathode under faradaic condition. As anticipated, the pH near the anode shifts to acidic pH while the pH near the cathode turns basic, confirming the presence of faradaic reactions. Figure 4.7a shows that, in the anode, while charging, the pH between points I and II (i.e., non-faradaic regime; < 1.2 V), follows the non-faradaic trend, i.e., pH increase. However, between point II and III which includes rest of the charging step and initial discharging step, the pH starts to decrease indicating faradaic reactions. When the cell voltage again reaches the non-faradaic regime during the rest of the discharging step between III and V, the pH should decrease as seen in non-faradaic experiments. However, the pH decreases only between point III and IV before starting to increase between IV and V. Although the exact mechanism causing the pH increase between IV and V is unclear, the low cell voltage during pH increase indicates that the increase must be due to non-faradaic process(es).

Meanwhile, in the cathode (figure 4.7b), the pH in the non-faradaic regime (i.e., between point I and II) increases in line with observations from non-faradaic experiments. When the cell voltage reaches the faradaic regime (point between II and III) during charging step and the beginning of discharge step, the pH keeps increasing due to faradaic reactions. When the cell voltage falls in the non-faradaic regime again (between point III and IV), the pH decreases in line with previous observation from non-faradaic condition.

The experiments with pH indicators also confirm that the anode reaches acidic pH and the cathode reaches basic pH when faradaic condition is applied, figure 4.6c and d.

4.4. Conclusion

In conclusion, our desalination experiments with NaCl feed water in MCDI revealed distinctive pH changes in various compartments, including the anode, cathode, and effluent. We studied pH changes under two experimental conditions: non-faradaic and faradaic. Under non-faradaic condition, both anode and cathode pH fluctuated around the feed pH, with a pH increase during charging and a pH decrease during discharging. Notably, the cathode pH exhibited the same pH direction as the anode pH. This observation is different from the theoretical predictions in the literature where anode and cathode pH changes are opposite in direction. Under faradaic condition, the anode pH became acidic, while the cathode pH turned basic due to H^+ and OH^- ions production by the faradaic reactions. When the cell is charged, until the onset of faradaic reactions the pH in the electrode compartment followed non-faradaic pH trends, but deviations occurred when faradaic reactions started to take place. This understanding about pH changes in MCDI compartments can help to reduce mineral scaling and to facilitate the removal of pH-sensitive compounds, such as boric acid.

Annex C

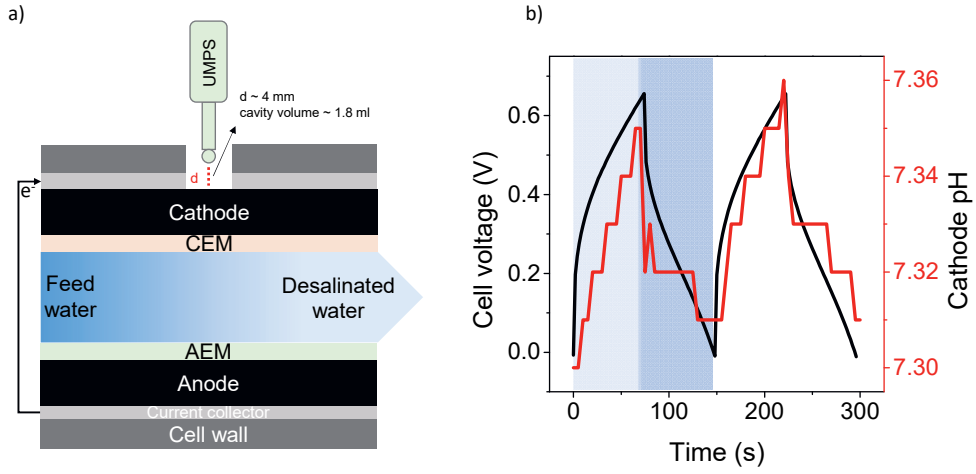

Figure S4.1. Schematic representation of pH measurements with larger cavity (a) and the measured pH (b)

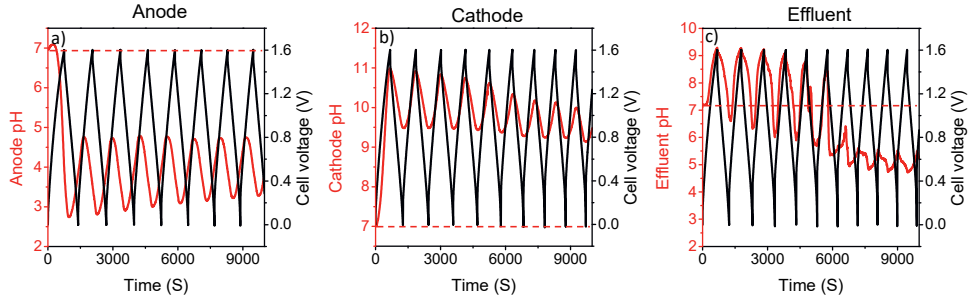

Figure S4.2. The pH changes at anode (a), cathode (b) and effluent (c) during initial desalination cycles under Faradaic conditions.

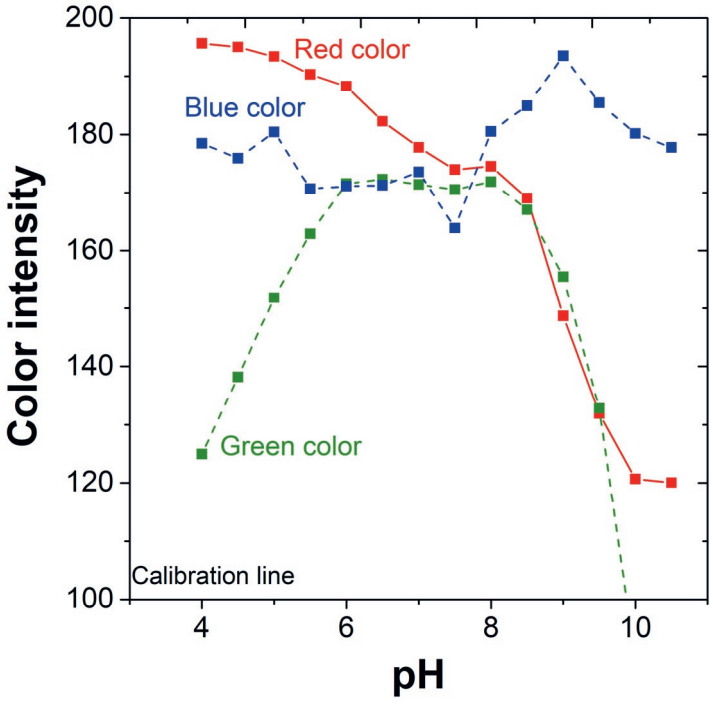

Figure S4.3. Calibration of Red, blue and green color intensities with respect to pH

Chapter 5. Exceptional Water Desalination Performance with Anion-selective Electrodes

This chapter was published as:

Antony C. Arulrajan, Deepika L. Ramasamy, Mika Sillanpää, Albert van der Wal, P.M. Biesheuvel, Slawomir Porada, and Jouke E. Dykstra. Exceptional Water Desalination Performance with Anion-Selective Electrodes. *Adv. Mater*. 1806937 (2019)

Abstract

Capacitive Deionization (CDI) typically uses one porous carbon electrode that is cation-adsorbing and one that is anion-adsorbing. In 2016, Smith and Dmello proposed an innovative CDI cell design based on two cation-selective electrodes and a single anion-selective membrane, and thereafter this design was experimentally validated by various authors. In this design, anions pass the membrane once, and desalinated water is continuously produced. In the present work, this idea is extended, and it is experimentally shown that also a choice for anion-selective electrodes, in combination with a cation-selective membrane, leads to a functional cell design that continuously desalinates water. Anion-selective electrodes are obtained by chemical modification of the carbon electrode with (3-aminopropyl)triethoxysilane. After chemical modification, the activated carbon electrode shows a substantial reduction of the total pore volume and BET surface area, but nevertheless maintains excellent CDI performance, which is the first time that a low porosity carbon electrode has been demonstrated as a promising material for CDI.

5.1. Introduction

Capacitive Deionization (CDI) is a method of water desalination based on electrodes that adsorb ions and later release them again.[36,125] Traditionally, CDI uses a cell design with one electrode that adsorbs and releases the cations (cathode), and another electrode that adsorbs the anions (anode). Unmodified carbons do not have a significant natural preference for the adsorption of either anions or cations, but instead can adsorb both, dependent on electrode potential.[126,127] A design with two such unmodified carbons can be used to desalinate water. However, because of the large co-ion expulsion effect, the charge efficiency of such a cell is low, and thus much charge is needed to achieve a certain desalination performance.[37]

To enhance charge efficiency, and thus to reduce the energy input corresponding to a certain desalination performance, it is advantageous to make the electrodes ion selective, either for anions or cations. This can be done by chemically modifying the electrodes,[55,93,128–133] or by placing ion-exchange membranes (also called ion-selective membranes) in front of the electrodes: an anion-exchange membrane in front of the anode, and a cation-exchange membrane in front of the cathode. In this way, one electrode becomes cation selective, the other anion selective. Another option is to use intercalation materials, for instance based sodium manganese oxide (NMO) or Prussian Blue analogues (PBA; e.g., nickelhexacyanoferrate).[134] These materials are cation-selective, thus can be used as the cathode. In typical cell designs with such selective electrodes, a cell is built with one anion-selective, and one cation-selective electrode. Typically, we have a spacer channel between two electrodes, and during half of the cycle time we adsorb salt ions, and during the other half, salt ions are released. If membranes are used, an ion typically passes a certain membrane twice, once during adsorption, and once during desorption.

In 2016, Smith and Dmello published their theoretical report that showed that a novel, and very different, CDI cell design is possible. In this design both electrodes are purely cation selective, and one anion-exchange membrane is

used, which is placed between two spacer channels.[135] In 2017, this cell design was experimentally validated by various authors using electrodes based on intercalation materials,[134,136,137] or using porous carbon electrodes coated with a cation-selective resin.[138] In this design, only anions pass the membrane, and do so only once in a cycle, while at the same time cations are adsorbed in one electrode and simultaneously released in the other. Therefore, while a certain moment channel 1 is desalinating and channel 2 is producing

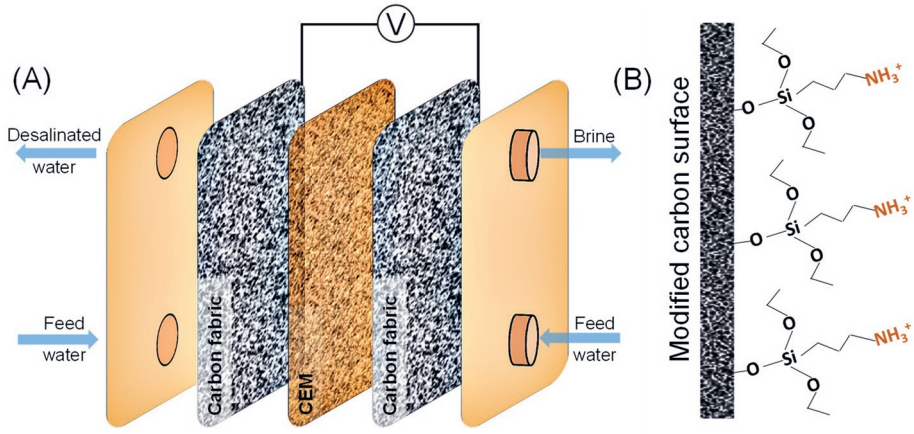

Figure 5.1. A) Schematic overview of desalination with anion-selective electrodes with a single cation exchange membrane (CEM) and two identical activated carbon fabric electrodes, either both modified or both unmodified. In this cell, water flows through the porous electrodes [162]. When current runs in one direction, one channel produces desalinated water (freshwater), while the other produces concentrate (brine). When a certain voltage is reached, the direction of the current is reversed until a lower endpoint for voltage is reached, and now freshwater is produced in the channel that previously was producing concentrate, and vice-versa. (B) Schematic view of modified carbon surface with silanes bearing terminal amines.

a concentrated stream, when the current direction is reversed, channel 1 now produces brine and channel 2 produces water of a lower salinity. Thus, at all moments in time, desalinated water is produced. In this design, intercalation electrodes based on NMO and PBA are used that are cation selective, but as we argue below, this concept is more general and can be extended to other electrode types.

In the present work we extend the approach of Dmello and Smith, which is based on cation selective electrodes, and we show that also a reverse design is possible, using anion selective electrodes and a cation-exchange membrane (figure 1). We will show that desalination is possible with unmodified carbon electrodes (which have no significant natural preference for either anion- or cation-adsorption) and with carbon electrodes modified by silylation with an amino silane (covalent attachment of silane), which results in a positive chemical charge on the surface of the electrode material (neutral and acidic pH conditions) that makes the electrode anion-selective.

5.2. Materials and methods

5.2.1. Cell assembly and desalination experiments

For the desalination experiments, we used either the unmodified (ACC 5092-15, Kynol, Germany) or modified electrodes (chemical modification with silanes bearing a terminal amine group) in a symmetric cell where the same type of electrode was used both as anode and cathode. A cation exchange membrane (CEM, Neosepta CMX, ASTOM Corp., Japan) was placed between these two identical electrodes (See table 5.1 for details). Graphite sheets were used as current collectors to connect the electrodes with the external electrical circuit and a potentiostat (Ivium Technologies, The Netherlands). A salt solution was pumped through both electrodes, see figure 1, by Stepdos 08 RC dosing pumps (KNF Neuberger) with a flow rate of 4 mL/min per channel. The feed solution contains 20 mM of NaCl. The conductivity of the effluent of both channels was measured with an interval time of 1 s. We conducted constant current (CC) experiments[139,140] by alternatingly applying a constant positive current until a pre-set upper cell voltage, $V_{cell} = V_{max,}$ was reached, and thereafter applying the reversed current until the cell voltage reached the same pre-set value but with opposite sign, $V_{cell} = -V_{max}$. To analyze the desalination performance, we use the following metrics: average salt adsorption rate, ASAR; productivity, P; average current efficiency, λ; and energy consumption, EC, with and without considering the potential for energy recovery.

5.2.2. Electrode modification

The electrodes were chemically modified by a silanization reaction between silylating agent and hydroxyl groups on the carbon surface.[141] In the present work, we have used a non-aqueous solvent to attach silane groups onto the carbon surface, similar to previously reported procedures for surface modification of carbon material and inorganic nanoparticles with silanes.[141–144] To prepare the modified electrode, the electrode material (12 g) reacted with 150 mL of amino-silylating agent, APTES, (3-aminopropyl)triethoxysilane (99%, Sigma Aldrich, USA) in Toluene (99.8%, anhydrous, Sigma Aldrich, USA) solution (30% v/v in toluene solution) in an airtight container, which was stirred at 120 rpm for 24 h to ensure maximum chemical modification of the carbon surface. The modified electrode was washed multiple times with ultrapure water and thereafter dried at room temperature.

5.2.3. Electrode characterization

The electrode characterizations were done using a Fourier Transform Infrared Spectroscopy instrument (FTIR, Vertex 70 by B Bruker Optics), with a scanning rate of 100 scans/sample in ATR mode, ranging from 400 to 4000 cm^{-1}, with a 4 cm^{-1} resolution. To determine the mass fraction of N and H of the electrodes, an organic elemental analyzer (Flash 2000 Thermo Scientific, Germany) was applied. The sample mass of 2-3.5 mg was taken in tin capsules for organic elemental analysis (furnace temperature – 950 °C). An X-ray diffractometer (PANalytical-empyrean diffractometer) helped attain the diffraction patterns of the electrodes, where a Co K-α radiation source (λ = 1.78 Å) in the 2Θ range of 5-120° was employed with a 0.01° step size. The obtained data was manually converted to the Cu K-α radiation (λ = 1.54 Å) to better match the data with literature reports. Brunauer–Emmett–Teller (BET) surface area analyzer (Micromeritics Tristar® II plus) was used to measure the physical properties of the materials, i.e. surface area, pore size and volume. The N_2 adsorption–desorption isotherms measurements were performed at a temperature of 77 K. The samples were degassed over a

period of 12 hours, at 60 °C in vacuum (VacPrep), before the BET analyses. The scanning electron microscope (SEM) imaging and energy dispersive X-ray spectra (EDS) were obtained from JSM-6480 LV electron microscopy (JOEL, USA) equipped with X-act SSD-10 mm^2 EDS detector (Oxford Instruments, UK).

5.2.4. Boehm titration experiments

To quantify the basic functional groups on the carbon surface, we titrated the modified and unmodified electrode material using the Boehm's method. To that end, 0.5 g of the electrode material was submerged into 50 mL of HCl solution (0.1 M) for 24 hours, which was occasionally shaken to neutralize the basic surface groups on the carbon surface. Thereafter, 40 ml of solution was filtered, and the filtrate was titrated slowly by dosing 0.6 ml of 0.1 M NaOH solution every 3 to 5 minutes by an automatic titration station (Metrohm 888 Titrando). To eliminate the influence of atmospheric CO_2 on the titration curves, experiments were conducted under gaseous N_2 atmosphere. After titrating the filtrate, a solution of 40 mL of 0.1 M HCl was titrated, following the same procedure as described for the sample. To calculate the amount of basic functional groups in the carbon sample, we determined the volume of titrant required to obtain the equivalence point, both for the sample and blank, and we subtracted the second from the first value.[3,4] The resulting value was then multiplied with the concentration of the titrant and thereafter divided by the mass of the sample to obtain a value for the concentration of the basic functional groups on the carbon surface.

5.2.5. Analysis of the desalination performance

To analyze the desalination performance, we calculate for each experiment the average salt adsorption rate, ASAR, the water productivity, P, and the energy consumption, both with and without considering energy recovery during discharge. To calculate ASAR, we integrate the difference between the inflow salt concentration, c_{inflow}, and the effluent salt concentration, c_{eff}, over time, of the channel that is desalinating ($c_{\mathrm{eff}} < c_{\mathrm{inflow}}$). The resulting

value is multiplied with the flow rate through the channel, Φ_v, and divided by the duration of the period when $c_{eff} < c_{inflow}$ for this channel, and by the surface area of the cell, A_{cell}, to come to a value of ASAR in μmol/min/cm^2. Values for current density are reported in A/m^2, and are calculated by dividing the cell current by Faraday's constant, F, and by A_{cell}. The water productivity is calculated by dividing the flow rate of one channel (during operation, one channel produces desalinated water), Φ_v, by A_{cell}.

The energy consumption with 100% energy recovery is calculated by multiplying the current and voltage signal, and integrating the resulting signal over time, for one full cycle, which includes a discharge step, when a negative current runs and V_{cell} goes from V_{max} to $-V_{max}$, and a charging step, when a positive current runs and V_{cell} goes from $-V_{max}$ to V_{max}, where V_{max} is a pre-set value for the maximum cell voltage. To calculate energy consumption without recovery, we only integrate the product of the current and voltage signal for the periods that current and voltage have the same sign. The values for energy consumption are reported in Wh/m^3 water produced.

5.3. Theory

To describe the experimental results, we derive a dynamic model including transport of ions across the ion exchange membrane (IEM), and the adsorption of ions in the micropores of the carbon electrodes. We model two electrode compartments, separated by an IEM, see figure 1 (manuscript). We assume that the aqueous phase in the electrode compartments is well-mixed, thus, we do not consider concentration gradients across the electrode, both in the direction of the flow, or in the direction perpendicular to the flow. To model ion adsorption in the electrodes, we use the amphoteric Donnan (amph-D) model, which has shown to describe experimental data well.[55,84,140] The amph-D model considers two types of pores: the macropores, where electroneutrality holds for the electrolyte, and where the salt concentration is equal to the concentration in bulk solution (if the assumption is made that there are no concentration gradients across the electrode); the micropores, where electronic charge is stored in the carbon, and is compensated by

chemical charge on the surface of the electrode material, and by ionic charge stored in the electrical double layers.

The amph-D model describes two types of micropore regions: the acidic region, A, which contains negative chemical surface charge, and the basic region, B, which considers positive chemical surface charge. We consider that the electrolyte contains only one monovalent salt.

Firstly, for each electrode compartment, we set up an overall mass balance for one of the ions present in solution. The overall mass balance includes the ions present in the macropores and micropores of the electrode, and is given by

$$p_{\mathrm{mA}} \cdot \frac{\partial c_{\mathrm{mA}}}{\partial t} + p_{\mathrm{mi}} \sum_{R=A,B} \alpha_R \cdot \frac{\partial c_{\mathrm{mi},R}}{\partial t} = \frac{\Phi_{\mathrm{v}}}{V_{\mathrm{elec}}} \cdot (c_{\mathrm{inflow}} - c_{\mathrm{mA}}) + z_{\mathrm{c}} \frac{A_{\mathrm{cell}}}{V_{\mathrm{elec}}} \cdot j_{\mathrm{ion}}. \quad (5.1)$$

where p_{mA} is the porosity of the macropores, p_{mi} of the micropores, c_{mA} is the ion concentration in the macropores (note that c_{mA} is the concentration of one ion, or the salt concentration, and not the total concentration of ions), and $c_{\mathrm{mi},R}$ is the ion concentration in region R in the micropores, where R can be A or B. Parameter Φ_{v} is the volumetric flow of electrolyte through the electrode compartment, c_{inflow} is the salt concentration in the influent, A_{cell} is the surface area of the electrode, j_{ion} is the flux of the ionic species across the ion exchange membrane and V_{elec} is the volume of the the electrode, given by $V_{\mathrm{elec}} = A_{\mathrm{cell}} \cdot L_{\mathrm{elec}}$, where L_{elec} is the thickness of the electrode. Parameter z_{c} gives the sign of the last term in Eq. (5.1), which is $z_{\mathrm{c}} = +1$ for the anode, and $z_{\mathrm{c}} = -1$ for the cathode.
The concentration of ions in the micropores is given by

$$c_{\mathrm{mi},R} = c_{\mathrm{mA}} \cdot \exp\left(-z_i \cdot \Delta\phi_{\mathrm{D,R}}\right). \quad (5.2)$$

where z_i is the valence of an ion and $\Delta\phi_{\mathrm{D,R}}$ is the dimensionless Donnan potential in region R. The ionic charge in the micropores, σ_{ionic}, is given by

$$\sigma_{\text{ionic},R} = \sum_i^{\square} z_i \cdot c_{\text{mi},R}. \quad (5.3)$$

Furthermore, for each micropore region electroneutrality holds

$$\sigma_{\text{ionic},R} + \sigma_{\text{chem},R} + \sigma_{\text{elec},R} = 0. \quad (5.4)$$

where σ_{elec} is the electronic charge density, and σ_{chem} the chemical charge density. The average electronic charge density in the acidic and basic region is given by

$$\sigma_{\text{elec,AV}} = \sum_{R=\text{A,B}}^{\square} \alpha_R \cdot \sigma_{\text{elec},R}. \quad (5.5)$$

We assume that no Faradaic reactions occur, and that the sum of $\sigma_{\text{elec,AV}}$ in the anode and cathode is equal to zero, thus $\sigma_{\text{elec,AV,AN}} + \sigma_{\text{elec,AV,CAT}} = 0$. The potential drop over the electrical double layer, $\Delta\phi_{\text{EDL}}$, which is the sum of the Donnan and Stern potential, $\Delta\phi_{\text{EDL},R} = \Delta\phi_{\text{D},R} + \Delta\phi_{\text{St},R}$, is the same for the acidic and basic region, thus $\Delta\phi_{\text{EDL,A}} = \Delta\phi_{\text{EDL,B}}$. To calculate the potential drop over the Stern layer, we use

$$\Delta\phi_{\text{St},R} \cdot V_{\text{T}} \cdot C_{\text{S}} = \sigma_{\text{elec},R} \cdot F. \quad (5.6)$$

where $\Delta\phi_{St,R}$ is the potential drop over the Stern layer in region R, C_S the Stern layer capacity, and V_T the thermal voltage, which is given by $V_T = \frac{RT}{F}$, where R is the gas constantand F the Faraday constant (note that, only in the last equation for V_T, we use symbol R for the gas constant; in the other equations R is used as an index for the micropore region). The evolution of the average electronic charge density is related to the ionic charge density across the IEM, j_{charge}, for one of the two electrodes; we give the relation for the anode (for the cathode, the right-hand side of Eq. (5.7) should be multiplied with factor “-1”)

$$p_{\mathrm{mi}} \frac{\partial \sigma_{\mathrm{elec,AV}}}{\partial t} = \frac{\mathrm{j_{charge}}}{L_{\mathrm{elec}}}. \quad (5.7)$$

Variable $\mathrm{j_{charge}}$ is related to the current density, I, in unit A/m^2 by $I = \mathrm{j_{charge}} \cdot A_{\mathrm{cell}} \cdot F$.

To describe the ion transport across the IEM, $\mathrm{j_{ions,mem}}$, we assume that the IEMs are in steady-state, and we use

$$j_{\mathrm{ions,mem}} = -\frac{D}{L_{\mathrm{mem}}} (\Delta cT_{\mathrm{mem}} - \omega X \Delta \phi_{\mathrm{mem}}). \quad (5.8)$$

where D is the diffusion coefficient of the salt, L_{mem} the thickness of the membrane, ωX the background charge of the membrane, ΔcT_{mem} the difference in the total ion concentration inside the membrane, between both sides of the membrane, and $\Delta \phi_{\mathrm{mem}}$ the potential drop over the membrane. The ionic current across the IEM is given by

$$j_{\mathrm{charge}} = -\frac{D}{L_{\mathrm{mem}}} (\langle cT_{\mathrm{mem}} \rangle \cdot \Delta \phi_{\mathrm{mem}}). \quad (5.9)$$

where $\langle cT_{\mathrm{mem}} \rangle$ is the average of the total ion concentrations on both sides of the membrane.

The flux of one ionic species, e.g. Na^+ across the IEM, j_{ion}, as used in Eq. (5.1), can be related to the total flux of ions across the membrane, $j_{\mathrm{ions,mem}}$, using $j_{\mathrm{ion}} = \frac{1}{2}\left(j_{\mathrm{charge}} + j_{\mathrm{ions,mem}}\right)$. On both sides of the membrane, we relate the concentration just inside the membrane (at the membrane -electrode compartment interface), to the salt concentration in the electrode compartment, by

$$cT_{\mathrm{mem}}^2 = \omega X^2 + (2 \cdot c_{\mathrm{mA}})^2. \quad (5.10)$$

Furthermore, at the membrane – electrode compartment interface, we have a Donnan potential, which is given by

$$cT_{\mathrm{mem}}^2 = 2 \cdot c_{\mathrm{mA}} \cdot \cosh\left(\Delta\phi_{\mathrm{D,mem}}\right). \tag{5.11}$$

Lastly, the cell voltage is related to all potential drops, using

$$\frac{V_{cell}}{V_{\mathrm{T}}} = \Delta\phi_{\mathrm{EDL},R}\big|_{\mathrm{an}} - \Delta\phi_{\mathrm{EDL},R}\big|_{\mathrm{cat}} - \Delta\phi_{\mathrm{mem}} - \Delta\phi_{\mathrm{D,mem}}\big|_{\mathrm{an}} + \Delta\phi_{\mathrm{D,mem}}\big|_{\mathrm{cat}}. \tag{5.12}$$

where subscript "an" refers to the anode, and "cat" to the cathode, and where R can be either A or B.

Table 5.1. Overview of parameters

Experimental parameters			
A_{cell}	Surface area of electrode and membrane	20	cm^2
L_{elec}	Electrode thickness	0.53	mm
L_{mem}	Membrane thickness	140	µm
c_{inflow}	Inflow salt (NaCl) concentration	20	mM
Φ_{v}	Solution flow rate through each electrode compartment	4	mL/min
ρ_{elec}	Electrode mass density Modified electrode Unmodified electrode	 0.39 0.51	 g/mL g/mL
R	Gas constant	8.314	J/mol/K
F	Faraday's constant	96485	C/mol
Theoretical parameters			
D	Average diffusion coefficient of NaCl	$1.68*10^{-9}$	m^2/s
ωX	Background charge of the cation exchange membrane	-4	M

$C_{St,vol}$	Stern layer capacity	160	F/mL
p_{mi}	Microporosity	0.19	
p_{mA}	Macroporosity	0.61	
σ_{chem}	Chemical surface charge unmodified electrodes Acidic region Basic region Chemical surface charge modified electrodes Acidic region Basic region	 -50 +450 +450 +900	mM

5.4. Results and Discussion

5.4.1. Electrode material characteristics

The electrode was subjected to various material characterization to understand material properties as shown in figure 5.2. The SEM image (figure 5.2A) shows that the structure of the surface of the electrode did not change much after modification, and thus that the modification is uniform and thin. The SEM-EDS elemental mapping (figure S5.2) of Si and C gives evidence for the uniformity of chemical modification with silane. The N_2 adsorption and desorption isotherms as function of relative pressure P/P_o at 77 K are presented in figure 5.2b and the pore volume distributions are presented in figure 5.2C. The unmodified electrode shows the characteristics of microporous materials, exhibiting a Type I Langmuir monolayer isotherm (IUPAC classification). The unmodified electrode has a BET surface area of 1100 m^2/g and a pore volume of 0.55 mL/g. The surface area (~18 m^2/g) and pore volume (7.0 μL/g) of the modified electrode are significantly reduced as a consequence of surface functionalization, probably due to the blocking of micropores by the (3-aminopropyl)triethoxysilane, APTES, modification. This is the first time that a low porosity carbon electrode has shown such excellent performance for desalination in CDI.

The ATR-FTIR spectra (figure 5.2d) of the modified electrode has peaks that were not observed for the unmodified electrodes. The peak at 665 cm^{-1} is

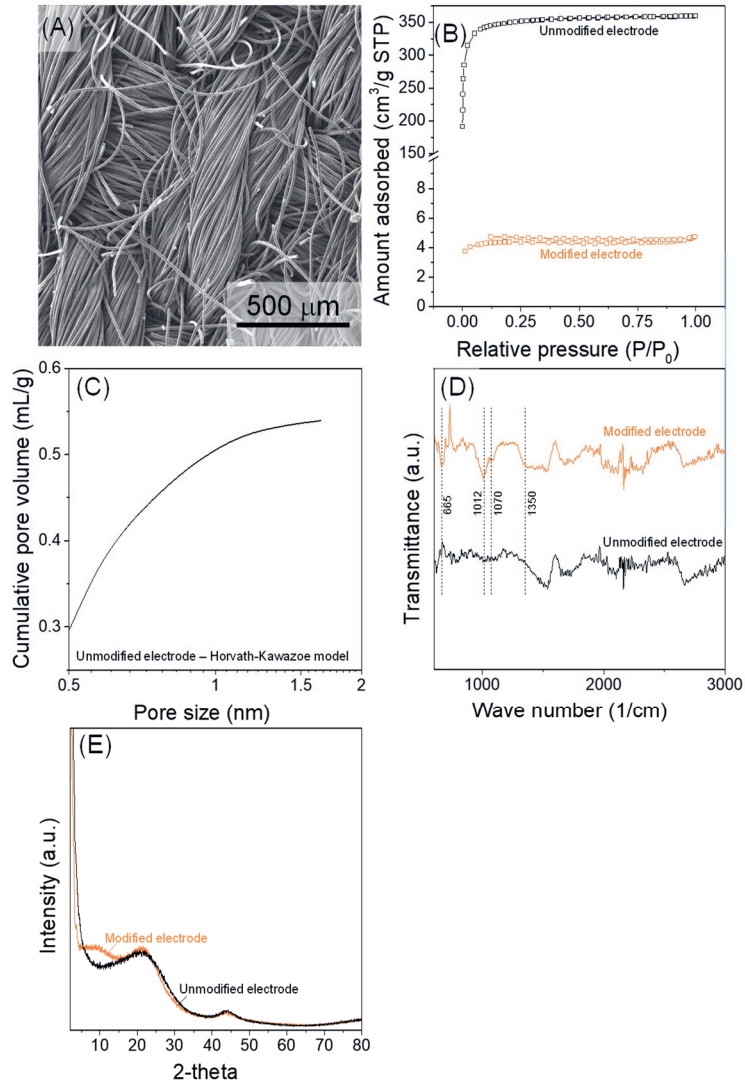

Figure 5.2. (A) SEM image of the modified electrode. (B) N_2 adsorption and desorption isotherms attained as function of relative pressure P/P_o at 77 K. (C) Pore volume distribution in the microporous region of modified electrode (D) ATR-FTIR spectra obtained of unmodified and modified electrodes. (D) XRD patterns of unmodified and modified electrodes.

related to Si-O-C bending vibration, and at 1012 cm^{-1} to Si-O-C stretching vibration.[145] The peak at 1070 cm^{-1} is due to the Si-O-Si stretching vibration.[146,147] Thus, these peaks confirm the presence of silane on the carbon surface. Furthermore, possible polymerization of APTES on the carbon surface is confirmed, as the presence of Si-O-Si bonds can be inferred from the spectra. In addition, there is a broad peak at 1350 cm^{-1} that is convoluted with the peak at 1550 cm^{-1}, which is due to the C-N stretching vibration.[146]

The XRD patterns (figure 5.2e) obtained for the modified and unmodified electrodes have the signature peaks of amorphous carbon (002) at 22.5^0 and graphitized carbon (101) at 44^0, and thus we can conclude that both electrodes contain a significant amount of graphitized carbon.[148] In addition, there is a broad peak around 10^o in the spectrum of the modified electrode that could be due to the silane modification of the carbon.

The elemental composition of the modified electrode is given in Table S5.1. The amount of N was determined by CHNS analysis, and the amounts of C, Si and O were determined by EDS analysis. Furthermore, figure S5.3 shows the results of cyclic voltammetry scans for the modified and unmodified electrodes.

5.4.2. Desalination performance

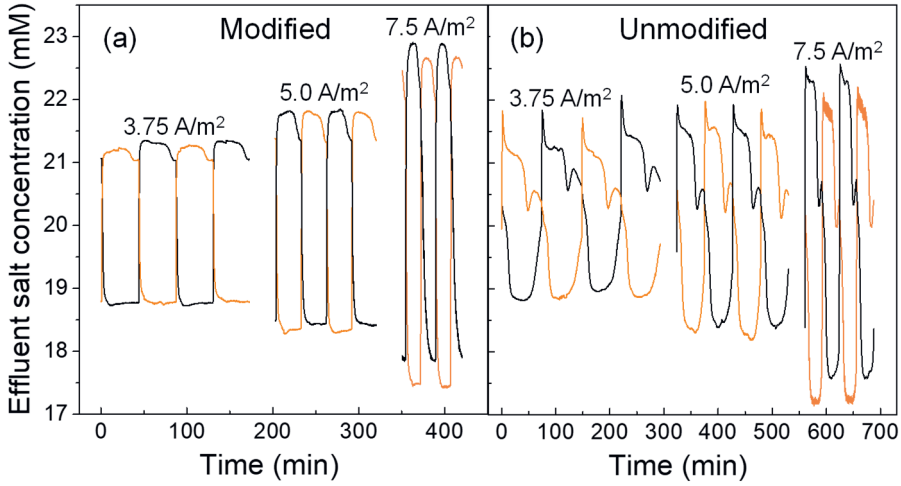

Figure 5.3. Continuous desalination using new cell design with modified electrodes (a) and unmodified electrodes (b). The black lines represents the effluent concentration from one side of the cell while the orange lines represents the effluent from the other side of the cell.

The new cell design with modified electrodes enables continuous desalination by producing desalinated water at one of the compartments at any given time (i.e., during charging as well as discharging) whereas with unmodified electrodes, though the desalination can take place, its efficiency is lower than the modified electrodes as shown in figure 5.3. During charging, one channel (black lines in figure 5.3) produces desalinated water which can be seen from the reduction in the effluent concentration while the other channel (orange line in figure 5.3) produces concentrated water which can be seen by the concentration increase in the effluent from the feed concentration of 20 mM. When the cell is discharged, the previously desalinating side started to produce concentrated water and the other side started to produce desalinated water resulting in continuous desalination during the operation of the cell. The cell voltage during charging and discharging are shown in figure S5.1.

To describe ion adsorption, the amphoteric Donnan model is used, which describes ion adsorption in electrical double layers located inside carbon micropores combined with the effect of chemical surface charge.[55,84,140] Figure 5.4 shows the dynamics of charging and discharge, experimentally and theoretically. We find that the time dependence of the effluent concentration

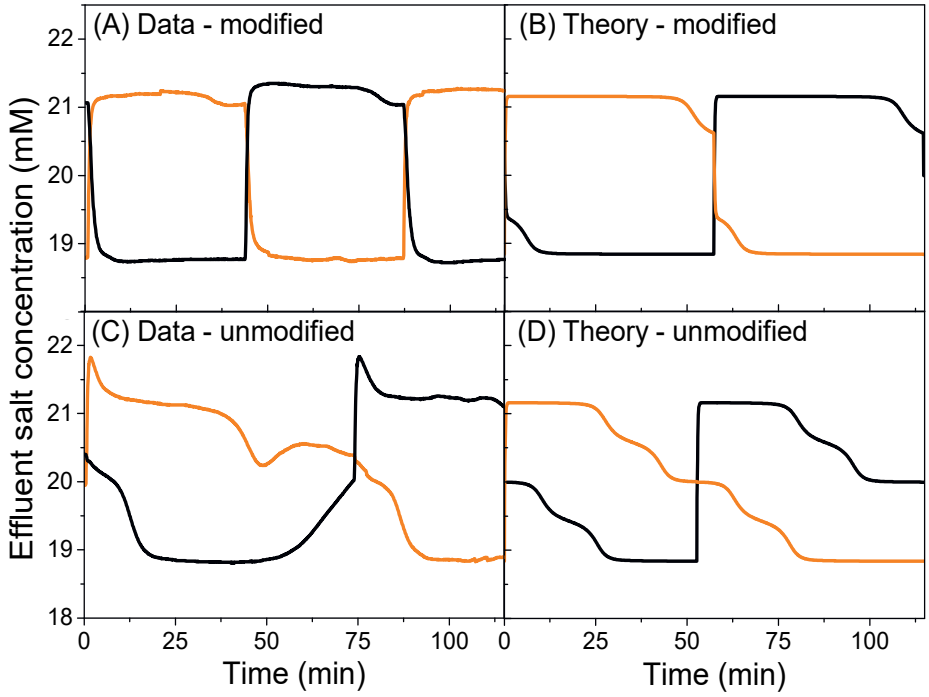

Figure 5.4. Effluent concentration of both channels (**Figure 5.3**) as function of time for the modified (A, B) and unmodified electrodes (C, D). Experimental (A,C) and theoretical (B,D) data are shown. During charging, the current density, I, was 3.75 A/m^2, and the pre-set upper cell voltage during charging V_{max}= 0.9 V. During discharge, both I and V_{max} have the same pre-set value but with opposite sign. Other parameters are listed in **Table 5.1.**

of both channels are well reproduced by the dynamic model (which includes the amphoteric Donnan approach for ion adsorption in carbon pores), both for the modified and unmodified electrodes. The theory reproduces that after switching from the charging to the discharge mode, the effluent salt

concentration rapidly increases in the channel that starts to produce a concentrated stream, and slowly decreases in the channel that is desalinating.

The desalination performance of the new cell design can be analyzed on the basis of the average salt adsorption rate (ASAR) and energy consumption (EC), which both depend on current density. We report results of ASAR in figure 5.5 and EC in figure 5.6, and we also plot the maximum theoretical current efficiency, $\lambda=1$, which is calculated by dividing ASAR by current density (after converting current to the unit μmol/min/cm^2). For $\lambda=1$, each electron transferred between the electrodes results in the adsorption of one cation and one anion when we have a monovalent salt. If λ has a value lower than unity, this must imply that undesired processes, such as co-ion desorption, also take place. We find, for unmodified electrodes, an average value (averaged over all experiments conducted with unmodified electrodes) of $\lambda \sim 0.80$ which is significantly below the theoretical maximum of $\lambda=1$. For the modified electrodes we find a much higher value, close to the theoretical maximum, of $\lambda \sim 0.99$.

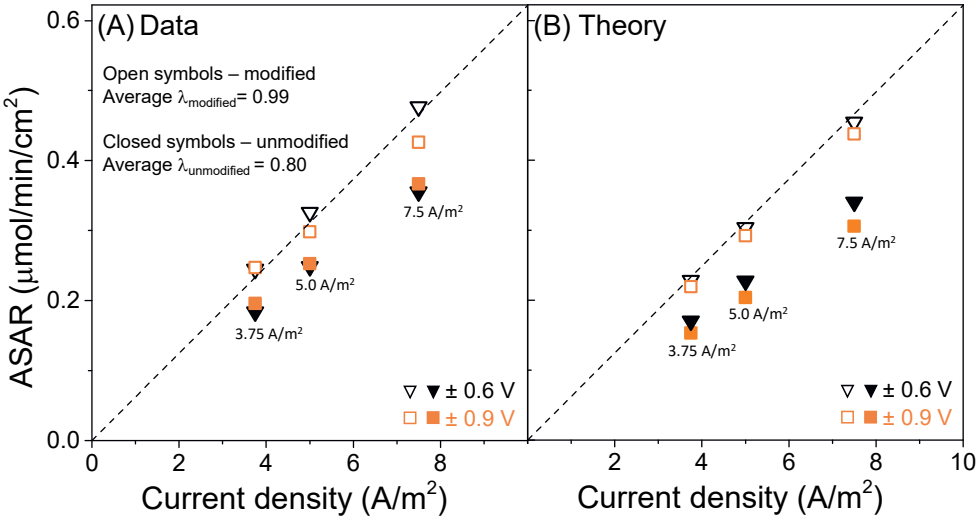

Figure 5.5. Average salt removal rate, ASAR, as function of current density for chemically unmodified and modified activated carbon electrodes and for different values of V_{max}, (A) experimental and (B) theoretical results. Current efficiency, λ, of unity is represented by the dashed line. Theoretical results are calculated using the amphoteric Donnan model.

As shown in figure 5.5, theory describes experimental data well, both for the modified and unmodified electrodes. In order to fit the theory to the data, we assume that the electrodes, also without modification, have a moderate concentration of positive chemical surface charge (see Table 5.1). For the modified electrodes, this positive charge is significantly increased, in line with results of Boehm titration, which reveal that the concentration of basic groups on the surface of the modified electrodes, ~0.91 mmol/g, is about two times larger than on the unmodified electrodes, ~0.43 mmol/g).

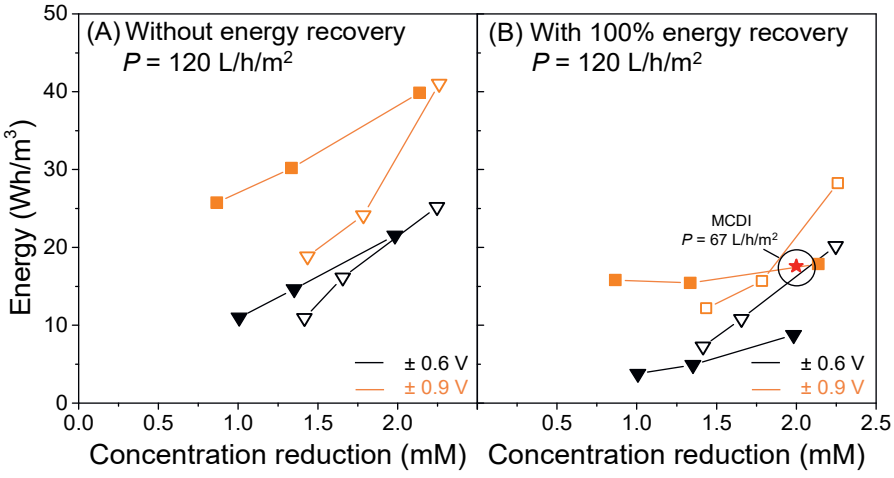

Figure 5.6. Energy consumption (EC) per m^3 of desalinated water produced of CDI with modified (open symbols) and unmodified electrodes (closed symbols), (A) without energy recovery (ER) and (B) with 100% ER. Values of EC for 100% ER are benchmarked against a standard MCDI system,[72] operated with a salt concentration reduction of Δc=2 mM and a lower water productivity of P_{MCDI}=67 L/h/m^2.

Figure 5.6 shows data for energy consumption (EC), both for modified and unmodified electrodes, with and without energy recovery (ER) during discharge. In figure 5.6 we show that EC for desalination with modified electrodes is lower, and we show that for V_{max} = 0.6 V EC is lower than for V_{max} = 0.9 V. Furthermore, we compare EC of our novel cell design with EC of a standard MCDI system.[72] We find that EC of our design is significantly lower, especially with modified electrodes and for V_{max} = 0.6 V. Compared to the standard MCDI system, we not only find lower EC, but also obtain a

much higher water productivity, which is the flow rate of desalinated water per membrane area, P = 120 L/h/m^2, instead of P = 67 L/h/m^2.

5.5. Conclusion

In conclusion, we demonstrated that a choice for anion-selective electrodes, in combination with a cation-selective membrane, leads to a functional cell design that continuously desalinates water. We showed that theory describes experimental data well, and we find that with 100% energy recovery, energy consumption of the new cell design is much lower than a standard MCDI system. Furthermore, we show that, after chemical modification, the porosity is reduced from 0.55 mL/g to 7.0 μL/g, and the BET-area of our electrodes is reduced from ~1100 m^2/g to ~18 m^2/g, while the desalination performance of the electrodes is increased. In conclusion, we demonstrated for the first time that a low porosity carbon electrode with additional surface charge as a promising material for CDI.

Annex D

Table S5.1. Elemental composition of modified and unmodified electrode

Element	Method	Unmodified electrode (wt%)	Modified electrode (wt%)
C	EDS	94.2	79.3
Si		0	4.75
O		4.5	8.36
N	Organic elemental analysis	0.4	2.5
H		0.8	2.45

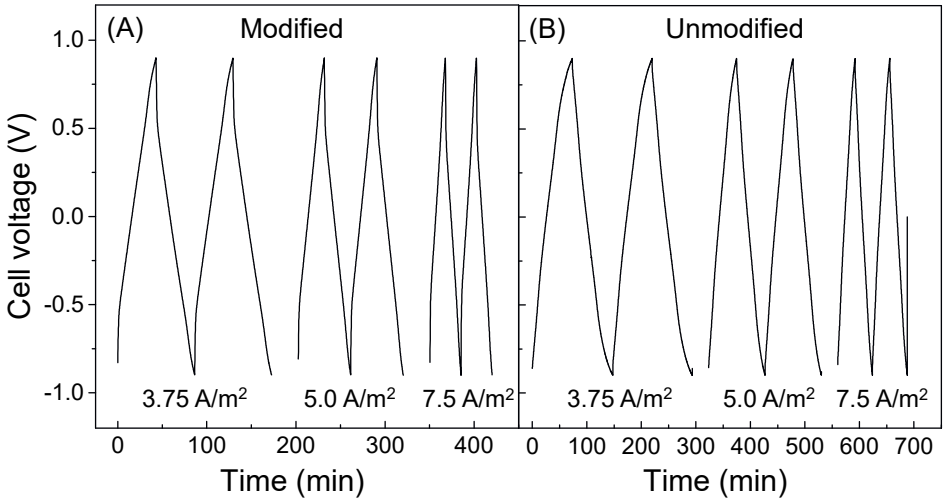

Figure S5.1. Cell voltage as function of time for desalination cycles using (A) modified and (B) unmodified activated carbon electrodes at a constant current of 3.75 A/m^2, and 5.0 A/m^2 and 7.5 A/m^2 in 20 mM NaCl.

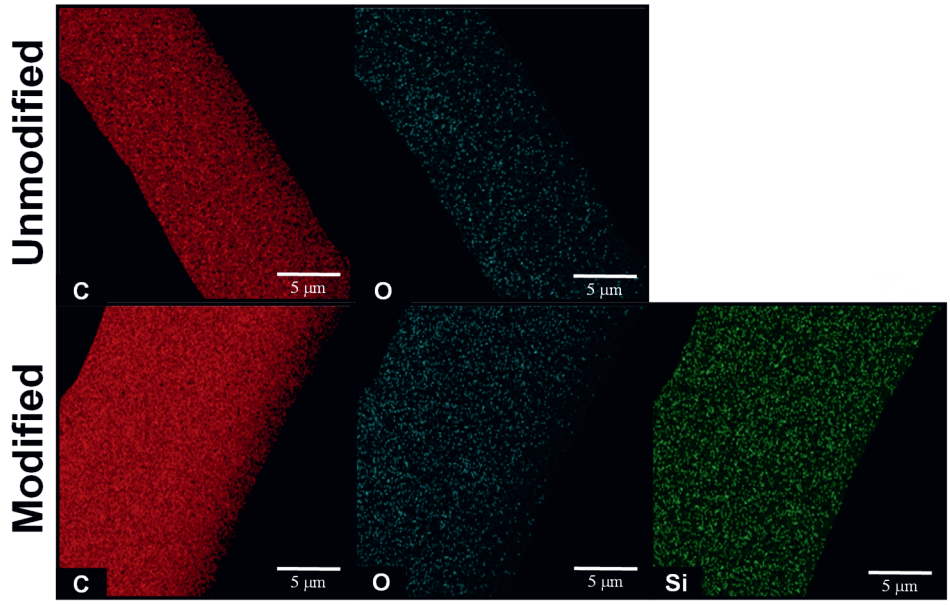

Figure S5.2. SEM-EDS elemental mapping of C, O and Si on both the unmodified and modified electrode.

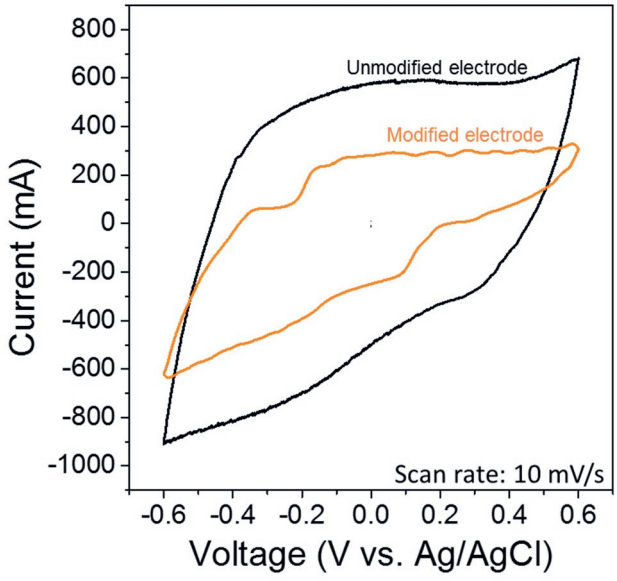

Figure S5.3. Cyclic voltammograms (CV) of the unmodified and modified electrode. Experiments were conducted in an electrochemical cell in a 3-electrode configuration. A porous separator was placed between the working and counter electrode. An Ag/AgCl reference electrode was used, and a platinum mesh counter electrode. The working electrode was either the unmodified or modified electrode (area 20 cm^2). The electrolyte was a 1 M Na_2SO_4 solution and was continuously pumped through the cell at a constant flowrate of 20 mL/min.

Chapter 6. General discussion and outlook

6.1. General discussion

Membrane Capacitive Deionization (MCDI) is an emerging electrochemical desalination technology which has a potential to be an alternative to conventional desalination technologies. However, to establish itself as a potential and sustainable solution for diverse applications, MCDI must address several critical challenges that hinders its development as an alternative as mentioned in the introduction of this thesis.

The challenges include scaling and fouling,[67,149] chemical usage for cleaning,[3] lack of ion-selectivity,[68] and the cost implications of scaling up.[150] All of these challenges are connected to the pH changes that occur during MCDI operation. Most existing studies carried out with NaCl solutions have identified faradaic reactions as primary cause for pH changes. However, it was also shown that non-faradaic processes can cause pH changes. Mineral scaling and associated salt removal efficiency loss are direct impacts of these pH changes. In addition, pH changes can also impact ion-selective removal especially for the ions that are pH sensitive. Therefore, it is important understand the exact reasons behind pH changes to effectively develop suitable mitigation strategies to control and manipulate pH changes. Though there have been attempts made to understand pH changes, there are knowledge gaps that limit effective solutions to pH changes. An important knowledge gap is that the pH changes were studied in model feed water (NaCl), and the understanding about pH changes during real brackish water desalination are limited.

Therefore, in this thesis, chapter 2 and 3 are focused on understanding pH changes during the desalination of real brackish water (i.e., tap water), aiming to identify the underlying mechanisms driving the pH changes, its consequences and potential solution. We showed the role of HCO_3^- ions on pH changes and the role of AEM thickness on reducing mineral scaling. In chapter 4 and 5, we studied pH changes in electrode compartments of MCDI during desalination of NaCl solution using a micro-pH sensor. We showed that, near the electrodes, the pH fluctuates around feed pH under non-faradaic

conditions and deviates to acidic and basic pH under faradaic conditions. Finally, we also demonstrated that pH sensitive chemical groups can be attached to activated carbon electrodes to improve their selectivity towards anions and to enable new cell designs.

In this chapter, we firstly discuss the findings of this thesis and its implications on the possible development of MCDI as a chemical-free desalination method for environmentally friendly and sustainable desalination, highlighting the importance of reducing chemical usage in water treatment. Secondly, we discuss the significance of the new insights gained on near electrode pH, the development of a new cell design, and the effect of these findings on the costs associated with water treatment using MCDI. Finally, we discuss avenues for advancement of MCDI technology in terms of scaling mitigation and ion-selectivity towards pH sensitive ions.

6.2. New understanding on effluent pH changes in MCDI and mineral scaling

Most existing studies on pH changes in MCDI are carried out in model feed water (i.e., NaCl) and concluded that faradaic reactions such as water splitting are the primary reason for pH changes in MCDI. Existing strategies proposed to limit pH changes were therefore focused to control the faradaic reactions. However, it is also possible that non-faradaic processes such as differences in ion mobilities can cause pH changes.

In this thesis, a model feed water (i.e., NaCl) as well as real brackish water (i.e., tap water with multiple ions present) are desalinated to study pH changes. An important observation made is that the effluent pH changes between NaCl and tap water are different in terms of the direction of pH changes. We showed that pH changes during NaCl desalination are due to the differences in ion mobilities (which is a non-faradaic process) between H^+, OH^-, Na^+ and Cl^- ions leading to a pH increase during charging and a pH decrease during discharging. Whereas with tap water desalination, the removal of HCO_3^- ions from the spacer channel (spacer channel) during

charging decreases pH and the increased concentration of HCO_3^- ions in the spacer channel during discharge increases the pH. The removal of HCO_3^- ions is also a non-faradaic process. This finding is contrary to the previous understanding that faradaic reactions are the cause of pH changes in MCDI.[88,114] Further investigation on pH changes revealed the role of HCO_3^- ions on pH changes during tap water desalination. The HCO_3^- ion is a constituent of DIC in tap water. The DIC concentration controlled by the chemcial equilibrium influences the tap water pH. The change in concentration of HCO_3^- ions resulting from its removal and up-concentration induces changes in the concentration of all other DIC species and thus results in pH changes.

As mentioned previously, pH changes have a direct consequence on mineral scaling. The pH increases during discharge (i.e., when concentrate is produced) can cause mineral scaling in the spacer channel due to the high concentration of hardness ions. We studied mineral scaling at different WR conditions and showed that the scaling increases with increasing WR. An increase in the thickness of the AEM is demonstrated as a strategy to decrease mineral scaling.

6.3. The implications of the understanding gained on effluent pH changes

6.3.1. A path towards chemical free MCDI operation

Mineral scaling poses a significant challenge in desalination technologies. This also applies to MCDI where salt removal efficiency is reduced and components such as electrodes and membranes degrade over time due to mineral scaling.[115,149,151,152] In CDI, during long-term operation, when mineral scaling and fouling occur, the impact on salt removal efficiency is significantly higher, i.e., an efficiency reduction from ~88% on day 1 to about 55% on day 15 of operation is found.[153] Similarly, when MCDI is used to desalinate water containing hardness ions such as Ca^{2+} and organic foulants, about 35% loss on salt removal was experienced over 15 days of operation.[149] When the cleaning procedure is performed by using anti-scaling chemicals,

the salt removal efficiency increased, back to the original level of 88%.[153] These anti-scaling chemicals are often costly and may negatively impact the aquatic system.[154]

In chapter 2 we showed that the mineral scaling can be minimised 1.35 times when two AEMs are placed on top of each other hence doubling the thickness. The reduction in mineral scaling indicates a proportional decrease in the frequency of cleaning cycles, subsequently reducing the amount of cleaning chemicals used and discharged into environment. This new approach paves the way for achieving chemical-free and sustainable desalination using MCDI.

6.3.2. The mineral scaling mitigation strategy and its effect on desalination costs

When comparing low pressure RO (LPRO) and MCDI for brackish water desalination, the sum of capital costs and operational costs (such as cleaning) for both the technologies are similar. However, the replacement costs of components (i.e., membranes) in MCDI is about 5 times higher than that of LPRO.[155] This indicates that the IEMs' replacement costs are significantly contributing to the overall water treatment costs. A model developed to calculate the technoeconomic feasibility of MCDI shows that when the IEMs' lifetime can be increased from 2 to 5 years, the water treatment costs can be decreased by 50% from ~0.5 $/m^3 to ~0.25 $/m^3.[150]

The mineral scaling mitigation strategy proposed in this thesis can help to reduce the costs of water treatment by MCDI systems by reducing the usage of cleaning chemicals and by increasing the lifetime of the electrodes and membranes. However, it is also important to understand that increasing the IEM thickness as a strategy to limit scaling can also increase the capital cost. Therefore, alternative cost-effective strategies as mentioned in 6.5.2 of this chapter have be developed to mitigate mineral scaling and reduce the costs of water treatment.

6.4. New understanding on near electrode pH changes

In chapter 4, we studied the pH changes near the anode and cathode during charging and discharging steps under faradaic and non-faradaic conditions, using NaCl feed water. We showed that under non-faradaic conditions, pH changes near the electrode fluctuate around the feed water pH, whereas under faradaic conditions, pH changes deviate from the feed pH and the pH reaches acidic values near the anode and basic values near the cathode. These insights on near electrode pH changes in MCDI can be used to control the operational conditions in such a way that it is suitable for removing pH-sensitive ions such as borates and phosphates which can exist either as ions (for example, BO_3^{3-} and PO_4^{3-}) or neutral species (for example, H_3BO_3 and H_3PO_4) depending upon the pH.

6.5. Implications of understanding gained on near electrode pH

6.5.1. Near electrode pH and electrode modification for ion-selective separation

Chapter 5 shows that chemical modification of electrodes (i.e., electrodes chemically modified with pH sensitive amino silane groups) can enable a continuous desalination cell design with both electrodes being anion selective. The introduction of pH sensitive chemical groups results in a significant improvement, offering a means to enhance the capacity of the electrodes while simultaneously improving selectivity towards specific ions.[156,157] In chapter 4, we showed that based on the applied voltage, faradaic or non-faradaic processes can be driven at the electrode, and that these processes can induce pH changes. By controlling the extent of these processes, one can manipulate the local pH and thus the adsorption and desorption of pH sensitive ions such as the group of phosphate ions, with species that are of different valency (i.e., PO_4^{3-}, HPO_4^{2-}, $H_2PO_4^{-}$).[158]

6.5.2. Near electrode pH on enabling new cell designs and its effect on desalination cost

When comparing desalination technologies in terms of economic feasibility and competitiveness, LCOW is used as a primary metric for technology comparison. The LCOW calculated for RO is 0.125 $/m^3 whereas the LCOW calculated for MCDI is 0.30 $/m^3.[46] The breakdown of LCOW of RO and MCDI is shown in figure 6.1. The IEM's capital expenditure (CapEx) and operational expenditure (OpEx) such as replacing the membranes are the primary factors behind the high LCOW of MCDI as they contribute to 65% of the LCOW. This implies that the further improvement of IEMs to reduce the costs and to increase its life span should be one of the primary focuses to improve the economic competitiveness of MCDI for brackish water desalination.

In Chapter 5 of this thesis, we demonstrated a novel continuous desalination system featuring two chemically modified electrodes and one CEM (i.e.,

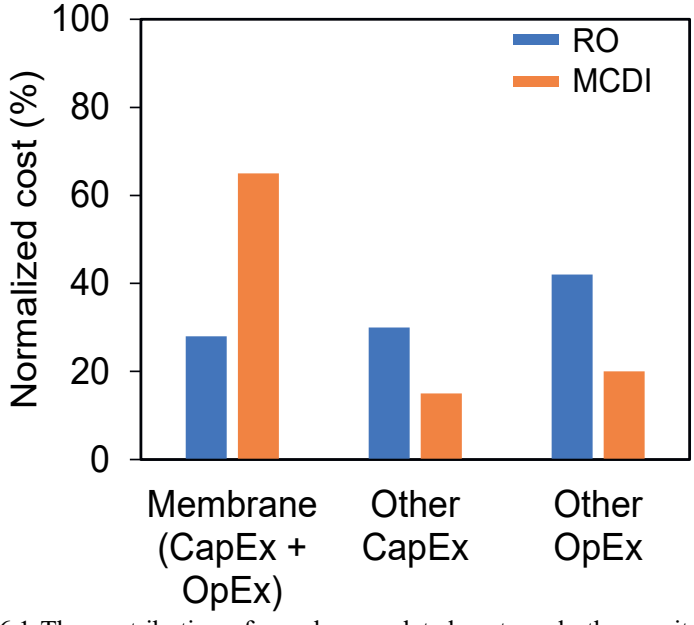

Figure 6.1 The contribution of membrane related costs and other capitol and operational expenditure to the overall LCOW of RO and MCDI.

single-IEM MCDI). This new design eliminates the need of an AEM from the conventional MCDI cell. Therefore, it is expected to have a proportional reduction in the cost contribution of IEMs to LCOW, decreasing from 65% to 32.5%.[46] The cost savings from reducing the number of IEMs can result in a proportional LCOW reduction to bring down the LCOW from 0.3 to ~0.2 $/m^3 as shown in figure 6.2. Though the LCOW of RO is still lower than the demonstrated single IEM MCDI, the novel configuration boasts twice the productivity (P) compared to standard MCDI cells, thereby offering additional cost savings by lowering the MCDI stack size and associated capital and operational costs to be competitive with RO.

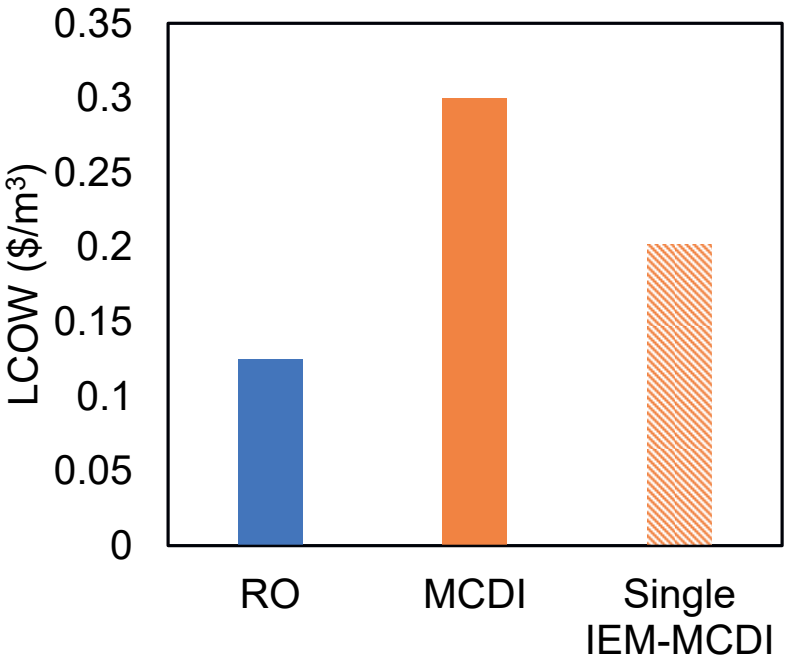

Figure 6.2. The calculated LCOW of RO, conventional MCDI and the expected LCOW of single-IEM MCDI design demonstrated in chapter 5.

However, as the water flows through the electrodes in this design, a notable challenge arises from the exposure of electrodes to dissolved oxygen in the water which can significantly impact the electrode degradation, thereby compromising the efficiency and lifetime of electrodes. A conventional CDI

cell operated at a charging voltage of 1.2 V and a discharging voltage of 0 V is shown to loose ~90 % of its initial salt adsorption capacity within 70 desalination cycles. [159,160] Therefore, further research is needed to understand the electrode degradation in such designs and to develop mitigation strategies.

6.6. Future perspectives

We have discussed the implications of understanding gained on effluent pH changes and near the electrodes. Though the understandings gained on this thesis gives valuable information for the improvement of MCDI technology, there is still a need for focused research on specific directions for further improvements of MCDI to overcome process limitations such as a lack of cost-effective mineral scaling mitigation strategies and improved ion-selectivity towards amphoteric ions. In this section, we discuss these focus points to set future research directions for further improvements on MCDI.

6.6.1. Way towards cost effective mineral scaling mitigation strategies

In this thesis, we showed that the increase on AEM thickness reduces mineral scaling. We also mentioned that increasing AEM thickness can increase the costs associated with IEMs. Therefore, in-depth research to understand the role of AEM on pH changes and associated mineral scaling in MCDI can lead to development of cost-effective mineral scaling mitigation strategies.

To understand the role of AEMs on influencing the pH changes, we carried out simple acid-base titration experiments on AEMs. Two separate AEM pieces are titrated with one having Cl^- as counterion while the other having HCO_3^- counterions (by equilibrating the membranes in NaCl or $NaHCO_3$ solution prior to titration experiments). The results revealed that the AEM loaded with Cl^- counterions displayed no additional buffer capacity while the AEM loaded with HCO_3^- counterions exhibited extra buffer capacity as can be seen in figure 6.3. This indicates that AEMs together with specific

counterions (i.e., HCO_3^- and CO_3^{2-}) possess buffer capacity in the spacer channel.

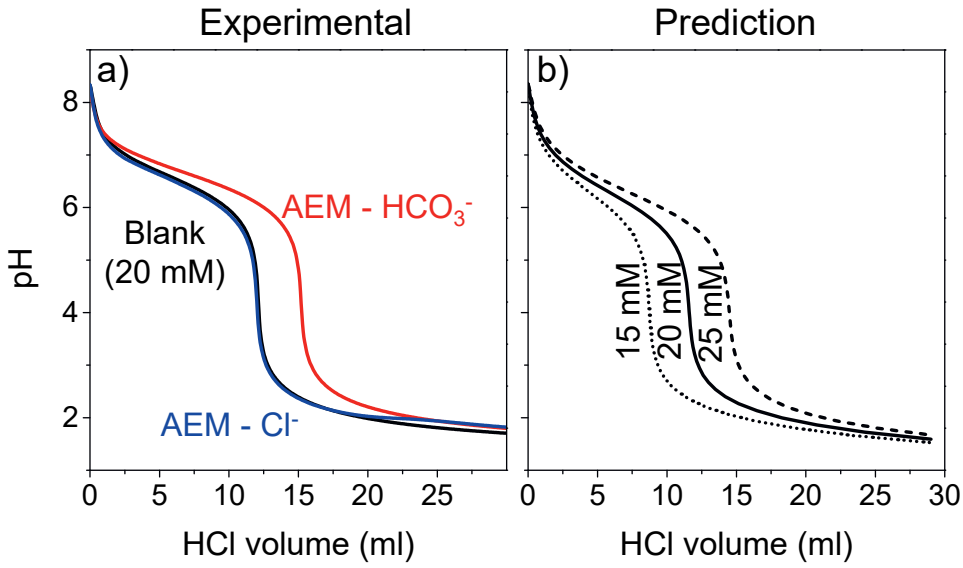

Figure 6.3. The titration curves of titrating AEMs with different counterion against HCl (a). Titration curves for various concentration of HCO_3^- ions present in the system (b).

An alternative cost-effective method to have buffer capacity at the spacer could be developed by modifying spacer material at the spacer channel with ion exchange groups (especially with positively charged chemical groups). Ion exchange resins or polyelectrolyte coatings can be used to modify spacer materials to increase the ion exchange capacity (IEC) of the spacer to develop alternative strategies to mitigate mineral scaling in MCDI.[158]

6.6.2. Need for better understanding on pH changes during desalination of water with amphoteric ions

In Chapter 2, we showed that the presence of bicarbonate ions (HCO_3^-), which are amphoteric ions, causes pH changes in MCDI. In natural water, often more than one type of amphoteric ion is present. The tap water used in chapter

2 and 3 predominantly contained bicarbonate ions. Natural brackish water can contain different amphoteric ions often together with other amphoteric ions. Therefore, it is important to improve the understanding on pH changes in MCDI with other amphoteric ions in order to understand the directions of pH changes and adjust the mineral scaling mitigation strategies accordingly. In addition, understanding gained on pH changes with different amphoteric ions in water can also help to improve targeted removal of specific amphoteric ions.

To gain insights for future research, we theoretically calculated the effluent pH changes with sodium phosphate water with different feed pH. Phosphate ions exists in multiple forms such as charged species $H_2PO_4^-$, HPO_4^{2-}, PO_4^{3-} and neutral species H_3PO_4 based on the pH.[161] The effluent pH changes were calculated (as described in the box) for three different feed pH values namely

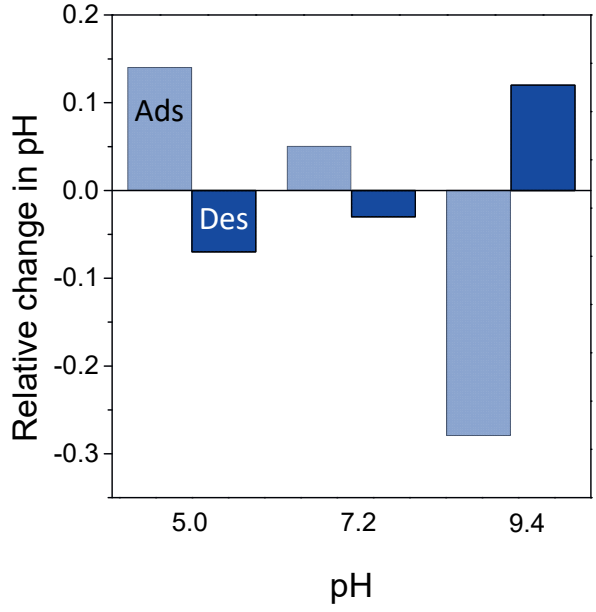

Figure 6.4 Relative averaged effluent pH changes for desalination of phosphate containing water with different feed water pH.

Effluent pH prediction for desalination of phosphate containing water

The calculations were carried out similar to the pH calculations described in chapter 3 using Aqion Pro software. To calculate the feed water composition at given pH, the pH and Na^+ ion concentration (5 mM) are used as fixed inputs and the concentration of P (in the form of PO_4) was calculated based on charge and mass balances. Once the feed water composition is derived for the given pH, to mimic the adsorption, the concentration of Na^+ was adjusted to 1.6 mM (i.e., 3.4 mM of Δc) and the P concentration was adjusted proportionally. For this new composition, the pH is calculated by balancing charge and mass. Similarly, to calculate the pH of the concentrate, the concentration of Na^+ is increased to 8.4 mM, the P concentration was adjusted proportionally, and the charge and mass balances were solved for the concentrate composition.

5.0,7.2 and 9.4. While pH 7.2 is equal to the pKa_2 value of phosphate, the other two pH values are 2.2 pH units away from the pKa value. Interestingly, with feed pH 5 and 7.2, the effluent pH increased during charging (i.e., adsorption of ions into the electrodes from spacer channel) and decreased during discharging (desorption of ions from the electrode to spacer channel) which is opposite to the observations reported in chapter 2 and 3 for carbonate containing water. However, when the feed pH is 9.4, the pH changes during charging and discharging are in the same direction as seen for carbonate containing water, i.e., a pH decrease during charging and pH increase during discharge, see figure 6.4. This also indicates, for phosphate containing water, that the scaling behaviour can be different from that of carbonate containing water. Therefore, the scaling mitigation strategies may also need to be adjusted accordingly. To gain further clarity on this, future research should focus on understanding pH changes containing multiple amphoteric ions.

Summary

MCDI is an emerging electrochemical desalination which has a potential for attractive technology for brackish water desalination and ion-selective separation. An MCDI cell is made up of activated carbon electrodes and ion-exchange membranes. When the electrodes are electrically biased by applying a voltage or current, it adsorbs ions of opposite charge resulting in desalination of water. When the electrodes are saturated with ions, they are discharged to produce concentrated water. Thus, desalinated water and a concentrated stream are cyclically produced. MCDI faces certain challenges such as pH changes, mineral scaling, and poor ion-selectivity which has to be addressed to make it an efficient and economically competitive technology. As pH changes are one of the primary factors affecting mineral scaling and ion selectivity, many studies were carried out to study the mechanisms resulting in these changes. Previous studies attributed faradaic reactions as the primary cause. However, most of the existing studies were carried out in ideal conditions with pristine electrodes, NaCl solutions and limited operational time, i.e., only several cycles of desalination were studied.

Chapter 2 of this thesis presents experiments conducted with aged electrodes, using tap water and NaCl over multiple operational cycles in MCDI and inverted-MCDI configuration. The study revealed a pH increase during charging and a decrease during discharging for NaCl whereas the pH directions during charging and discharging are reversed during tap water desalination. We showed that the reason for pH changes in NaCl is the difference in ion mobilities while the reason for pH changes during tap water desalination is the adsorption and desorption of HCO_3^- ions. Interestingly, both processes causing pH changes are non-faradaic. These findings underscore the complex interplay between solution composition and pH changes in real water systems.

In **chapter 3**, the primary focus was to understand how the presence of HCO_3^- ions in tap water affects the pH dynamics, and the direction of pH changes in particular. Crucially, experiments carried out with NaCl and $NaHCO_3$ feed

waters exhibited the inversion in the direction of pH changes between these two systems revealing that pH changes in HCO_3^- containing water are directly linked to HCO_3^- (which is part of the DIC) removal, establishing it as a key factor in causing pH changes during tap water desalination. Further investigations and calculations showed how HCO_3^- removal affects the concentrations of dissolved inorganic carbon (DIC) species, and consequently causes a shift in the carbonic acid equilibrium, inducing pH changes. Additionally, the research also showed that desalination of tap water or synthetic water with hardness ions under higher water recovery conditions resulted in mineral scaling. Increasing the thickness of the AEM resulted in minimized mineral scaling and is therefore suggested as a practical strategy to mitigate mineral scaling.

After studying effluent pH changes with tap water and NaCl, we measured the local pH in the electrode compartments while desalinating NaCl feed water. **Chapter 4** shows the experimentally measured pH near the anode, cathode and at the effluent. The pH changes were examined under two different experimental conditions namely, non-faradaic conditions and faradaic conditions. Under non-faradaic conditions, faradaic reactions such as water splitting were absent, whereas, under faradaic conditions, faradaic reactions are possible. We showed that both anode and cathode pH fluctuated around the feed pH (pH 7) under non-faradaic conditions, with a pH increase during charging and subsequent decrease during discharging. This observation is contradictory to theoretical expectations of cathode and anode showing opposite behaviour in terms of pH direction. Transitioning to faradaic conditions, the anode pH shifted to acidic, while the cathode pH became basic as expected.

The insights gained on near electrode pH changes hold practical implications to prepare electrodes with pH sensitive chemical groups for ion-selective adsorption. In **chapter 5**, we demonstrated the effectiveness of a novel cell design combining anion-selective electrodes with a cation-selective membrane for continuous water desalination. The anion-selective electrodes are prepared using pH sensitive amino-silane chemical groups which exist in

protonated form under pH 10 and thus acts as an anion selective chemical group. The desalination performance observed was also theoretically validated. The new cell design achieved significantly lower energy consumption compared to standard MCDI systems while having increased water productivity.

Chapter 6 discusses the relevance of the findings of this thesis to scientific advancement of MCDI research and to the possible technical improvements to make MCDI economically competitive. We discussed how the demonstrated mineral scaling mitigation strategy can pave the way to develop MCDI as an environmentally friendly technology by reducing the need for cleaning chemicals. We also showed how the new cell design used in this thesis can reduce the costs of water treatment by MCDI. This chapter also discusses the future research directions needed to improve mineral scaling mitigation strategies and selective separation of amphoteric ions.

References

1. Williams, J. Desalination in the 21st Century: A Critical Review of Trends and Debates. *Water Altern.* **15**, 193–217 (2022).
2. Ercin, A. E. & Hoekstra, A. Y. Water footprint scenarios for 2050: A global analysis. *Environ. Int.* **64**, 71–82 (2014).
3. Wang, Y., Zhang, Y., Sun, W. & Zhu, L. The impact of new urbanization and industrial structural changes on regional water stress based on water footprints. *Sustain. Cities Soc.* **79**, 103686 (2022).
4. Kharraz, J. El, El-Sadek, A., Ghaffour, N. & Mino, E. Water scarcity and drought in WANA countries. *Procedia Eng.* **33**, 14–29 (2012).
5. Mekonnen, M. M. & Hoekstra, A. Y. Four billion people facing severe water scarcity. *Sci. Adv.* **2**, 1–7 (2016).
6. Montgomery, M. A. & Elimelech, M. Water And Sanitation in Developing Countries: Including Health in the Equation. *Environ. Sci. Technol.* **41**, 17–24 (2007).
7. Dhakal, N. *et al.* Is Desalination a Solution to Freshwater Scarcity in Developing Countries? *Membranes (Basel).* **12**, 381 (2022).
8. Ba, W. *et al.* Urban water scarcity in China: A systematic review of research advances and future directions. *Appl. Geogr.* **159**, 103069 (2023).
9. Jadeja, N. B., Banerji, T., Kapley, A. & Kumar, R. Water pollution in India – Current scenario. *Water Secur.* **16**, 100119 (2022).
10. Guhathakurta, P. & Saji, E. Detecting changes in rainfall pattern and seasonality index vis-à-vis increasing water scarcity in Maharashtra. *J. Earth Syst. Sci.* **122**, 639–649 (2013).
11. Asif, Z., Chen, Z., Sadiq, R. & Zhu, Y. Climate Change Impacts on Water Resources and Sustainable Water Management Strategies in North America. *Water Resour. Manag.* **37**, 2771–2786 (2023).
12. Norton-Brandão, D., Scherrenberg, S. M. & van Lier, J. B. Reclamation of used urban waters for irrigation purposes - A review of treatment technologies. *J. Environ. Manage.* **122**, 85–98 (2013).
13. Shen, Y.-Y. Y., Sun, S.-H. H., Tsai, S.-W. W., Chen, T.-H. H. & Hou,

C.-H. H. Development of a membrane capacitive deionization stack for domestic wastewater reclamation: A pilot-scale feasibility study. *Desalination* **500**, 114851 (2021).

14. Fang, K. *et al.* Recovering ammonia from municipal wastewater by flow-electrode capacitive deionization. *Chem. Eng. J.* **348**, 301–309 (2018).

15. Liu, E., Lee, L. Y., Ong, S. L. & Ng, H. Y. Treatment of industrial brine using capacitive deionization (CDI) towards zero liquid discharge – challenges and optimization. *Water Res.* **183**, 116059 (2020).

16. Ghyselbrecht, K. *et al.* Desalination of an industrial saline water with conventional and bipolar membrane electrodialysis. *Desalination* **318**, 9–18 (2013).

17. Tong, T. & Elimelech, M. The Global Rise of Zero Liquid Discharge for Wastewater Management: Drivers, Technologies, and Future Directions. *Environ. Sci. Technol.* **50**, 6846–6855 (2016).

18. Zarzo, D. & Prats, D. Desalination and energy consumption. What can we expect in the near future? *Desalination* **427**, 1–9 (2018).

19. Kim, J., Park, K., Yang, D. R. & Hong, S. A comprehensive review of energy consumption of seawater reverse osmosis desalination plants. *Appl. Energy* **254**, 113652 (2019).

20. Altaee, A., Zaragoza, G. & van Tonningen, H. R. Comparison between Forward Osmosis-Reverse Osmosis and Reverse Osmosis processes for seawater desalination. *Desalination* **336**, 50–57 (2014).

21. Patel, S. K., Biesheuvel, P. M. & Elimelech, M. Energy Consumption of Brackish Water Desalination: Identifying the Sweet Spots for Electrodialysis and Reverse Osmosis. *ACS ES T Eng.* **1**, 851–864 (2021).

22. Porada, S., Zhang, L. & Dykstra, J. E. Energy consumption in membrane capacitive deionization and comparison with reverse osmosis. *Desalination* vol. 488 at https://doi.org/10.1016/j.desal.2020.114383 (2020).

23. Curto, D., Franzitta, V. & Guercio, A. A Review of the Water Desalination Technologies. *Appl. Sci.* **11**, 670 (2021).

24. Al-Shammiri, M. & Safar, M. Multi-effect distillation plants: state of the art. *Desalination* **126**, 45–59 (1999).

25. El-Dessouky, H. T., Ettouney, H. M. & Al-Roumi, Y. Multi-stage flash desalination: present and future outlook. *Chem. Eng. J.* **73**, 173–190 (1999).

26. Darwish, M. A. & El-Dessouky, H. The heat recovery thermal vapour-compression desalting system: A comparison with other thermal desalination processes. *Appl. Therm. Eng.* **16**, 523–537 (1996).

27. Ghazi, Z. M. *et al.* An overview of water desalination systems integrated with renewable energy sources. *Desalination* **542**, 116063 (2022).

28. Ahmed, F. E., Khalil, A. & Hilal, N. Emerging desalination technologies: Current status, challenges and future trends. *Desalination* **517**, 115183 (2021).

29. Abdel-Fatah, M. A. Nanofiltration systems and applications in wastewater treatment: Review article. *Ain Shams Eng. J.* **9**, 3077–3092 (2018).

30. Oatley-Radcliffe, D. L. *et al.* Nanofiltration membranes and processes: A review of research trends over the past decade. *J. Water Process Eng.* **19**, 164–171 (2017).

31. Biesheuvel, P. M., Porada, S., Elimelech, M. & Dykstra, J. E. Tutorial review of reverse osmosis and electrodialysis. *J. Memb. Sci.* **647**, 120221 (2022).

32. Mubita, T. M., Porada, S., Biesheuvel, P. M., van der Wal, A. & Dykstra, J. E. Strategies to increase ion selectivity in electrodialysis. *Sep. Purif. Technol.* **292**, 120944 (2022).

33. Patel, C. G., Barad, D. & Swaminathan, J. Desalination using pressure or electric field? A fundamental comparison of RO and electrodialysis. *Desalination* **530**, 115620 (2022).

34. Al-Amshawee, S. *et al.* Electrodialysis desalination for water and wastewater: A review. *Chem. Eng. J.* **380**, 122231 (2020).

35. Ghyselbrecht, K. *et al.* Desalination feasibility study of an industrial NaCl stream by bipolar membrane electrodialysis. *J. Environ. Manage.* **140**, 69–75 (2014).

36. Biesheuvel, P. M. *et al.* Capacitive Deionization -- defining a class of desalination technologies. 1–3 (2017).

37. Suss, M. E. *et al.* Water desalination via capacitive deionization: What is it and what can we expect from it? *Energy Environ. Sci.* **8**, 2296–2319 (2015).

38. Porada, S., Zhao, R., van der Wal, A., Presser, V. & Biesheuvel, P. M. M. Review on the science and technology of water desalination by capacitive deionization. *Prog. Mater. Sci.* **58**, 1388–1442 (2013).

39. Biesheuvel, P. M. & van der Wal, A. Membrane capacitive deionization. *J. Memb. Sci.* **346**, 256–262 (2010).

40. Omosebi, A. *et al.* Energy recovery in capacitive deionization systems with inverted operation characteristics. *Environ. Sci. Water Res. Technol.* **6**, 321–330 (2020).

41. Jones, E., Qadir, M., van Vliet, M. T. H., Smakhtin, V. & Kang, S. The state of desalination and brine production: A global outlook. *Sci. Total Environ.* **657**, 1343–1356 (2019).

42. Zhao, R., Porada, S., Biesheuvel, P. M. & van der Wal, A. Energy consumption in membrane capacitive deionization for different water recoveries and flow rates, and comparison with reverse osmosis. *Desalination* **330**, 35–41 (2013).

43. Qin, M. *et al.* Comparison of energy consumption in desalination by capacitive deionization and reverse osmosis. *Desalination* **455**, 100–114 (2019).

44. Hasseler, T. D., Ramachandran, A., Tarpeh, W. A., Stadermann, M. & Santiago, J. G. Process design tools and techno-economic analysis for capacitive deionization. *Water Res.* **183**, 1–9 (2020).

45. Bales, C. *et al.* Predictive performance and costing model for Membrane Capacitive Deionization (MCDI) at operational scale. *Desalination* **557**, 116595 (2023).

46. Liu, X., Shanbhag, S., Bartholomew, T. V., Whitacre, J. F. & Mauter, M. S. Cost Comparison of Capacitive Deionization and Reverse Osmosis for Brackish Water Desalination. *ACS ES&T Eng.* **1**, 261–273 (2021).

47. Alghoul, M. A., Poovanaesvaran, P., Sopian, K. & Sulaiman, M. Y.

Review of brackish water reverse osmosis (BWRO) system designs. *Renew. Sustain. Energy Rev.* **13**, 2661–2667 (2009).

48. Gude, V. G. Energy consumption and recovery in reverse osmosis. *Desalin. Water Treat.* **36**, 239–260 (2011).

49. Li, X., Hasson, D., Semiat, R. & Shemer, H. Intermediate concentrate demineralization techniques for enhanced brackish water reverse osmosis water recovery – A review. *Desalination* **466**, 24–35 (2019).

50. Rolf, J. *et al.* Inorganic Scaling in Membrane Desalination: Models, Mechanisms, and Characterization Methods. *Environ. Sci. Technol.* **56**, 7484–7511 (2022).

51. Al-Shammiri, M., Ahmed, M. & Al-Rageeb, M. Nanofiltration and calcium sulfate limitation for top brine temperature in Gulf desalination plants. *Desalination* **167**, 335–346 (2004).

52. Remmen, K. *et al.* Layer-by-layer membrane modification allows scandium recovery by nanofiltration. *Environ. Sci. Water Res. Technol.* **5**, 1683–1688 (2019).

53. Dražević, E., Košutić, K. & Freger, V. Permeability and selectivity of reverse osmosis membranes: Correlation to swelling revisited. *Water Res.* **49**, 444–452 (2014).

54. Kim, M., Cerro, M. del, Hand, S. & Cusick, R. D. Enhancing capacitive deionization performance with charged structural polysaccharide electrode binders. *Water Res.* **148**, 388–397 (2019).

55. Gao, X. *et al.* Complementary surface charge for enhanced capacitive deionization. *Water Res.* **92**, 275–282 (2016).

56. Singh, K. *et al.* Nickel hexacyanoferrate electrodes for high mono/divalent ion-selectivity in capacitive deionization. *Desalination* **481**, 114346 (2020).

57. Su, X. & Hatton, T. A. Redox-electrodes for selective electrochemical separations. *Adv. Colloid Interface Sci.* **244**, 6–20 (2017).

58. Tas, S., Miedema, H. & Nijmeijer, K. Ion Exchange Membranes for the Selective Separation of Monovalent Cation. *Procedia Eng.* **44**, 1101–1102 (2012).

59. Ahdab, Y. D., Rehman, D., Schücking, G., Barbosa, M. & Lienhard, J.

H. Treating Irrigation Water Using High-Performance Membranes for Monovalent Selective Electrodialysis. *ACS Environ. Sci. Technol. Water* **1**, 117–124 (2021).

60. Choi, J., Lee, H. & Hong, S. Capacitive deionization (CDI) integrated with monovalent cation selective membrane for producing divalent cation-rich solution. *Desalination* **400**, 38–46 (2016).

61. Abdel-Jawad, M. *et al.* Fifteen years of R&D program in seawater desalination at KISR part II. RO system performance. *Desalination* **135**, 155–167 (2001).

62. Abdel-Jawad, M. *et al.* Fifteen years of R&D program in seawater desalination at KISR part I. Pretretment technologies for RO systems. *Desalination* **135**, 141–152 (2001).

63. Tong, T., Liu, X., Li, T., Park, S. & Anger, B. A Tale of Two Foulants: The Coupling of Organic Fouling and Mineral Scaling in Membrane Desalination. *Environ. Sci. Technol.* **57**, 7129–7149 (2023).

64. Matin, A., Rahman, F., Shafi, H. Z. & Zubair, S. M. Scaling of reverse osmosis membranes used in water desalination: Phenomena, impact, and control; future directions. *Desalination* **455**, 135–157 (2019).

65. Tong, T., Wallace, A. F., Zhao, S. & Wang, Z. Mineral scaling in membrane desalination: Mechanisms, mitigation strategies, and feasibility of scaling-resistant membranes. *J. Memb. Sci.* **579**, 52–69 (2019).

66. Wang, T. *et al.* Scaling behavior of iron in capacitive deionization (CDI) system. *Water Res.* **171**, 115370 (2020).

67. Mossad, M. & Zou, L. Study of fouling and scaling in capacitive deionisation by using dissolved organic and inorganic salts. *J. Hazard. Mater.* **244**–**245**, 387–393 (2013).

68. Shocron, A. N., Roth, R. S., Guyes, E. N., Epsztein, R. & Suss, M. E. Comparison of Ion Selectivity in Electrodialysis and Capacitive Deionization. *Environ. Sci. Technol. Lett.* **9**, 889–899 (2022).

69. Oyarzun, D. I., Hemmatifar, A., Palko, J. W., Stadermann, M. & Santiago, J. G. Ion selectivity in capacitive deionization with functionalized electrode: Theory and experimental validation. *Water Res. X* **1**, 100008 (2018).

70. Avraham, E., Noked, M., Soffer, A. & Aurbach, D. The feasibility of boron removal from water by capacitive deionization. *Electrochim. Acta* **56**, 6312–6317 (2011).

71. Shocron, A. N. *et al.* Electrochemical removal of amphoteric ions. *Proc. Natl. Acad. Sci.* **118**, e2108240118 (2021).

72. Hawks, S. A. *et al.* Performance metrics for the objective assessment of capacitive deionization systems. *Water Res.* **152**, 126–137 (2019).

73. He, D. *et al.* Faradaic Reactions in Water Desalination by Batch-Mode Capacitive Deionization. *Environ. Sci. Technol. Lett.* **3**, 222–226 (2016).

74. Yu, F. *et al.* Faradaic reactions in capacitive deionization for desalination and ion separation. *J. Mater. Chem. A* **7**, 15999–16027 (2019).

75. Rudie, A. & Hart, P. Mineral scale management. Part II, Fundamental chemistry. *TAPPI J.* **5**, 17–23 (2006).

76. Ghasemian, J. & Riahi, S. Effects of salinity and ionic composition of smart water on mineral scaling in carbonate reservoirs during water flooding. *Pet. Explor. Dev.* **48**, 421–429 (2021).

77. Andersen, C. B. Understanding Carbonate Equilibria by Measuring Alkalinity in Experimental and Natural Systems. *J. Geosci. Educ.* **50**, 389–403 (2002).

78. Sharifian, R., Wagterveld, R. M., Digdaya, I. A., Xiang, C. & Vermaas, D. A. Electrochemical carbon dioxide capture to close the carbon cycle. *Energy Environ. Sci.* **14**, 781–814 (2021).

79. Gude, V. G. Desalination and sustainability – An appraisal and current perspective. *Water Res.* **89**, 87–106 (2016).

80. Uwayid, R., Seraphim, N. M., Guyes, E. N., Eisenberg, D. & Suss, M. E. Characterizing and mitigating the degradation of oxidized cathodes during capacitive deionization cycling. *Carbon N. Y.* **173**, 1105–1114 (2021).

81. Lado, J. J., Pérez-Roa, R. E., Wouters, J. J., Isabel Tejedor-Tejedor, M. & Anderson, M. A. Evaluation of operational parameters for a capacitive deionization reactor employing asymmetric electrodes. *Sep. Purif. Technol.* **133**, 236–245 (2014).

82. Chen, T., Neville, A. & Yuan, M. Calcium carbonate scale formation—assessing the initial stages of precipitation and deposition. *J. Pet. Sci. Eng.* **46**, 185–194 (2005).

83. Gabrielli, C., Maurin, G., Poindessous, G. & Rosset, R. Nucleation and growth of calcium carbonate by an electrochemical scaling process. *J. Cryst. Growth* **200**, 236–250 (1999).

84. Dykstra, J. E., Keesman, K. J., Biesheuvel, P. M. & van der Wal, A. Theory of pH changes in water desalination by capacitive deionization. *Water Res.* **119**, 178–186 (2017).

85. Lee, J.-H., Bae, W.-S. & Choi, J.-H. Electrode reactions and adsorption/desorption performance related to the applied potential in a capacitive deionization process. *Desalination* **258**, 159–163 (2010).

86. Landon, J., Gao, X., Omosebi, A. & Liu, K. Emerging investigator series: local pH effects on carbon oxidation in capacitive deionization architectures. *Environ. Sci. Water Res. Technol.* **7**, 861–869 (2021).

87. Biesheuvel, P. M. M., Hamelers, H. V. M. V. M. & Suss, M. E. E. Theory of Water Desalination by Porous Electrodes with Immobile Chemical Charge. *Colloids Interface Sci. Commun.* **9**, 1–5 (2015).

88. Zhang, C., He, D., Ma, J., Tang, W. & Waite, T. D. Faradaic reactions in capacitive deionization (CDI) - problems and possibilities: A review. *Water Res.* **128**, 314–330 (2018).

89. Zhao, R., Satpradit, O., Rijnaarts, H. H. M., Biesheuvel, P. M. & van der Wal, A. Optimization of salt adsorption rate in membrane capacitive deionization. *Water Res.* **47**, 1941–1952 (2013).

90. Cohen, I., Avraham, E., Bouhadana, Y., Soffer, A. & Aurbach, D. The effect of the flow-regime, reversal of polarization, and oxygen on the long term stability in capacitive de-ionization processes. *Electrochim. Acta* **153**, 106–114 (2015).

91. Cohen, I., Avraham, E., Bouhadana, Y., Soffer, A. & Aurbach, D. Long term stability of capacitive de-ionization processes for water desalination: The challenge of positive electrodes corrosion. *Electrochim. Acta* **106**, 91–100 (2013).

92. Gao, X., Omosebi, A., Landon, J. & Liu, K. Surface charge enhanced carbon electrodes for stable and efficient capacitive deionization using

inverted adsorption-desorption behavior. *Energy Environ. Sci.* **8**, 897–909 (2015).

93. Gao, X., Omosebi, A., Landon, J. & Liu, K. Enhanced Salt Removal in an Inverted Capacitive Deionization Cell Using Amine Modified Microporous Carbon Cathodes. *Environ. Sci. Technol.* **49**, 10920–10926 (2015).

94. Gao, X. *et al.* Polymer-coated composite anodes for efficient and stable capacitive deionization. *Desalination* **399**, 16–20 (2016).

95. Biesheuvel, P. M., Zhao, R., Porada, S. & van der Wal, A. Theory of membrane capacitive deionization including the effect of the electrode pore space. *J. Colloid Interface Sci.* **360**, 239–248 (2011).

96. Choi, J.-H. H. & Yoon, D.-J. J. The maximum allowable charge for operating membrane capacitive deionization without electrode reactions. *Sep. Purif. Technol.* **215**, 125–133 (2019).

97. Srimuk, P. *et al.* High performance stability of titania decorated carbon for desalination with capacitive deionization in oxygenated water. *RSC Adv.* **6**, 106081–106089 (2016).

98. Srimuk, P. *et al.* Enhanced performance stability of carbon/titania hybrid electrodes during capacitive deionization of oxygen saturated saline water. *Electrochim. Acta* **224**, 314–328 (2017).

99. Tang, W., He, D., Zhang, C., Kovalsky, P. & Waite, T. D. Comparison of Faradaic reactions in capacitive deionization (CDI) and membrane capacitive deionization (MCDI) water treatment processes. *Water Res.* **120**, 229–237 (2017).

100. Ogumi, Z. Gas Permeation in SPE Method. *J. Electrochem. Soc.* **131**, 769 (1984).

101. Dykstra, J. E. Desalination with porous electrodes : Mechanisms of ion transport and adsorption. (Wageningen University, 2018). doi:10.18174/443551.

102. van Limpt, B. & van der Wal, A. Water and chemical savings in cooling towers by using membrane capacitive deionization. *Desalination* **342**, 148–155 (2014).

103. Fritz, P. A., Boom, R. M. M. & Schroen, K. Polyelectrolyte-activated carbon composite electrodes for inverted membrane capacitive

deionization (iMCDI). *Sep. Purif. Technol.* **220**, 145–151 (2019).

104. Pan, S.-Y. Y., Haddad, A. Z., Kumar, A. & Wang, S.-W. W. Brackish water desalination using reverse osmosis and capacitive deionization at the water-energy nexus. *Water Res.* **183**, 116064 (2020).

105. Le Gouellec, Y. Calcium sulfate (gypsum) scaling in nanofiltration of agricultural drainage water. *J. Memb. Sci.* **205**, 279–291 (2002).

106. Zhou, D., Zhu, L., Fu, Y., Zhu, M. & Xue, L. Development of lower cost seawater desalination processes using nanofiltration technologies — A review. *Desalination* **376**, 109–116 (2015).

107. Esfahani, I. J., Rashidi, J., Ifaei, P. & Yoo, C. K. Efficient thermal desalination technologies with renewable energy systems: A state-of-the-art review. *Korean J. Chem. Eng.* **33**, 351–387 (2016).

108. Al-Rawajfeh, A. E., Glade, H. & Ulrich, J. Scaling in multiple-effect distillers: the role of CO2 release. *Desalination* **182**, 209–219 (2005).

109. Karabelas, A. J., Mitrouli, S. T. & Kostoglou, M. Scaling in reverse osmosis desalination plants: A perspective focusing on development of comprehensive simulation tools. *Desalination* **474**, 114193 (2020).

110. Zhang, Z., Wadekar, S. S., Lokare, O. R. & Vidic, R. D. Comparison of calcium scaling in direct contact membrane distillation (DCMD) and nanofiltration (NF). *J. Memb. Sci.* **638**, 119647 (2021).

111. Ayala-Bribiesca, E., Araya-Farias, M., Pourcelly, G. & Bazinet, L. Effect of concentrate solution pH and mineral composition of a whey protein diluate solution on membrane fouling formation during conventional electrodialysis. *J. Memb. Sci.* **280**, 790–801 (2006).

112. Liu, Q., Xu, G.-R. & Das, R. Inorganic scaling in reverse osmosis (RO) desalination: Mechanisms, monitoring, and inhibition strategies. *Desalination* **468**, 114065 (2019).

113. van de Lisdonk, C. A. C., van Paassen, J. A. M. & Schippers, J. C. Monitoring scaling in nanofiltration and reverse osmosis membrane systems. *Desalination* **132**, 101–108 (2000).

114. Arulrajan, A. C., Dykstra, J. E., van der Wal, A. & Porada, S. Unravelling pH Changes in Electrochemical Desalination with Capacitive Deionization. *Environ. Sci. Technol.* **55**, acs.est.1c04479 (2021).

115. Wang, T. *et al.* Formation mechanism of iron scale in membrane capacitive deionization (MCDI) system. *Desalination* **495**, 114636 (2020).

116. Cole, J. J. & Prairie, Y. T. Dissolved CO2 in Freshwater Systems☆. in *Reference Module in Earth Systems and Environmental Sciences* 1–5 (Elsevier, 2014). doi:10.1016/b978-0-12-409548-9.09399-4.

117. Pines, D. *et al.* How Acidic Is Carbonic Acid? *J. Phys. Chem. B* **120**, 2440–2451 (2016).

118. Donnelly, F. C. *et al.* Synthesis of CaCO 3 nano- and micro-particles by dry ice carbonation. *Chem. Commun.* **53**, 6657–6660 (2017).

119. Welgemoed, T. J. & Schutte, C. F. Capacitive Deionization Technology^{TM}: An alternative desalination solution. *Desalination* **183**, 327–340 (2005).

120. Oren, Y. Capacitive deionization (CDI) for desalination and water treatment — past, present and future (a review). *Desalination* **228**, 10–29 (2008).

121. Shapira, B., Avraham, E. & Aurbach, D. Side Reactions in Capacitive Deionization (CDI) Processes: The Role of Oxygen Reduction. *Electrochim. Acta* **220**, 285–295 (2016).

122. Liu, F., Coronell, O. & Call, D. F. Effect of cross-chamber flow electrode recirculation on pH and faradaic reactions in capacitive deionization. *Desalination* **492**, 114600 (2020).

123. Hemmatifar, A. *et al.* Equilibria model for pH variations and ion adsorption in capacitive deionization electrodes. *Water Res.* **122**, 387–397 (2017).

124. Ogumi, Z., Takehara, Z. & Yoshizawa, S. Gas Permeation in SPE Method: I . Oxygen Permeation Through Nafion and NEOSEPTA. *J. Electrochem. Soc.* **131**, 769–773 (1984).

125. Ratajczak, P., Suss, M. E., Kaasik, F. & Béguin, F. Carbon electrodes for capacitive technologies. *Energy Storage Mater.* **16**, 126–145 (2019).

126. Yang, Z.-Y. *et al.* Sponge-Templated Preparation of High Surface Area Graphene with Ultrahigh Capacitive Deionization Performance. *Adv. Funct. Mater.* **24**, 3917–3925 (2014).

127. Yin, H. *et al.* Three-Dimensional Graphene/Metal Oxide Nanoparticle Hybrids for High-Performance Capacitive Deionization of Saline Water. *Adv. Mater.* **25**, 6270–6276 (2013).

128. Cohen, I., Avraham, E., Noked, M., Soffer, A. & Aurbach, D. Enhanced Charge Efficiency in Capacitive Deionization Achieved by Surface-Treated Electrodes and by Means of a Third Electrode. *J. Phys. Chem. C* **115**, 19856–19863 (2011).

129. Wu, T. *et al.* Asymmetric capacitive deionization utilizing nitric acid treated activated carbon fiber as the cathode. *Electrochim. Acta* **176**, 426–433 (2015).

130. Omosebi, A., Gao, X., Rentschler, J., Landon, J. & Liu, K. Continuous operation of membrane capacitive deionization cells assembled with dissimilar potential of zero charge electrode pairs. *J. Colloid Interface Sci.* **446**, 344–350 (2015).

131. Qian, B. *et al.* Sulfonated Graphene as Cation-Selective Coating: A New Strategy for High-Performance Membrane Capacitive Deionization. *Adv. Mater. Interfaces* **2**, 1–9 (2015).

132. Su, X., Kulik, H. J., Jamison, T. F. & Hatton, T. A. Anion-Selective Redox Electrodes: Electrochemically Mediated Separation with Heterogeneous Organometallic Interfaces. *Adv. Funct. Mater.* **26**, 3394–3404 (2016).

133. Liu, P. *et al.* Grafting sulfonic and amine functional groups on 3D graphene for improved capacitive deionization. *J. Mater. Chem. A* **4**, 5303–5313 (2016).

134. Porada, S., Shrivastava, A., Bukowska, P., Biesheuvel, P. M. & Smith, K. C. Nickel Hexacyanoferrate Electrodes for Continuous Cation Intercalation Desalination of Brackish Water. *Electrochim. Acta* **255**, 369–378 (2017).

135. Smith, K. C. & Dmello, R. Na-Ion Desalination (NID) Enabled by Na-Blocking Membranes and Symmetric Na-Intercalation: Porous-Electrode Modeling. *J. Electrochem. Soc.* **163**, A530–A539 (2016).

136. Kim, T., Gorski, C. A. & Logan, B. E. Low Energy Desalination Using Battery Electrode Deionization. *Environ. Sci. Technol. Lett.* **4**, 444–449 (2017).

137. Lee, J., Kim, S. & Yoon, J. Rocking Chair Desalination Battery Based on Prussian Blue Electrodes. *ACS Omega* **2**, 1653–1659 (2017).

138. Lee, J. *et al.* Rocking-Chair Capacitive Deionization for Continuous Brackish Water Desalination. *ACS Sustain. Chem. Eng.* **6**, 10815–10822 (2018).

139. Qu, Y. *et al.* Energy consumption analysis of constant voltage and constant current operations in capacitive deionization. *Desalination* **400**, 18–24 (2016).

140. Mubita, T. M., Porada, S., Biesheuvel, P. M., van der Wal, A. & Dykstra, J. E. Capacitive deionization with wire-shaped electrodes. *Electrochim. Acta* **270**, 165–173 (2018).

141. Buqa, H., Grogger, C., Santis Alvarez, M. V., Besenhard, J. O. & Winter, M. Surface modification of graphite anodes by combination of high temperature gas treatment and silylation in nonaqueous solution. *J. Power Sources* **97**–**98**, 126–128 (2001).

142. Ramasamy, D. L., Repo, E., Srivastava, V. & Sillanpää, M. Chemically immobilized and physically adsorbed PAN/acetylacetone modified mesoporous silica for the recovery of rare earth elements from the waste water-comparative and optimization study. *Water Res.* **114**, 264–276 (2017).

143. Sharma, R. K., Mittal, S. & Koel, M. Analysis of Trace Amounts of Metal Ions Using Silica-Based Chelating Resins: A Green Analytical Method. *Crit. Rev. Anal. Chem.* **33**, 183–197 (2003).

144. Pasternack, R. M., Rivillon Amy, S. & Chabal, Y. J. Attachment of 3-(Aminopropyl)triethoxysilane on Silicon Oxide Surfaces: Dependence on Solution Temperature. *Langmuir* **24**, 12963–12971 (2008).

145. Orel, B., Ješe, R., Lavrenčič Štangar, U., Grdadolnik, J. & Puchberger, M. Infrared attenuated total reflection spectroscopy studies of aprotic condensation of (EtO)3SiRSi(OEt)3 and RSi(OEt)3 systems with carboxylic acids. *J. Non. Cryst. Solids* **351**, 530–549 (2005).

146. Aneja, K. S., Bohm, S., Khanna, A. S. & Bohm, H. L. M. Graphene based anticorrosive coatings for Cr(<scp>vi</scp>) replacement. *Nanoscale* **7**, 17879–17888 (2015).

147. Niemirowicz, K. *et al.* Bactericidal activity and biocompatibility of

ceragenin-coated magnetic nanoparticles. *J. Nanobiotechnology* **13**, 32 (2015).

148. Elazari, R., Salitra, G., Garsuch, A., Panchenko, A. & Aurbach, D. Sulfur-Impregnated Activated Carbon Fiber Cloth as a Binder-Free Cathode for Rechargeable Li-S Batteries. *Adv. Mater.* **23**, 5641–5644 (2011).

149. Wang, C., Chen, L. & Zhu, L. Effect of combined fouling on desalination performance of membrane capacitive deionization (MCDI) during long-term operation. *J. Dispers. Sci. Technol.* **41**, 383–392 (2020).

150. Hand, S., Guest, J. S. & Cusick, R. D. Technoeconomic Analysis of Brackish Water Capacitive Deionization: Navigating Tradeoffs between Performance, Lifetime, and Material Costs. *Environ. Sci. Technol.* **53**, 13353–13363 (2019).

151. Lee, B., Oh, C., An, J., Yeon, S. & Oh, H. J. Optimizing Operational Conditions of Pilot-Scale Membrane Capacitive Deionization System. *Sustainability* **15**, 16809 (2023).

152. Wu, J., Chen, Z., Zhang, J. & Li, Y. Insight into the scaling behavior of capacitive deionization for the removal of multiple cation components in the single-pass mode. *Sep. Purif. Technol.* **340**, 126718 (2024).

153. Zhang, W., Mossad, M. & Zou, L. A study of the long-term operation of capacitive deionisation in inland brackish water desalination. *Desalination* **320**, 80–85 (2013).

154. Belkin, N., Rahav, E., Elifantz, H., Kress, N. & Berman-Frank, I. The effect of coagulants and antiscalants discharged with seawater desalination brines on coastal microbial communities: A laboratory and in situ study from the southeastern Mediterranean. *Water Res.* **110**, 321–331 (2017).

155. Ben Saad, M. *et al.* Environmental and Economic Assessment of Membrane Capacitive Deionization (MCDI) and Low-Pressure Reverse Osmosis (LPRO) for Sustainable Irrigation in the Mediterranean Region. *Sustain.* **16**, (2024).

156. Kumar, S., Aldaqqa, N. M., Alhseinat, E. & Shetty, D. Electrode Materials for Desalination of Water via Capacitive Deionization.

Angew. Chemie - Int. Ed. **62**, (2023).

157. Xiao, Q. *et al.* Membrane capacitive deionization (MCDI) for selective ion separation and recovery: Fundamentals, challenges, and opportunities. *J. Memb. Sci.* **699**, 122650 (2024).

158. Gao, F., Shi, W., Dai, R. & Wang, Z. Effective and Selective Removal of Phosphate from Wastewater Using Guanidinium-Functionalized Polyelectrolyte-Modified Electrodes in Capacitive Deionization. *ACS Environ. Sci. Technol. Water* **2**, 237–246 (2022).

159. Lu, D., Cai, W. & Wang, Y. Optimization of the voltage window for long-term capacitive deionization stability. *Desalination* **424**, 53–61 (2017).

160. Liu, X., Shanbhag, S. & Mauter, M. S. Understanding and mitigating performance decline in electrochemical deionization. *Curr. Opin. Chem. Eng.* **25**, 67–74 (2019).

161. Bian, Y., Chen, X. & Ren, Z. J. PH Dependence of Phosphorus Speciation and Transport in Flow-Electrode Capacitive Deionization. *Environ. Sci. Technol.* **54**, 9116–9123 (2020).

162. Suss, M. E. *et al.* Capacitive desalination with flow-through electrodes. *Energy Environ. Sci.* **5**, 9511 (2012).

List of publications (This thesis)

1. Arulrajan, A. C., Dykstra, J. E., van der Wal, A. & Porada, S. Unravelling pH Changes in Electrochemical Desalination with Capacitive Deionization. *Environ. Sci. Technol.* **55**, acs.est.1c04479 (2021).
2. Arulrajan, A. C. *et al.* Mitigation of mineral scaling in membrane capacitive deionization – Understanding the role of pH changes and carbonates. *J. Water Process Eng.* **60**, 105094 (2024).
3. Arulrajan, A. C. *et al.* Exceptional Water Desalination Performance with Anion-Selective Electrodes. *Adv. Mater.* 1806937 (2019).

Acknowledgements

The PhD has been a great journey with many good things, and many surprices along the way. It wasn't easy, but I managed to reach the destination after all. So, I have to give myself credit for taking on this journey, not giving up, remembering to make memories, and adapting to many surprises along the way. Thanks to "me"! However, finishing this adventure is not done alone. There are many people who directly and indirectly helped me along the way, to whom I am deeply grateful.

I want to start by expressing my deepest gratitude to my promotor, **Bert van der Wal,** for his invaluable time, expertise, and guidance throughout my PhD journey. From our first meeting at a train station to our many meetings in Leeuwarden, I learned so much from you. Traveling all the way to Leeuwarden for our meetings and providing feedback that helped me dive deep into science meant a lot. Your appreciation for the little steps I made served as a tremendous source of energy and motivation. Having someone with your entrepreneurial and industrial involvement as my promotor definitely influenced how I see science and its relevance to societal problems. Your involvement and support during the final stages of my PhD journey were great boost. Thank you Bert!

I'm also immensely grateful to my co-promotor and daily supervisor, **Slawomir Porada** (or Slawek, as I always call you). Your support whenever I needed it was invaluable. Your casual and informal way of communication from day one made me comfortable. The way you pay attention to details and your scientific curiosity have greatly influenced and shaped my thought process over the years. Teaching me CDI experiments in the lab and our insightful discussions gave me a great start. Your supervision has been crucial in improving my experimental skills, the way I think, and how I plan my projects. I'm sure these skills will be a treasure for my future endeavours.

I also extend my sincere thanks to my other co-promotor and daily supervisor, **Jouke Dykstra**. I still remember our very first interview and meeting. Your teaching on CDI concepts, providing theoretical insights, and fostering an in-depth analytical mindset were instrumental in my research. The way you tuned my scientific writing and presentation skills is something I will always cherish. Every time you asked a question, my research direction became more

focused and clear. Your timely feedbacks (sometimes, even during your holidays) on my papers, presentations, and results were invaluable.
A heartfelt thanks to **Maarten Biesheuvel**. Your guidance in the initial stages when I was exploring the research field as a newbie was crucial. The discussions, scientific arguments, and your support as a theme coordinator helped me become better at research and presenting myself to a wider audience. Your encouraging expressions during my presentations boosted my confidence while presenting.
A big thanks to **Cees, Johannes, Bert,** and **Jan Post** for making Wetsus a great place to work. Your efforts created an inspiring and supportive environment that significantly contributed to the progress of my research. And Jan, thanks again for your support as a theme coordinator and during the NEW-ttt project, which is a stepping stone for my next adventure.
A special shoutout to the wonderful fellows from office 1.18E. **Carlo**, (or Carlo"s", or Belloniiiii or Mr.Mottaiii) you were always there in this entire journey. Thanks for many dinner and party invites and making "the castle" a memorable place. The times we spent in the office, cycling, and in pubs are among my best memories. Thanks for all the delicious Italian treats, and sorry I couldn't treat you to some nice and spicy food from India as planned. You've always been a great support, friend, and a great human being :). **Angel**, I thought you were a real "angel" until that 400% Windows update made me wait forever. It was wonderful sharing the office with you, ensuring we had coffee, chocolate, and "Simpsons" breaks :). Especially I loved all the cycling days you organized. Your little secret in India stays a secret for now :P. **Vania**, thanks for the nice times and support, especially when the PhD journey got tough. It was great having you as an officemate during the PhD and at the water campus afterwards :) Those Christmas and New Year's evenings and card games are memories to cherish!. **XiaoXia**aaaa! You're an amazing person. I felt at home when you and Farid brought me medicine when I got COVID <3. My craziest memories are at the dinners you organized. Thanks for being "the Xiaoxia", for all the delicious Chinese food and for introducing me to Farid :). **Yujia**, my "enemy" (just kidding!), it was amazing having you as an "enemy". Thanks for tolerating me for years, especially when we had to face each other in the office all the time. We had so much fun (remember the insect box, Tulip visit, lelystad and Groningen trips!). **Sebastian** (Canizales), thanks man, for the great talks, dinners, and

other crazy parties (especially the night after the Wetsus Congress) at your place. **Olga** (Olgitaaaa!), thanks for all the nice talks, fun moments, and discussions on everything from politics to pets, and for the polish treats you brought!. **Ettore**eeee, you, being part of the castle, made it the best place filled with many memories. From an officemate to the theme coordinator, you've always been encouraging and supportive, especially during the tough times, Thanks. **Ruben**, the only Dutch in the office, always giving the Dutch perspective in our discussions. It was fun seeing your mischievous side whenever you teamed up with Yujia to tease me. **Nouran and Yicheng**, though we didn't spend as much time together, it was nice and fun having you both around.

My good times at Wetsus weren't limited to office 1.18E. From coffee breaks and lab adventures to cycling and partying, I cherished many moments with amazing people who made this journey memorable. **Prashanth**, wow, so many memories—talks, walks, movie and music nights, Tamil movie jokes, and "naai kodai" days etc. You're a great friend I could rely on. I admire your worldview and how you handle things. Your positive words, especially during the pandemic, helped me a lot. I cherish the memories of your last weeks in Leeuwarden and the "amma thaaye" moment (and many more)!! **Suyash and Indresh**, I can't thank you two separately because you're like family to me. From dinners and walks to office chats and birthday parties, and so many more good times we've shared, you've always been there and stood by me through the good times and the tough ones, and I've always felt I could knock on your door anytime for anything. Thank you for the comfort and support you've given me. **Avi**, thanks for accepting me as a friend and always showing love and affection. I don't know if you can relate at this moment to what I say, but I wish, even after10 years, we'll read this together with the same bond we share now. **Sam**, I wish I could call you by the usual nicknames, but I'll be polite here. Thanks for your support throughout my PhD journey, especially in the final stages when you kept me motivated with your kind words and support. Though the pandemic restricted our initial interactions, we have soon become close. Having you in India on my wedding was truly special (Now, I cannot escape from seeing your face often on the photos :P). You showing up with a coffee mug for coffee breaks were my best stressbusters. Thanks for always understanding the unspoken words and prioritizing people, a big hug to you!. **Kestral**, you went from a newbie I

rarely spoke with to someone I'm very comfortable with. Thanks for the all nice memories and moments at Wetsus, Leeuwarden, cycling, in India, and for handling the "kid". Also, thanks to **Kikko** for welcoming me warmly when I go to your home (I assume your barks are a sweet way of saying hello :D). **Farid**, my brother, so many "crazy" evenings we shared (wow, that evening with the life jacket!) It's great to see you as an entrepreneur, embarking on another wild journey and sharing your experiences with me. **Ruizhe**, I remember many of the office talks (even though you weren't officially part of 1.18E), cycling days, and all the other nice moments in and out of Wetsus. Having you as an "additional office mate" was fun! **Sebas** (Castaño), the funniest memory is cycling from the city centre to your home in the middle of the night just to say goodnight. The dance workshop, lunchtimes, Wetsus congress, and ETE times were always joyful. It was great having you on many good days, especially in India, though it isn't your go-to country :P. **Nimmy and Haniel**, thanks for all the nice evenings with the little Indian gatherings and awesome food. The pandemic reduced the time we could spend together, but I hope we can spend more time in the future! **Shuyana**, I have got many nice movements to remember from our time being neighbours at Auke Stellingwerfstraat! Nice discussions about mindfulness, and your initiatives at Wetsus. These helped me in crucial times. **Catarina**, my lab and second-floor office neighbour, thanks for the great times in the lab, office, and during cycling evenings. You introduced me into organising student presentations and also pushed me into joining whatsapp group :D. **Kaustub**, we only spent a short time together at Wetsus, but it was nice chatting, discussing CDI, and sharing opinions. **Deepika**, though we've never met in person, we still share something in common—Thoothukudi! And I enjoyed working with you on my first project at Wetsus. **Jen** (min-chen), it was nice having you at Wetsus and working together on projects. Our time in the lab was productive and fun :). **Viann**, my only student at Wetsus, it was wonderful having you on the project. With your enthusiasm and dedication, you managed the project successfully. I learnt a lot from you :).

Rose, Louis, Tania, & **Emad**, though we didn't spend as much time as I would have liked, I cherish the moments we shared—from Rose showing me around Wetsus during the waterseed challenge, to first lab experiments with Tania, to an awesome week in China with Louis, to many nice moments with Emad in the castle and at wetsus. **Marianne, Chris, Barbara,** and **Qingdian,**

my waterseed mates, it was nice starting at Wetsus together, discussing science, and having fun inside and outside Wetsus! **Daniele**, my theme mate, man, we discussed a lot of things together, and I admire your energy and enthusiasm. **Selin**, wow, we had many crazy days, trips, and conference days together. I always had company whenever I come to Wageningen. I hope you finally agree that CDI is the BEST! :P. **Wanda**, so many fun days, personal talks, games, and many many supportive words! It was a short time, but thanks for being there in the crucial period :). **Shangeetha**, thank you, machi. When I first arrived, I was super happy to meet you because I could keep speaking in Tamil. We shared a lot of nice moments and long chats, which are all good memories to remember.

Though I could not spend much time I did have nice moments and memories with **Sara** (nice Wetsus congress days and light festival), **Rita** (memorable A1 course to get to know you to many other office/coffee time discussions to remember), **Margo** (great discussions during NEW-ttt project and the business challenge. Thank you for all the nice and supporting words!). **Amanda, Arunitha, Edward, Sanjay, Sara, Dhayana, Mu, Lester, Mirvahid,** & **Sofie**, though we didn't spend much time together, there were many fun and special moments throughout the PhD from cycling to coffee breaks to Paddy's with you guys. Thanks! **Madhu, Keerthana,** & **Kayal** thanks for all the nice moments we shared at Wetsus and outside, especially with nice Indian food. Special thanks to Madhu for always boosting positivity around him.

The technical team of Wetsus, starting with **Jan Jurjen**, you did magic with my experimental setups, and every problem I faced. Thanks for always being a phone call away; your energy and enthusiasm are a big boost to everyone around you and specially to me. I don't remember you ever saying "not possible" to my crazy ideas or complicated experimental designs I asked for. A big thank you for making my setup and my life easier :). I got help from everyone in the technical team, thanks **Wim, Ernst, Harm, John, Jan, Wiebe** & **Johan**. I appreciate you always being ready to help, especially with last-minute requests! **Rienk,** thanks for your support during my PhD, helping me with every software struggle I ran into! **Gerrit**, you made sure every order I requested arrived on time!,

The analytical team, **Janneke, Jan-Willem, Jelmer, Marianne, Mieke, Lisette, Bianca**, and many others who helped directly and indirectly during

my PhD by carrying out analysis, sharing expertise, helping me work on Saturdays and more. The people on the second floor, **Christina, Michele, Roel, Philip, Lucia, Wokke, Thomas, Leon, Michele, Jan de Groot**, and anyone I forgot to mention, thanks for the nice discussions, dinners, cycling days, and many nice moments and discussions we shared.

The HR, secretaries, and receptionists who ensure Wetsus functions smoothly, a big thanks! Especially **Nynke, Anke,** and **Alexander**, thanks for all your support during this journey, from job contracts to travel arrangements to any kind of help I asked for. Thanks to all secretaries for supporting in many different occasions. Thanks, **Jannie** and **Anita**, for welcoming everyone with a warm smile in the morning and for our little talks :) The Wetsus energy suppliers- THE CANTEEN team! Thank you **Gerben, Katarina, Riet** and **Karen** for keeping Wetsus energetic!

Ronald, A special thanks for being involved in my next professional adventure. The WCBC you organized during my final year of PhD was a turning point in my career. Since then, you've been a constant support, guide, and a great coach. **Ramesh**, I remember our first meeting and ever since, you never miss to pass your energy and insights to me. Thank you for believing in me and for encouraging me to run the extra mile. It means a lot to me. **Jasper**, my partner in crime in IonIQs, thank you for spreading the energy and motivation to move forward, perfect timing to finish PhD and explore new adventures!

Hanna (Damhuisss), you're the best neighbour anyone could ask for. We've shared so many memories, from our crazy, childish door-knocking fights to movie nights, cycling together, traveling, snow-walks, and so much more. You made my days in Auke Stellingwerfstaart truly special. Thank you for making me a part of (y)our family. **Ageeth**, or Mom as I always call you, your love and care have been incredible. Thank you for treating me like your (adopted :D) son. The dinners, jokes, and endless laughter reminded me of my family in India. Thanks to you and Hanna, I can now say that I have a Dutch family too :). **Dany**, man, though we met relatively recently, we've already shared so many great times. Our dinners were filled with laughter, and fun! Cheers to many more nice memories!.

My **teachers and seniors** from Kamaraj college, NIT-T (**Professors, Jerome, Ugin, and Sathiskumar**) Twente (**Stanley and Serge**), Ariel (**Palaniappan and Alex**) are the reason that I have made it to here. Thanks

to everyone, especially **Pon Sathieshkumar** who was instrumental in beginning my research journey!

Kishore, thank you, machan! From 2006 till now, you've always been by my side through everything. Those long phone calls, bike rides, day outs, and the support whenever I need mean the world to me. Memories like tachaku tachaku are the best :D. **Tamil, Don,** and **Jeya**, so many great and fun times in India whenever I show up. Thanks, machans! My favorite kutties, **Bharathi** and **Suguna**, your long phone calls always lifted my spirits when I felt down. Thank you so much my dear sisters.

Aishu, my dear pakki, thank you for all the times we've spent together, whether in person or on our phones. From Trichy to Enschede to Ariel to Leeuwarden, you've been there through it all. Our discussions helped me stay practical and move forward in many situations. I am super happy to have you just a few hours' drive away!. **Giri**, Machaaan, from crazy singing to traveling around to doing stupid things, we've never changed since our NIT-T hostel days. The same crazy bond and activities will continue forever (Machan naa pass aagitaennn :D). **Dheepi**, from a barely known classmate to one of my best friends. Thanks a lot pakki, for being there during my toughest times and keeping me sane when life threw unexpected surprises, it means a lot to me. Thank you for all those unlimited phone calls, meetings, and great memories. **Sathya**, my "crazy" twin, ours has always been a long-distance friendship, but it never felt that way. Thank you for always making time for me, helping me think things through, and for the craziest topics I've ever discussed :D. **Arthi**, from a senior to one of my closest!. Thank you, crazy fellow, my guru in many things, for pushing me to keep writing my thesis when I badly wanted to take a break and, for always helping me find out what I want :D.

My dear paranymphs, **Marko** (Markitooo), I can't believe I made it to the finish line and you are next to me :)! We've shared so many incredible moments: cooking together, walking, city trips, video games, our unforgettable Wageningen days, the Wetsus congress, and (y)our adventures in India. From our scientific discussions and philosophical talks to the simple joy of spending time together, each memory is precious. I still remember inviting you to give a student presentation when you first arrived at Wetsus, and then relying on your help in the lab during the pandemic. Your visit to India was another highlight. There's always so much to reminisce about and

celebrate every time we meet. Thank you for being such an amazing part of this journey and a friend for life!
Nandini, or Nands! Haha, where do I even begin? Let's kick off with a war—Tamil movies are better than Malayalam movies :P. We've had so many crazy times, from your precise geography lessons about Jamshedpur, and (y)our "perfectly" reversed car drive, to countless dinners at Jamuna, movies, day outs, and music (AR Rahman with "special effect"). Those midnight atrocities and endless discussions about your wedding preparations were such fun. And wow, we even share a similar love story in how we found our partners! Each moment with you has been a blast, and I cherish them all. Thank you for always being there. :)

And, here comes the biggest support forever, my family!
Amma and **Appa**, words cannot express how grateful I am for your flawless belief in me. Through many tough moments when I felt like giving up, it was your unconditional love and support that kept me going. Your faith in me never wavered, even when I doubted myself. You were always there, guiding me through every twist and turn. Your endless encouragements have been my rock. You've supported me through deserts and oceans, always believing in my potential and dreams. Without your strength and faith, I wouldn't be experiencing this joyous moment. You are the reason I continued this journey, pushing through the tough times and coming out stronger on the other side. I dedicate all my achievements—not just this PhD, but everything I have done and will do—to you both. Love you both so much <3. **Divine**, you've been more than a brother to me. You've been my friend, philosopher, and even my fortune teller, always keeping me grounded and showering me with love. Your wisdom and support have been invaluable, and I can't thank you enough for always being there for me (cringe :P, but true <3). **Jeny** and **Venba kutty**, you both have been there during the crucial times of my journey. Your joy and unwavering support have lifted my spirits when I needed it the most. Venba's hugs, kisses and smiles are the greatest and most lovely boost I received. **Paati**, I'm sure you will be super happy as well. Thank you for your love and many prayers. My **Aunts, uncles** and **cousins** (Jeffin, Jelsi, Rithin and Nithil), so much of love and so many good memories. Love you all <3.
Mama, Athai, Sankavi, and **Silambarasan**, you've welcomed me into the family with such warmth and joy. Your encouragement and unwavering

belief in my journey have been a boost, especially as I pushed towards the finish line with my PhD. Sankavi & Silambarasan your positive words and persistent encouragement kept me focused on writing my thesis. Thank you! <3

Last but certainly not least, my wife, **Vergi**! Thank you, sweetheart, for being the incredible, positive person who has helped me navigate through so many clueless moments. Your unwavering understanding of the journey I've been on has added countless little joys along the way. Without you by my side, I truly don't know if I would be here after all the highs and lows I've experienced in the final stretch. I often find myself wishing I had met you a few years earlier—it would have made life so much easier. Your patience, support, and encouragement have been my anchor. You've pushed me to keep chasing my dreams, and now, my dreams go beyond just obtaining a PhD. Your belief in me has been the reason for many of the steps I've taken confidently over the past few years. Thank you for being my motivation, and my biggest cheerleader. Your love and support have made all the difference, and I am endlessly grateful to have you in my life. Here's to many more adventures and dreams to chase together!

About the author

Antony Cyril Arulrajan was born in Thoothukudi, Tamil Nadu, India in 1993. He earned his bachelor's and master's degrees in chemistry from Kamaraj College (MS University, Tirunelveli) and the National Institute of Technology-Tiruchirappalli, India, respectively. His master's thesis focused on fuel cell catalysis. Following his master's, Antony spent about a year each at the University of Twente in the Netherlands and Ariel University in Israel, where he conducted research on understanding and developing electrocatalysts for fuel cell applications.

In 2018, Antony began his Ph.D. in the Environmental Technology group at Wageningen University and Research, in collaboration with Wetsus (European Centre of Excellence for Sustainable Water Technology) in Leeuwarden, The Netherlands. During his Ph.D., he investigated the pH changes during electrochemical desalination to mitigate mineral scaling and improve ion-selectivity. Since 2023, Antony has been developing an innovative water treatment technology through his startup, IonIQs B.V. (formerly VerSi-watertech).

Netherlands Research School for the
Socio-Economic and Natural Sciences of the Environment

D I P L O M A

for specialised PhD training

The Netherlands research school for the
Socio-Economic and Natural Sciences of the Environment
(SENSE) declares that

Antony Cyril Arulrajan

born on the 30th of May 1993 in Thoothukudi, India

has successfully fulfilled all requirements of the
educational PhD programme of SENSE.

Wageningen, 9th of September 2024

SENSE coordinator PhD education

Dr Ir Peter Vermeulen

The SENSE Director

Dr Jampel Dell'Angelo

The SENSE Research School declares that **Antony Cyril Arulrajan** has successfully fulfilled all requirements of the educational PhD programme of SENSE with a work load of 41.8 EC, including the following activities:

SENSE PhD Courses

- Environmental research in context (2019)
- Research in context activity: Scientific outreach of CDI research to wider audience (2023)

Other PhD and Advanced MSc Courses

- Scientific Artwork - Vector graphics and images, Wageningen University (2019)
- Presentation skills, Wetsus (2019)
- Communication style, Wetsus (2019)
- How to supervise students, Wetsus (2019)
- Talents, Wetsus (2019)
- Wetsus Personal development course starting day (2019)
- Project and Time management (2019)
- Career perspectives, Wetsus (2021)
- Environmental Electrochemical Engineering, Wageningen University (2022)
- European water campus business challenge, Water Campus Leeuwarden (2023)

Management and Didactic Skills Training

- Supervising a MSc student with thesis titled: 'Water desalination and ion-selectivity with novel flow-electrode in capacitive deionization' (2021-2022).

Oral Presentations

- *Anion selective electrodes for water desalination.* CDI and Electrosorption- 2019 (CDI&E-2019), 20-23 May 2019, Beijing, China
- *pH changes in electrochemical water desalination.* 12th European symposium on electrochemical engineering (ESEE), 14-17 June 2021, Leeuwarden, the Netherlands

Poster Presentations

- *Unravelling the pH changes in electrochemical water desalination with CDI.* CDI and Electrosorption- 2021 (CDI&E 2021), 11-14 May 2021
- *Understanding pH changes in Membrane Capacitive Deionization (MCDI) during long operation*. International Society of Eelectrochemistry-29th topical meeting, 18-21 April, 2021

This work has been done within the cooperation framework of Wetsus, European Centre of Excellence for Sustainable Water Technology (www.wetsus.eu). Wetsus is co-funded by the Dutch Ministry of Economic Affairs and Climate Policy, the European Union Regional Development Fund, the City of Leeuwarden, the Province of Fryslân, Northern Netherlands Provinces, and the Netherlands Organization for Scientific Research. Wetsus also coordinates the WaterSEED project that received funding from European Union's Horizon 2020 research and innovation program under Marie Skłodowska-Curie grant agreement No. 665874. Thanks to the members of the "Desalination & Concentrates" for their financial support and fruitful discussions.

Financial support from Wetsus and Environmental Technology group (Wageningen University) for printing this thesis is gratefully acknowledged.